Aus dem Adolf-Butenandt-Institut der Ludwig-Maximilians-Universität Lehrstuhl
für Molekularbiologie
Vorstand: Prof. Dr. rer. nat. Peter Burkhard Becker

The Epigenetic Regulation of Ciliogenesis by *Xenopus laevis* Suv4-20h Histone Methyltransferases

Dissertation zum Erwerb des Doktorgrades der Medizin
an der Medizinischen Fakultät der Ludwig-Maximilians-Universität
zu München

N. B. Ohnmar Hsam
aus Mandalay

2015

Mit Genehmigung der Medizinischen Fakultät
der Universität München

Berichterstatter:	Prof. Dr. Ralph A. W. Rupp
Mitberichterstatter:	Prof. Dr. med. Thomas Cremer Prof. Dr. Andreas Ladurner Prof. Dr. Michaela Smolle
Dekan:	Prof. Dr. med. Dr. h.c. M. Reiser, FACR, FRCR
Tag der mündlichen Prüfung:	29.01.2015

Eidesstattliche Versicherung

Ich erkläre hiermit an Eides statt, dass ich die vorliegende Dissertation selbständig verfasst, mich außer der angegebenen keiner weiteren Hilfsmittel bedient und alle Erkenntnisse, die aus dem Schrifttum ganz oder annähernd übernommen sind, als solche kenntlich gemacht und nach ihrer Herkunft unter Bezeichnung der Fundstelle einzeln nachgewiesen habe.

Ich erkläre des Weiteren, dass die hier vorgelegte Dissertation nicht in gleicher oder in ähnlicher Form bei einer anderen Stelle zur Erlangung eines akademischen Grades eingereicht wurde.

_____ _____

Ort, Datum Unterschrift

Dedicated to my parents & sister

Sai Long Kyio Hsam

Daw Khin Than Mya

& Siri

The most exciting phrase to hear in science, the one that heralds new discoveries, is not 'Eureka!', but 'That's funny ...'

- Isaac Asimov

TABLE OF CONTENTS

ABBREVIATIONS

5’ or 3’-UTR	5’ or 3’ untranslated region
AC	animal cap
AP	alkaline phosphatase
ATP	adenosine triphosphate
BB	basal body
BCIP	5-bromo-4-chloro-3-indolyl-phosphate
BMP	bone morphogenetic proteins
bp	base pairs
BSA	bovine serum albumin
CCP	ciliated cell progenitor
ChIP	chromatin immunoprecipitation
CNS	central nervous system
Co	control
DEPC	diethylpyrocarbonate
DIG	digoxigenin
DKO	double knockout
dll1	delta-like 1
dn	double null
DNA	deoxyribonucleic acid
dnah9	dynein axonemal heavy chain 9
Dvl	dishevelled
et al.	et alii
FGF	fibroblast growth factor
Fig.	figure
for	forward
foxj1	forkhead box J1
GFP	green fluorescent protein
GRP	gastrocoel roof plate
h	hour
H4K20me2/me3	di-methylation/tri-methylation on histone H4 at lysine position 20
hCG	human chorionic gonadotropin
HMT	histone methyltransferase

hpf	hours post fertilization
ICC	immunocytochemistry
IFT	intraflagellar transport
INC	intercalating non-ciliated cells
ISH	*in situ* hybridization
kb	kilobase
KMT	lysine methyltransferases
LNA	locked nucleic acid
mab	monoclonal antibody
MBS	modified Barth's saline
MBT	midblastula transition
MCC	multiciliated cell
mci	multicilin
MCP	multiciliated cell progenitor
min.	minute
miR	microRNA
MO	morpholino oligonucleotid
mRNA	messenger RNA
myb	myeloblastosis proto-oncogene
NF	Nieuwkoop Faber
ng	nanogram
NICD	notch intracellular domain
nm	nanometer
ODC	ornithine decarboxylase
OMIM	online Mendelian inheritance in man
ORF	open reading frame
pax2	paired box 2
PBS	phosphate buffered saline
PCD	primary ciliary dyskinesia
PCP	planar cell polarity
PCR	polymerase chain reaction
PFA	paraformaldehyde
PKD	polycystic kidney disease
PRMT	protein arginine N-methyltransferases

PTM	posttranslational modification
rev	reverse
RFP	red fluorescent protein
rfx2	regulatory factor X, 2
RNA	ribonucleic acid
RT	room temperature
SAM	*S*-Adenosyl methionine
SEM	scanning electron microscopy
SET domain	Suv39, E(z), Trx protein domain
Sh1	Suv4-20h1
siRNA	small interfering RNA
Suv	**su**ppressor of position effect **v**ariegation
TGF beta	transform growth factor beta
WT	wild type
X-Gal	5-Brom-4-chlor-3-indoxyl-β-D-galactopyranosid
xlim-1	xenopus LIM homeobox gene 1

1. SUMMARY/ ZUSAMMENFASSUNG

Summary

Cilia have vital functions ranging from extracellular transport, mechano- and chemosensors to signaling pathways. Due to their near ubiquitous distribution on human cells, defective cilia are associated with severe disorders of the lung, kidney and reproductive system, as well as tumor development. Preliminary work from our laboratory has indicated that cilia on the surface of the *Xenopus* larval skin are shortened in length and lessened in number, if the Suv4-20h1 and –h2 histone methyltransferases are absent. These enzymes are required for the di- and tri-methylation of H4K20 and play a critical role in embryogenesis. The aim of this dissertation is to examine the connection between histone methylation and cilia formation.

To elucidate the underlying causes for the Suv4-20h cilia phenotype, endogenous synthesis of the Suv4-20h proteins was inhibited by microinjection of antisense-morpholino. Subsequently, Suv4-20h target genes were investigated by immunostainings and RNA analysis in order to identify links between Suv4-20h enzymes and ciliogenic pathways. This dissertation shows that Suv4-20h HMTases control ciliogenesis in multiciliated cells of the epidermis and the kidney via a similar pathway.

There are two specific Suv4-20h functions in the larval epidermis during different stages of cilia formation. During gastrulation, Suv4-20h protein depleted embryos show more ciliated cell progenitors, most likely due to the upregulation of Delta-like 1 (Dll1), which perturbs cell fate selection. At the tadpole stage, a defect in cilia differentiation is observed. Four genes stimulating multiciliogenesis and encoding axonemal proteins respectively are downregulated concomitant with functional losses of cilia. Ciliogenesis is also strongly inhibited in the pronephric kidney of Suv4-20h morpholino injected embryos. The microRNA miR-449 that normally inhibits Dll1 is strongly reduced here and can act as the earliest link between Suv4-20h and ciliogenesis to date. Additionally, my data indicate stimulating effects of cilia on tubule differentiation. Taken together, my results demonstrate for the first time that ciliogenesis has an epigenetic root.

Zusammenfassung

Zilien übernehmen lebenswichtige Aufgaben, die vom extrazellulären Transport über Mechano- und Chemosensoren bis hin zur Beteiligung an Signalwegen reicht. Aufgrund ihrer fast ubiquitären Verbreitung ist deren Ausfall mit schweren Erkrankungen von Lunge, Niere und Reproduktionstrakt, sowie mit der Entwicklung von Tumoren verbunden. Die Vorarbeit in unserem Labor zeigte, dass die Länge und Anzahl der Zilien auf der Haut der Xenopuslarve abnahm, wenn die Suv4-20h1 und –h2 Histonmethyltransferasen abwesend waren. Die Enzyme sind zuständig für die Di- und Trimethylierung von H4K20 und spielen eine bedeutende Rolle in der Embryonalentwicklung. Das Ziel dieser Dissertation ist den Zusammenhang zwischen Histonmethylierungen und Zilienbildung zu erforschen.

Zur Entschlüsselung der zugrunde liegenden Ursachen für den Suv4-20h Zilien-Phänotyp wurde initial die endogene Synthese der Suv4-20h Proteine mittels der Mikroinjektion von antisense Morpholino-Oligonukleotiden inhibiert. Anschließend wurden Immunfärbungen und RNA-Analysen zur Untersuchung von Zielgenen der Suv4-20h Enzyme durchgeführt, um Verknüpfungen zwischen den Suv4-20h Enzymen und ziliogenen Netzwerke zu entdecken. Diese Doktorarbeit zeigt, dass die Suv4-20h HMTasen die Ziliogenese in multizilierten Zellen der Epidermis und der Niere über einen ähnlichen Signalweg kontrolliert.

In der Epidermis der Xenopuslarve zeigen sich zwei spezifische Funktionen der Suv4-20h Enzyme zu unterschiedlichen Stadien der Ziliogenese. Während der Gastrulation zeigen Suv4-20h Protein depletierte Embryonen vermehrt Zilienvorläufer-Zellen, am ehesten aufgrund einer Überproduktion von Delta-like 1 (Dll1), wodurch Störungen in der Zellspezifizierung bedingt sind. Während des Kaulquappenstadiums präsentiert sich ein Defekt in der Zilien-Differenzierung. Vier Gene, die die Multiziliogenese stimulieren bzw. Axonemproteine kodieren, sind vermindert exprimiert, was mit Funktionseinbußen der Zilien einhergeht. In der Vorniere zeigt sich ebenfalls eine erhebliche Hemmung der Ziliogenese in Suv4-20h Morpholino injizierten Embryonen. Die MikroRNA miR-449, die normalerweise Dll1 inhibiert, ist hier deutlich vermindert und kann den bisher frühesten Link zwischen den Suv4-20h Histonmethyltransferasen und der Ziliogenese darstellen. Zusätzlich gibt es Hinweise für stimulierende Einflüsse auf die Tubulus-Differenzierung durch Zilien. Zusammenfassend zeigen meine Ergebnisse zum ersten Mal, dass die Zilienbildung ihre Wurzeln in der Epigenetik hat.

2. INTRODUCTION

2.1 Developmental biology and medicine

Developmental biologists strive to understand the question of how a single zygote becomes a fully differentiated multicellular organism. It is one of the most magnificent events that a single fertilized cell gives rise to different cell types in tissues and organs, all in all forming a complex organism. Understanding how tissues and organs become differentiated is very valuable for medical and regenerative medicine purposes. Most, if not all, diseases can be viewed as failure of cellular differentiation and discoveries of embryonic development can help to gather information needed for a better diagnosis and treatment of diseases (Lewis Wolpert 2011).

2.2 Development of the multiciliated epithelium

2.2.1 Definition of cilia

A cilium (*lat*.: eyelash) is a vital membrane-covered cell-extension on the surface of almost all post-mitotic cells in vertebrates, which includes mammals and frogs. Discovered since the days of Antony van Leeuwenhoeck in 1675, cilia's steep rising as pivotal cell structures began in the past decade. Since then, modern science has linked these hair-like structures to profound functions in tissue development and homeostasis (Satir 1995; Oh and Katsanis 2012). Basically, cilia are classified into non-motile primary cilia and motile cilia. The primary cilium is a solitary cilium with sensory role (e.g. photoreceptors of the retina, chemo- and mechanosensors of the olfactory epithelium and inner ear) and functions in cellular (cell cycle, division) and signaling processes (e.g. Notch, Wnt pathways). Motile cilia cover the surfaces of brain ventricles, fallopian tubes, airways and the embryonic node. Cells can form a solitary cilum, as in the node, or multiple cilia, as in the airways. In the past, motile cilia were solely attributed to establishing a fluid flow along surfaces. But more recently, data suggest that all motile cilia perform sensory functions as well (Fliegauf, Benzing et al. 2007; Bloodgood 2010; Oh and Katsanis 2012). All motile cilia share a similar ciliary structure, which will be introduced in the next section.

2.2.2 Structure of motile cilia

Various classes of cilia may have different tissue-adapted functions, but their highly conserved basic structure remains constant. A cilium is basically divided into three subcompartments from base to top, i.e. basal body, transition zone and axoneme. After the exit from cell cycle, cells in G0/G1 can assemble one or two cilia or a cilia tuft (200-300 per cell). In order to assemble multiple cilia, those cells need to start massive centriole amplification. This huge amount of centriole amplification is achieved by two modes: a centriolar mother centriole-dependent amplification mode and an acentriolar *de novo* centriole biogenesis without a mother centriole. Centrioles later migrate via vesicle transport to the apical surface of the cell and become established as basal bodies (BB) (Klos Dehring, Vladar et al. 2013).

The basal bodies form the foundation for the axoneme to extend from the cell surface. Each basal body contains nine triplets of microtubules and has accessory structures attached, including a basal foot and striated rootlet. The basal foot is a lateral extension from the midregion of the BB that interacts with apical microtubules of the cytoskeleton. Ciliary rootlets are striated fibrous networks, originating from basal bodies and extending toward the cell nucleus. The striated ciliary rootlets are thought to be an anchor and support structure for the cilia (Boisvieux-Ulrich and Sandoz 1991; Kasuya and Miyoshi 2001; Yang, Liu et al. 2002; Fliegauf, Benzing et al. 2007). Figure 1.1 illustrates the main features of the motile cilia.

The transition zone marks the proximal region of the cilia and is thought to control entry and exit from the ciliary compartment (Fliegauf, Benzing et al. 2007).

The ciliary axoneme is elongated and maintained via intraflagellar transport (IFT) during ciliogenesis. The motile ciliary axoneme has a 9+2 structure surrounded by a specialized extension of the cell membrane, containing specific receptors and ion channel proteins. Nine microtubule doublets (A- and B-tubule) encircle a pair of singlet microtubules in its core. The peripheral microtubules are held in place by radial spokes. Inner and outer dynein arms connect A-tubules with adjacent B-tubules and mediate cilia motility based on peripheral microtubule sliding (Satir 1980; Fliegauf, Benzing et al. 2007; Satir and Christensen 2007). Motility is achieved by the interaction between dynein arms and microtubules. The ATPase

activity of the dynein motors causes dynein structural change and initiates the doublets to slide asynchronously against each other, thus generating a wave-like beating motion of the cilia (Satir, 1980).

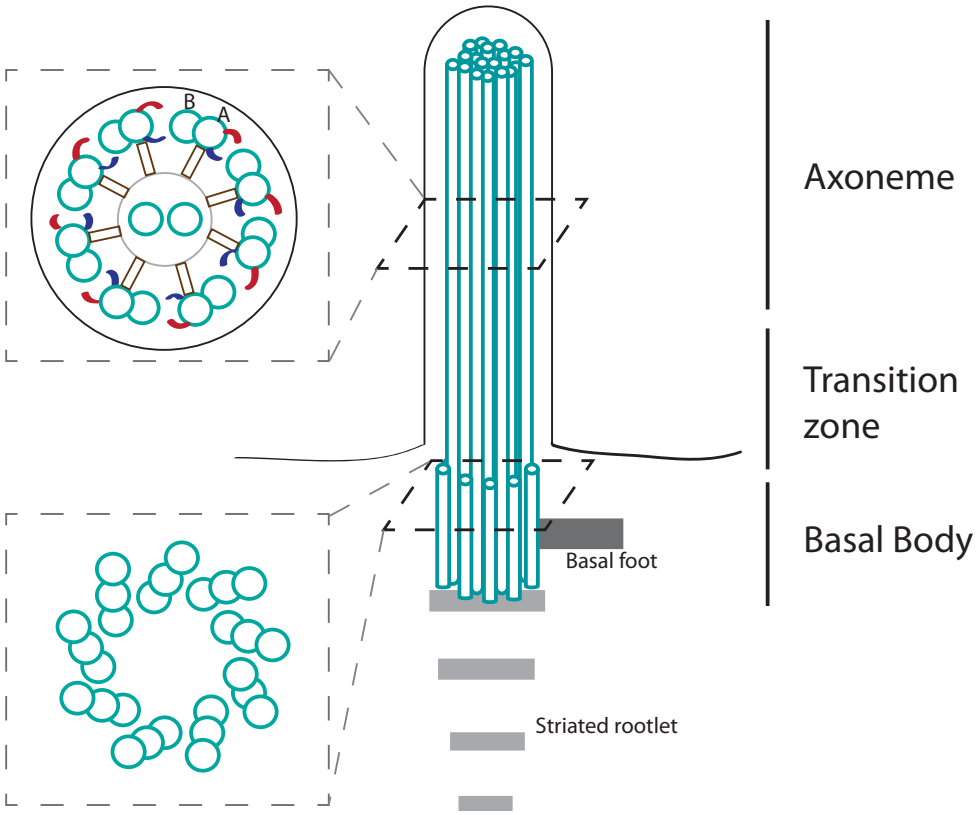

Fig. 1.1: Subcompartments of a '9+2' motile cilium.
Graphic shows a motile cilium with a '9+2' axonemal microtubule arrangement (cyan). The cross-sectional view is shown at the left side. Outer (red) and inner (blue) dynein arms, connecting two peripheral doublet microtubules, facilitate cilia motility. Radial spokes (brown) connect peripheral doublets to the central singlet microtubules. The basal body comprises nine microtubule triplets, which is the foundation for the axoneme extension. The basal foot connects the cilium to the internal cytoskeleton and the striated rootlet stabilizes the cilium. Modified after Fliegauf et al., Nat Rev Mol Cell Biol 8, (2007).

2.2.3 Ciliopathies: Cilia-related diseases

The term ciliopathy is used for a disease, which is caused by a dysfunction of any ciliary component. Cilia-related diseases often affect multiple organ systems due to their ubiquitous location. Motile cilia are present in various tissues and organs and are commonly attributable to establish a directed fluid flow on the surface of epithelia. In the fallopian tubes

for example, ciliary motion is involved in transport of an ovum toward the uterus ensuring fertility (Lyons, Saridogan et al. 2006). Furthermore, respiratory cilia are vital for a proper mucociliary clearance (Knowles and Boucher 2002). Defective ciliary structure and function are commonly associated with airway pathologies. Ciliary defects can arise from disease or environmental agents including primary ciliary dyskinesia, asthma, infection and pollutants such as smoking (Chilvers and O'Callaghan 2000). Smoking was linked to short cilia, likely leading to an impaired mucociliary clearance (Leopold, O'Mahony et al. 2009).

Primary Ciliary Dyskinesia

The respiratory system has a mucociliary epithelium, where hundreds of motile cilia from each ciliated cell protrude into the airway lumen. Cilia are surrounded by a watery solution, the periciliary layer, which again is covered by a layer of mucus. Ciliary beating generates an extracellular mucus-transporting current, which cleans the airways from dirt, cell debris and pathogens. Structural defects of respiratory cilia impair cilia motility and the mucociliary clearance, leading to a condition described as “primary ciliary dyskinesia” (PCD) or “immotile-cilia syndrome”. However, cilia motility is not always absent. Sometimes ciliary beating is present, but is incorrect in its frequency or beating pattern (Afzelius 1976; Zariwala, Knowles et al. 2007).

PCD (OMIM #244400) is an autosomal-recessive disorder, affecting approximately 1 in 15.000 live births in Europe. However, the prevalence might be an underestimation, because PCD is often misdiagnosed. Newborns can present unexplained tachypnea and chronic rhinitis. With dysmotile cilia being unable to clear mucus toward the natural exits mouth and nose, as a result, respiratory tract bacteria are able to grow and overcome the mucus barrier, infecting the underlying epithelium. During progression of disease, chronic upper and lower airway infection and inflammation arise as consequence. The disease eventually advances to bronchiectasis and lung failure. Since the progression of lung disease varies by age of diagnosis and treatment, early diagnoses can positively affect quality of life and slow down progression of disease. PCD is often caused by mutations in DNAH5 and DNAI1, which code components of outer dynein arms (www.omim.org/entry/244400 ; Zariwala, Knowles et al. 2007; Reiß 2009). Other disorders, which have been reported in PCD patients, are infertility due to defective sperm flagella or fallopian tube cilia, as well as retinal degeneration, hearing deficits, hydrocephalus and organ laterality defects. Dysfunctional motile cilia of the embryonic node are linked to abnormal left-right organ patterning, resulting in heterotaxy or

situs inversus. 50% of PCD patients have a situs inversus, a condition referred to as Kartagener's syndrome (Zariwala, Knowles et al. 2007).

Two other ciliopathies, called Alström Syndrome (OMIM #203800) and Bardet-Biedl Syndrome (OMIM #209900) possess many similarities, such as blindness due to rod-cone dystrophy, loss of hearing, childhood obesity, insulin resistance and type 2 diabetes mellitus. Apart from these characteristics, Bardet-Biedl Syndrome shows mental retardation, polydactyly and hypogonadism (http://www.omim.org/entry/209900). Chronic pulmonary symptoms also appear in 30-50% of patients with Alström and Bardet Biedl Syndrome, which suggests that motile respiratory cilia can also be dysfunctional in ciliopathies of the primary cilium (Marshall, Bronson et al. 2005; Zariwala, Knowles et al. 2007).

Hydrocephalus

Multiple motile '9+2' cilia lining the brain ventricles are important for the circulation of the cerebrospinal fluid, which surrounds brain and spinal cord. A dysfunctional ependymal flow was shown in several animal studies to be linked to the formation of enlarged brain ventricles, termed hydrocephalus (Ibanez-Tallon, Pagenstecher et al. 2004; Hagenlocher, Walentek et al. 2013). Dysmotile cilia lacking axonemal dynein heavy chain Dnahc5 caused an impairment of fluid flow. Furthermore, mice with mutations in the intraflagellar transport protein IFT88 demonstrated erroneous ciliogenesis of the choroid plexus epithelium. Therefore, it was thought that the hydrocephalus was caused by an overproduction of cerebrospinal fluid as an result of altered mechanosensory function in choroid plexus cilia (Fliegauf, Benzing et al. 2007). For a list of ciliopathies see Avasthi and Marshall, (2012).

2.3 *Xenopus leavis* – the South African claw-toed frog

2.3.1 A model organism in developmental biology

Xenopus laevis is a species, which naturally occurs only in South and Central Africa. Since the 1940s, it was widely used in Europe for comparative anatomy and endocrinology studies, e.g. in hospital laboratories as an indicator for human pregnancy. In the 1960s, *Xenopus* became increasingly popular with developmental biologists, because it could be induced to ovulate all season long (Gurdon and Hopwood 2000). In the 1980s, *Xenopus* molecular analysis was crucial to study developmental processes (Gurdon, Mohun et al.

1985). Decades later, *Xenopus* is nowadays one of the most widely used vertebrate species in developmental, cell and molecular biology (Gurdon and Hopwood 2000). Biologists use *Xenopus laevis* because of its ease in maintenance, resistance to diseases, and the large number of embryos (up to thousand eggs/day). Fertilized eggs are robust and survive well in petri dishes with saline solution. To manipulate gene expression and to study embryogenesis, mRNA, plasmid DNA and antisense morpholino oligonucteotides can be easily injected into the oocyte (Sive, Grainger et al. 2000). To study the molecular mechanisms in cilia development, *Xenopus* skin is widely used as an *in vivo* model. For this purpose, easy accessibility of the large egg size (∅1mm) offers enormous advantage compared to the internal location of mammalian airway epithelium. Additionally, the processes of early development are largely conserved from *Xenopus* to higher vertebrates. Thus, *Xenopus* has been helpful in detecting many concepts in modern developmental biology. Furthermore, eggs tolerate microsurgeries well due to their good tissue healing capabilities, which allows microdissections for animal cap assays. But above all, *Xenopus* is perennially reproductive and female frogs can be stimulated to lay eggs by injection of human chorionic gonadotropin (hCG) every three months. Moreover, embryos have a short life cycle (Fig. 1.2), enabling the researcher to follow the development from a zygote to a tadpole in only 44 hours (Nieuwkoop and Faber 1967).

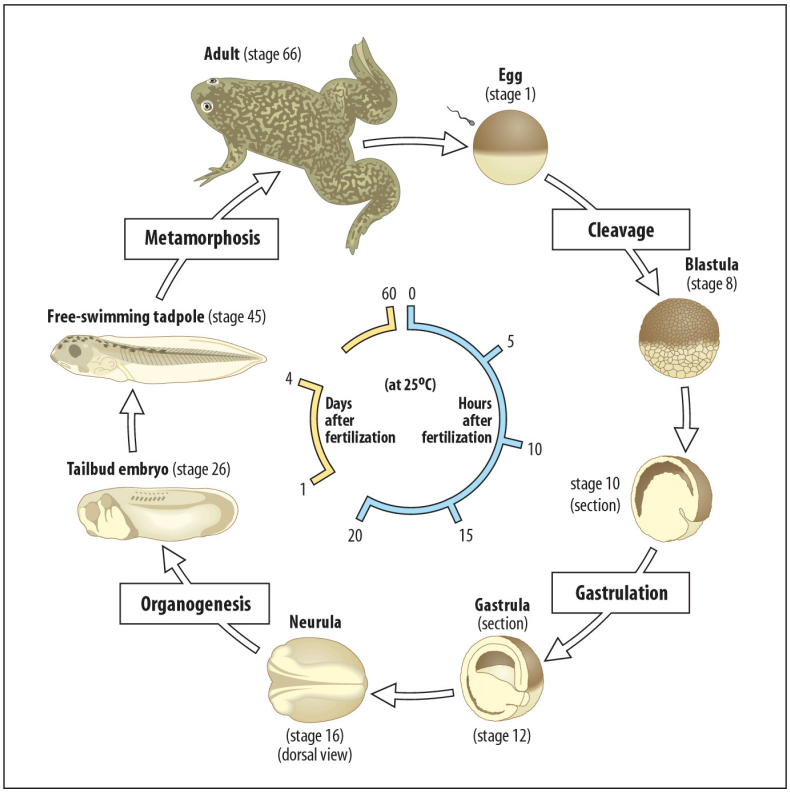

Fig. 1.2 Model of *Xenopus laevis* life cycle. Major stages of development are depicted according to Nieuwkoop and Faber (1967): cleavage, MBT (midblastula transition), gastrula, neurula, organogenesis and meta-morphosis. Pre-MBT embryos only translate maternal mRNA. After MBT during blastula stage (NF 8), zygotic gene transcription starts. (Modified after http://www.mun.ca/biology/desmid/brian/BIOL3530/DEVO_03/devo_03.html)

The pigmented surface of the upper half is termed animal pole, while the non-pigmented lower surface is called vegetal pole. Prominent factors in endoderm and mesoderm formation are maternal Vg1 and VegT that are restricted to the vegetal hemisphere. VegT is important for endodermal induction and lack of VegT results in embryos with no endoderm and less mesoderm (Zhang, Houston et al. 1998). Vg1 and Nodal genes are thought to play a role during gastrula when vegetal cells induce overlaying marginal zone cells to differentiate to mesoderm. It is noteworthy that cells lacking mesoderm- and endoderm-inducing signals form ectoderm, suggesting that ectoderm formation represents a default pathway (Dale, Matthews et al. 1993; Jones, Kuehn et al. 1995). Maternal factors play an important role for ectoderm specification. For instance, isolation of the pigmented blastocoel roof before the midblastula transition results in the formation of 'atypical epidermis', an ectodermal derivate. Ectoderm differentiates into two major groups: surface ectoderm and neuroectoderm. The surface ectoderm gives rise to the future skin and is specified by BMP (bone morphogenetic protein). The neuroectoderm is fated to form the central and the peripheral nervous system by secretion of BMP antagonists that inhibit BMP-signaling (Kühl and Gessert 2010).

2.3.2 Cilia in the *Xenopus* epidermis and ciliogenesis

Xenopus laevis skin resembles the human respiratory mucociliary epithelium and contains two categories of cells: ciliated and non-ciliated cells. In the surface layer of the non-neural ectoderm, fully differentiated multiciliated cells are evenly scattered between the non-ciliated cell types, including goblet cells, ionocytes and small secretory cells (Hayes, Kim et al. 2007; Dubaissi and Papalopulu 2011; Dubaissi, Rousseau et al. 2014).

So far, two major phases are involved in creating the ciliated spacing pattern. According to Deblandre et al. (1999), Notch signaling is a key regulator of ciliated cell fate, which occurs in the inner (sensorial) layer of the epidermis. It is involved in many organisms to ensure

certain developmental processes. It is responsible for binary cell-fate decisions in patterning events and controls specification of cells by direct cell-cell contacts (Fortini 2009).

A subset of cells with high levels of Delta-like 1 (*dll1*) gets committed to become ciliated cells (CCP; ciliated cell progenitor) in the inner skin layer during gastrulation stage (Fig. 1.3d). These progenitor cells express *dll1*, a notch ligand and are able to prevent neighboring cells from entering the ciliated cell fate by lateral inhibition. Dll1 triggers the Notch1 receptor of neighboring cells through direct cell-to-cell contact, which leads to activation of the Notch pathway. Subsequently, the notch intracellular domain (NICD) is then released by proteolysis, which in turn moves to the nucleus resulting in a transcriptional repression of ciliogenic genes (Deblandre, Wettstein et al. 1999; Fortini 2009; Stubbs, Vladar et al. 2012).

However, as CCPs begin to differentiate, they move from the inner ectodermal layer to the embryonic surface by radial intercalation through the junctions between at least three outer layer cells. Consequently, this second step secures the spaced alignment of ciliated cells in the outer skin layer, thereby restricting the number of intercalating cells. Lastly, ciliated cells reach the surface of the mucociliary epithelium where cilia can be detected by acetylated α-tubulin (Deblandre, Wettstein et al. 1999; Stubbs, Davidson et al. 2006).

It is known that *dll1*-expressing cells also give rise to other cell types of the mucociliary epithelium apart from MCCs. The so-called intercalating non-ciliated cells (INC), e.g. the small secretory cells and the ionocytes are specified in the inner layer and then intercalate to the surface (Stubbs, Davidson et al. 2006; Dubaissi and Papalopulu 2011).

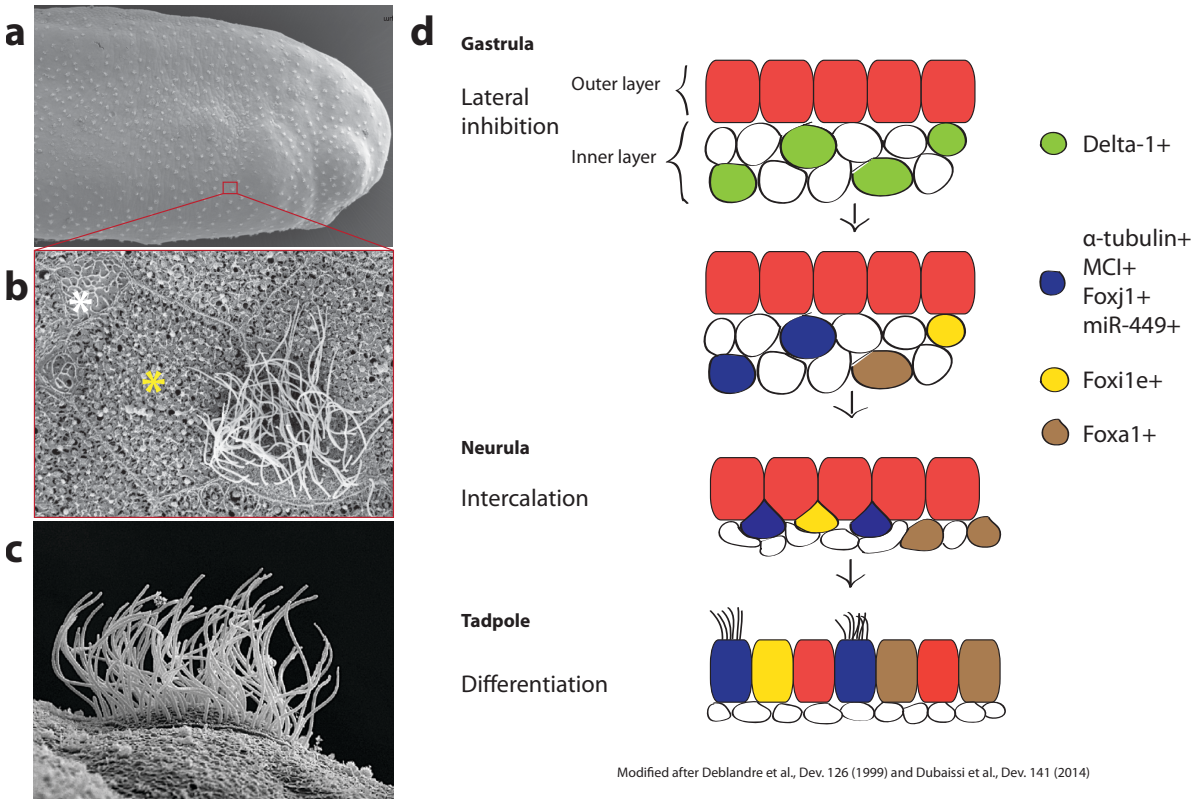

Fig. 1.3: *X. laevis* epidermis – a mucociliary epithelium and its development.
a-c: scanning electron microscopy images of the larval skin. **b:** higher magnification of red marked area in (**a**), showing a multiciliated cell, intercalating non-ciliated cell (white asterisk), and large goblet cells (yellow asterisk). **c**: lateral view of a multiciliated cell with multiple cilia tufts, from Hayes et al. 2007. **d**: a two-step model of the morphogenesis of the multiciliated skin. Gastrula (NF 10-13) - Delta-1/Notch-mediated cell fate specification and lateral inhibition; CCPs and INCs express Delta (green), whereas neighboring cells express Notch (white). Later CCPs express α–tubulin as a marker (blue). Neurula (NF 15-20) – intercalation into the outer cell layer and subsequent differentiation and proliferation (NF 20-22). Yellow: ionocytes; brown: small secretory cells.

At the molecular level, the mechanisms, by which a committed cell can differentiate and form cilia, are not fully understood. Studies in various animal models have highlighted the connection between Delta/Notch and the transcriptional program that drives cilia formation during ciliated cell differentiation (Fig. 1.4) (Deblandre, Wettstein et al. 1999; Liu, Pathak et al. 2007; Ma and Jiang 2007; Ezratty, Stokes et al. 2011).

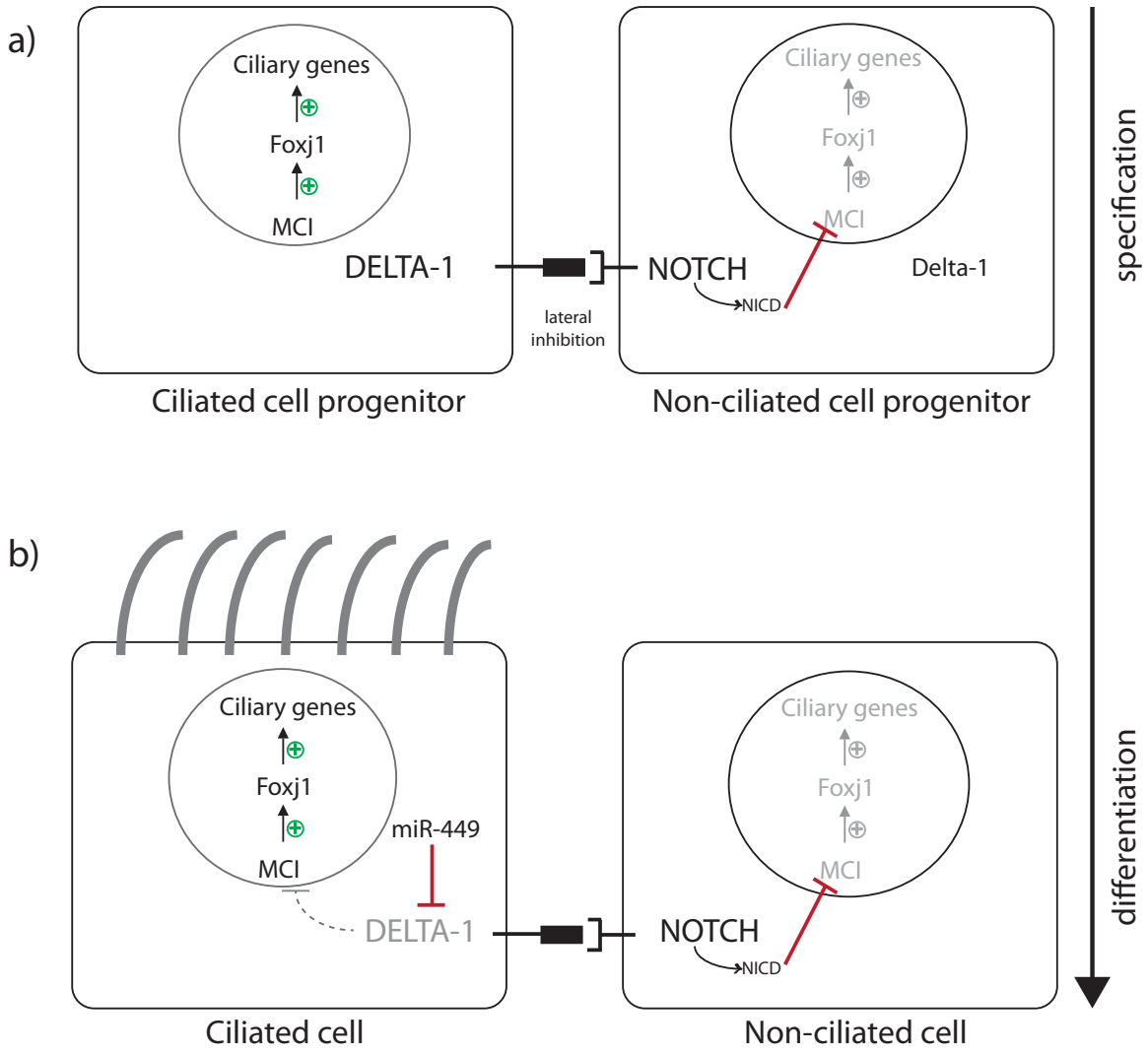

Fig. 1.4: Proposed molecular pathway for multiciliogenesis.
Multicilin acts as a critical target of Notch signaling during lateral inhibition. **a)** Delta/Notch-mediated lateral inhibition. CCPs are marked with high Delta-1 levels and can activate Notch signaling in adjacent cells. **b)** Notch activation represses multiciliogenesis by inhibition of Multicilin in future non-ciliated cells. In contrast, a high level of Multicilin is proposed to induce cell cycle exit and ciliogenesis in future multiciliated cells. The dashed line indicates that Delta-1 might repress multiciliogenesis through autocrine signaling. miR-449 represses Delta-1 from early neurula onward. Grey colour denotes inactive and black denotes active genes/pathways.

After ciliated fate specification, cells exit the cell cycle in order to assemble cilia. Multicilin (*mci*) promotes multiciliogenesis downstream of notch by inducing the cell-cycle exit (Stubbs, Vladar et al. 2012). Furthermore, it stimulates deuterosome-mediated (de novo) centriole amplification by induction of *myb*, which is a transcription factor involved in cell cycle regulation and progenitor cell proliferation. *Myb* then induces *foxj1* (forkhead box J1), a master regulator of many genes required for motile cilia formation (Ramsay and Gonda 2008; Stubbs, Oishi et al. 2008; Yu, Ng et al. 2008; Tan, Vladar et al. 2013). It is noteworthy that

Foxj1 is also expressed in human pulmonary and renal epithelium (Pelletier, Brody et al. 1998).

According to a recent study by Marcet et al. (2011) in *Xenopus* and HAECs (human airway mucuciliary epithelial cell), microRNAs of the miR-449 family (miR-449a, b and c) are key regulators of multiciliogenesis. Delta-like 1 expression in the epidermis is normally undetectable from early neurula onwards (Deblandre, Wettstein et al. 1999). miR-449 is induced during multiciliogenesis and it is thought that miR-449 represses Delta-like 1 expression, thus promoting centriologenesis and differentiation of multiciliated cells in epidermis and nephrostomes. Inhibition of miR-449 leads to an increase of α-tubulin mRNA positive MCPs with defective multiciliogenesis, suggesting that miR-449 regulates terminal differentiation rather than specification of MCCs (Marcet, Chevalier et al. 2011).

Taken together, these data suggest an evolutionary conserved cassette controlling the mucociliary epithelium formation among many different tissues and species. Thereby, *Xenopus* is a highly suited *in vivo* system to dissect this process.

Many epithelia are polarized within the plane of the tissue. This is generally termed as planar cell polarity (PCP). Cilia protruding from the surface of multiciliated cells are also polarized in order to produce a directed fluid flow by organized ciliary beating. Recent reports have shown that planar cell polarity signaling is central in regulation of cilia-mediated fluid flow (Konig and Hausen 1993; Park, Mitchell et al. 2008). Two modes of planar polarity are present in multiciliated cells: intra-cellular rotational planar polarity and inter-cellular tissue-level planar polarity (Fig. 1.5). The first mode refers to the unidirectional alignment of all basal bodies within a cell with the ciliary rootlet pointing in the direction of the return stroke (Fig. 1.5a) (Wallingford 2010). Disrupted Dishevelled (Dvl) function was shown to disorganize ciliary beating and impair flow. Aside from the above function, Dvl is important for ciliogenesis by promoting docking of basal bodies to the apical cell membrane. The PCP effector proteins Inturned and Fuzzy are also important for ciliogenesis. They control formation of the apical actin cytoskeleton downstream of Dvl and defects of these factors impair docking of basal bodies (Park, Mitchell et al. 2008). The latter mode states that basal bodies of different multiciliated cells of the tissue are parallel aligned (Fig. 1.5b). Tissue-level polarity is also controlled by PCP proteins such as Vangl2 and Frizzled (Wallingford 2010).

Collectively, the PCP pathway is associated with important events, including cilia formation and polarization.

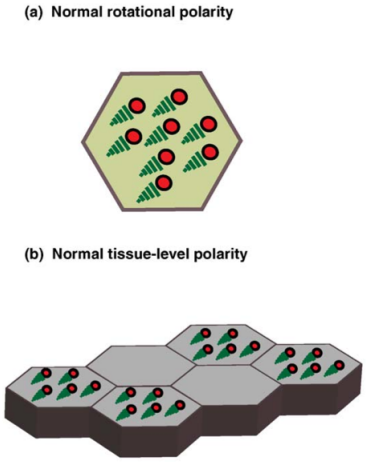

1.5: Modes of planar cell polarity in the *X. leavis* multiciliated skin. Basal bodies: red; ciliary rootlet: green. From Wallingford (2010).

2.3.3 Cilia in the pronephric kidney

Kidneys have various vital functions such as maintenance of homeostasis of water and ion balance by filtrating blood, reabsorbing useful molecules and excreting metabolic waste. Vertebrate kidneys develop within the intermediate mesoderm and can be divided into three sequential developing kidney forms: the pronephric, mesonephric and metaneprhric kidney (Vize, Seufert et al. 1997; Brandli 1999).

The three kidney forms are similar in their basic structure, but differ in the number of the nephrons. The mesonephric kidney is the adult form of amphibian and fish, while the metanephric kidney represents the functional form in other vertebrates. The metanephros is the most complex kidney form and can obtain one million nephrons. The mesonephros is less complex and has 10-50 nephrons (Vize, Seufert et al. 1997).

The pronephric kidney is the first and simplest kidney form, but already functional in early embryogenesis. The nephron is the basic functional unit of kidneys. In *Xenopus,* the pronephric kidney consists of one to three nephrons from the so-called nonintegrated type, where the glomerulus is not directly attached to the proximal tubule. Instead, wastes are filtered into the coelom as a cavity connecting glomerulus and tubules. Ciliated funnels called nephrostomes connect the coelom to the tubules and move filtrate from the coelom toward the tubules. There are normally three nephrostomes linking coelom and tubules (Fig. 1.6).

Multiciliated cells are present throughout the nephrostomes shown by markers for multiciliogenesis and immunostaining with acetylated α-tubulin (Vize, Seufert et al. 1997; Brandli 1999; Mobjerg, Larsen et al. 2000; Marcet, Chevalier et al. 2011; Stubbs, Vladar et al. 2012).

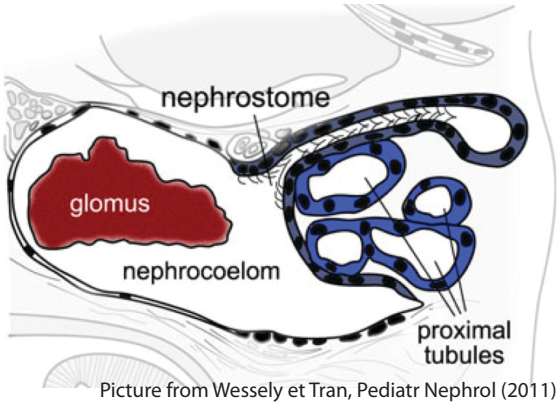

Fig. 1.6: Illustration of a sectioned amphibian pronephric kidney with ciliated nephrostome. From Wessely et Tran, Pediatr Nephrol (2011).

The Delta/Notch pathway is also important in the developing kidney, where it was shown to regulate pronephric cell fate specification (McLaughlin, Rones et al. 2000). Moreover, the Notch pathway plays an important role in the formation of multiciliated cells in the kidney. Previous studies in zebrafish have revealed that notch ligand Jagged2 is enriched in multiciliated cells (MCC) of the kidney. Jagged2 binds to notch3 receptor of neighboring cells and represses ciliogenesis via indirect downregulation of ciliogenic transcription factor *rfx2*. Blocking of Jagged2 leads to an increase in MCCs suggesting that notch signaling might regulate multiciliated cell specification via lateral inhibition in other tissues than epidermis (Liu, Pathak et al. 2007).

Studies by Kramer-Zucker et al. demonstrated in zebrafish that disruption of cilia motility affected fluid movement in the pronephros, thus leading to fluid accumulation and formation of tubular cysts (Kramer-Zucker, Olale et al. 2005).

2.4 Epigenetics and development

2.4.1 Epigenetics

Since its definition in 1942 by Conrad Waddington who called it “the branch of biology, which studies the causal interactions between genes and their products, which bring

the phenotype into being" (Waddington, 1942), the term "Epigenetics" has been revised several times. The Greek prefix "epi-" in "epigenetics" suggests features that are "on top of" genetics, indicating that epigenetic traits exist on top of the genetic basis for inheritance. Currently, epigenetics might be more specifically defined as "the study of any potentially stable and, ideally, heritable change in gene expression or cellular phenotype that occurs without change in Watson-Crick base-pairing of DNA" (Goldberg, Allis et al. 2007).

During development, it is essential that cells loose their pluripotent trait and become differentiated. Specified at just one time point, cells adopt different phenotypes and functions, although the genetic material of the cells stays the same (Li, Liu et al. 2012). Consequently, cell-lineage appropriate gene expression patterns have to be 'inherited'.
Analyses of the epigenetic landscape of pluripotent cells showed hyperdynamic genes and highly decondensed euchromatin, which is correlated with transcriptional active genes since DNA is accessible to the transcription complex. Differentiated cells however, need to establish and consolidate gene repression. This is, for example, achieved through condensation of chromatin (heterochromatin), resulting in less accessible DNA (Dambacher, Hahn et al. 2010; Tollervey and Lunyak 2012).
Epigenetic mechanisms are thought to modulate chromatin accessibility and therefore its transcriptional state. Five major mechanisms are known to alter chromatin structure: DNA methylation, posttranslational histone modification, non-coding RNA, as well as histone variants and chromatin remodeling (Dambacher, Hahn et al. 2010). Before going further into detail of epigenetic mechanisms, the basic of chromatin composition will be discussed in the next section.

2.4.2 Chromatin states

Chromatin consists of DNA wrapped around histones and can be classified in two major states: euchromatin and heterochromatin. Euchromatin is open chromatin that is accessible for the transcriptional machinery. Therefore, it marks regions of transcriptional active genes. Heterochromatin is the opposite; it is condensed and consequently less accessible. The repeating fundamental unit of DNA packaging is described as a nucleosome, consisting of a 147 bp long portion of superhelix DNA wrapped 1.65 turns around a histone

octamer. There are five types of histones: H1, H2A, H2B, H3 and H4. Two copies of each H2A, H2B, H3 and H4 form the histone core. The linker histone H1 binds the linker DNA, linking the core DNA between two neighboring nucleosomes, to the nucleosome core. Nucleosomes are stabilized by various interactions within the core octamer and electrostatic and hydrogen bonds between histones and the DNA. Each of the histones consists of a core domain and a flexible tail domain where most post-translational modifications (PTM) at amino-acid residues occur. The tails extend away from the core DNA and largely interact with adjacent nucleosomes or with nuclear factors (Luger, Dechassa et al. 2012; Tollervey and Lunyak 2012).

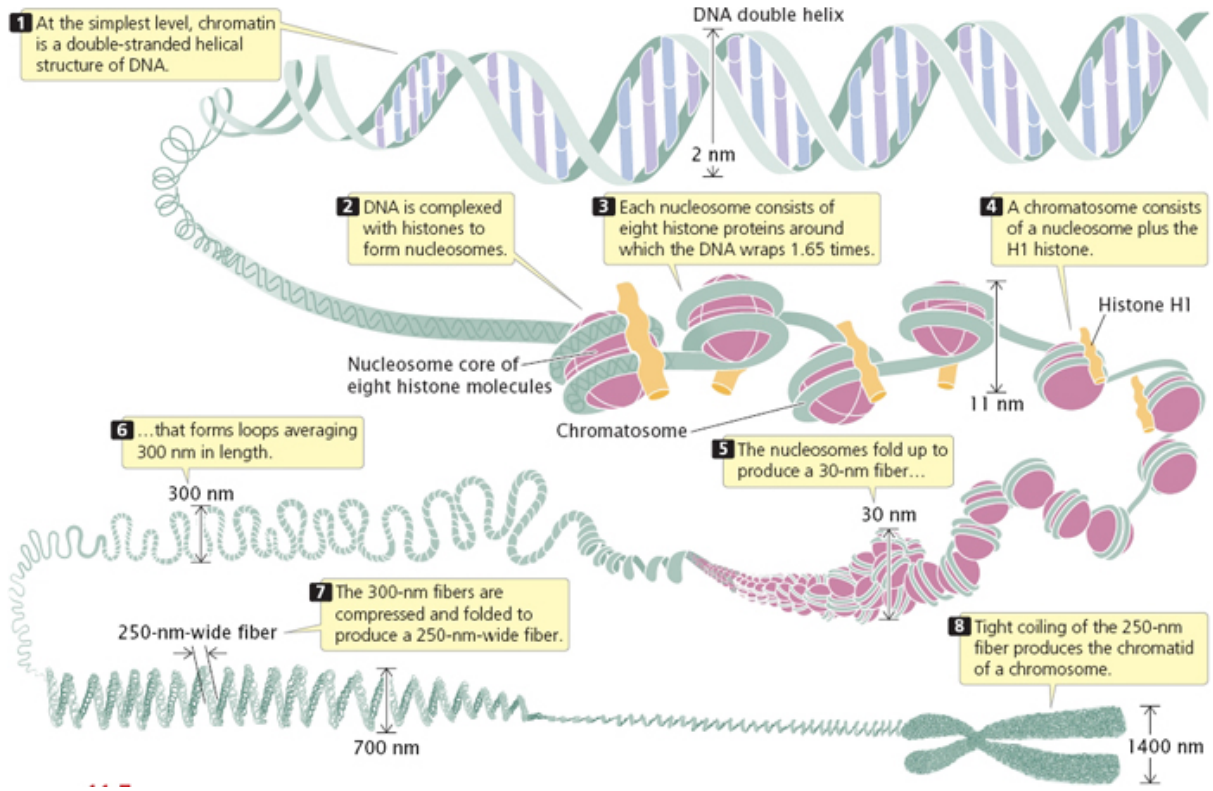

Fig. 1.6: Model of chromatin organizing
Chromatin is sequentially organized in 11nm beads-on-a string fiber (primary chromatin structure), 30nm fiber chromatin folding (secondary structure) and higher-order chromatin fiber (tertiary structure). From B. Pierce, Genetics: A Conceptual Approach, 4th edition (2011), 295.

Fig. 1.6 illustrates the basic features of chromatin organization. Although nucleosomes have been assumed to fold up into 30-nm chromatin fibers, their actual existence is controversial. Contemporary studies on human mitotic chromosomes detected no regular structures >11-nm and suggest that mitotic chromosomes rather contain irregularly folded nucleosome fibers (Hansen 2012; Nishino, Eltsov et al. 2012).

Recently, certain gene expression patterns have been associated with particular epigenetic modifications. Lightly packed euchromatin is transcriptionally active and shows several histone modifications, such as tri-methylated state of lysine residue in position 9 of histone H3 (=H3K4me3) and H3K9ac. These two modifications are related to an "open" state of chromatin, as observed in embryonic stem (ES) cells. In contrast, heterochromatin is densely packed and is enriched in H3K9me3, H3K27me3 and H4K20me3, which are associated with transcriptionally silent chromatin. Bivalent chromatin carries both activating H3K4me3 and repressive H3K27me3 lysine histone methylation marks at some promoters. It was thought that bivalent chromatin was characteristic for ES cells to poise key developmental genes during the pluripotent state, while to keep them available for lineage-specific activation. Nevertheless, the functions of bivalent chromatin domains remain to be further elucidated, since it also occurs in hematopoietic stem and progenitors cells, as well as in neural progenitors and terminal neurons (Mikkelsen, Ku et al. 2007; Dambacher, Hahn et al. 2010; Tollervey and Lunyak 2012).

2.4.3 Posttranslational histone modifications

The core histone proteins can be covalently modified at many sites and in many ways. Most covalent post-translational modifications target amino-acid residues near the N-termini of the core histones H3 and H4 (Fig. 1.7). Modifications include lysine and arginine methylation, lysine acetylation (Allfrey, Faulkner et al. 1964), serine, threonine and tyrosine phosphorylation and lysine ubiquitylation (Kouzarides 2007). The nomenclature of PTMs reflects the histone domain, the type and site of the modified residue and the type of modification (Turner 2005), for example, H4K20me3 would mean tri-methylation of lysine residue in position 20 of histone H4.

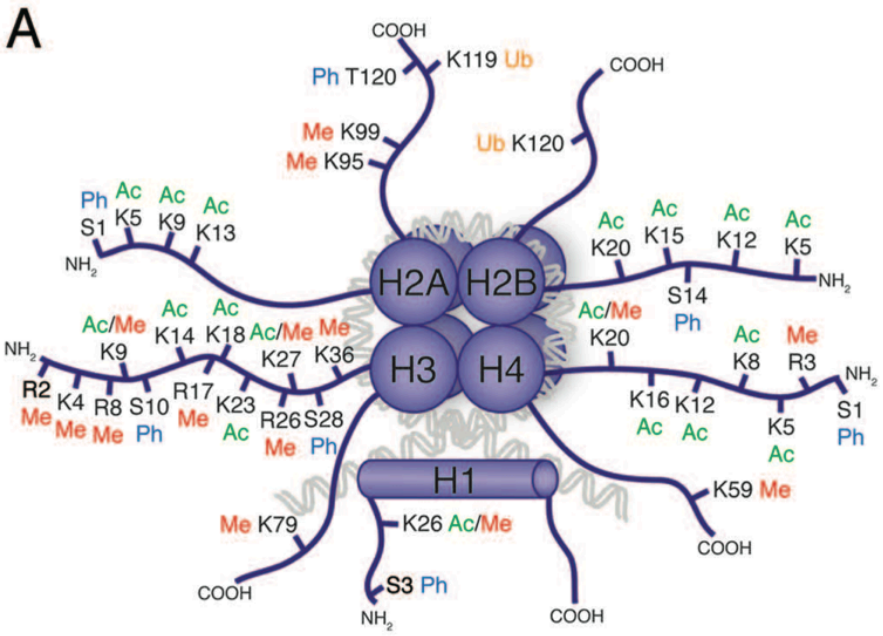

Fig. 1.7: Covalent post-translational histone modifications.
A model of a nucleosome is shown including core histones and unstructured histone tails. It is striking, that most modifications, such as acetylation (Ac), methylation (Me) and phosphorylation (Ph) occur in N-terminal tails, whereas ubiquitylation (Ub) appears in C-terminal tails of histone H2A and H2B. Note that some amino-acid residues can be both methylated and acetylated, e.g. H4K20. From Tollervey, J. R. and V. V. Lunyak, Epigenetics 7(8), (2012).

Histone modifications may affect higher-order chromatin organization with the different covalent post-translational histone modifications varying in their functions. Which mechanisms alter the chromatin structure? What are the mechanisms to elicit downstream biological outcomes?

Knowing that positively charged histone tails interact with the negatively charged DNA, it was first hypothesized, that modifications of amino acid residues would change charges of histones, resulting in stabilized or destabilized histone-histone and histone-DNA contacts. Additionally, the "histone code hypothesis", states that one or multiple histone marks in combination or in sequence can affect gene expression by recruiting other proteins that "read" the modified amino acid residues (Strahl and Allis 2000; Davey, Sargent et al. 2002; Kouzarides 2007). The enzymes binding to specific modifications are referred to as „readers", while "writers" (methyltransferase, acetyltransferase) catalyze the attachment of modifications to the amino acid residues, and "erasers" remove specific modifications (Gardner, Allis et al. 2011).

In summary, these three types of enzymes mediate histone modifications, which function can be divided into two main categories. Firstly, modifications help to establish global chromatin

environments by generating domains, which are accessible or inaccessible for transcription, e.g. euchromatin or heterochromatin. Furthermore, modifications coordinate the recruitment of enzyme complexes to manipulate DNA, thereby affecting biological processes (Kouzarides 2007). In the context of my thesis, the next section will focus on histone lysine methylation established by Suv4-20h enzymes.

2.4.4 Suv4-20h histone methyltransferases

Histone methyltransferases (HMTases) catalyze the transfer of one to three methyl groups to lysine or arginine residues of histones. Lysine can be mono- (me1), di- (me2) or tri-methylated (me3) by specific lysine methyltransferases (KMTs). In contrast, arginine can only be mono- or di-methylated by arginine methyltransferases (PRMTs). S-adenosyl-L-methionine (SAM) serves as the common methyl group donor (Zhang and Reinberg 2001). Lysine HMTases may or may not contain a SET-domain. The SET domain is an evolutionarily conserved sequence and its acronym refers to its common presence in the *Drosophila* **S**u(var)3-9, **E**nhancer of Zeste, and **T**rithorax proteins (Zhang and Reinberg 2001; Feng, Wang et al. 2002).

Histone lysine methylation can enable activation and repression of gene transcription. For instance, at active genes H3K4me3 is enriched at the promotor region and H3K36me3 is abundant at the gene body. In contrast, at inactive genes H3K27me3, H3K9me3 and H4K20me3 are enriched. H3K27 tri-methylation is mediated by polycomb-group proteins including Ezh1 (enhancer of zeste homolog1) and Ezh2, which form the polycomb repressive complex 2 (PCR2). H3K27me3 is often associated with gene silencing, while H3K9me3 and H4K20me3 mark repetitive genomic regions at telomeric and pericentromeric heterochromatin (Dambacher, Hahn et al. 2010).

Lysine methylation can occur at five different sites on histone H3, but only at K20 on H4. PR-Set7 catalyzes mono-methylation of H4K20, whereas Suvh4-20h1 and Suv4-20h2 enzymes catalyze di- and tri-methylation of H4K20. The Suv4-20h enzymes are termed according to their *Drosophila* homolog, which acts as **su**ppressor of position effect **v**ariegation (Rice, Nishioka et al. 2002; Jorgensen, Schotta et al. 2013).

According to Schotta et al. (2004), H4K20 methylation is evolutionary conserved from yeast to mammals and is "critically important for the biological processes that ensure genomic integrity, such as DNA damage repair, DNA replication and chromatin compaction" (Jorgensen, Schotta et al. 2013). Mono- and di-methylation of H4K20 are associated with DNA replication and DNA damage repair. H4K20 tri-methylation, however, is linked to heterochromatin formation. Heterochromatin regions contain both H4K20 and H3K9 tri-methylated states and both repressive methylation marks are established in a highly coordinated sequence. The Suv39h enzymes induce H3K9me3, which allows the HP1 proteins (heterochromatin protein 1α and β) to attach. HP1 proteins then recruit the Suv4-20h enzymes, which induce H4K20 tri-methylation (Schotta, Lachner et al. 2004; Jorgensen, Schotta et al. 2013).

In proliferating cells, the levels for H4K20 mono- and tri-metylation are very low, but H4K20me2 levels are high, indicating a cell-cycle dependent methylation of Histone H4. During S-phase, newly incorporated H4 histones lack all K20 methylation. Due to low expression levels of PR-Set7, very few H4K20me1 marks are added during this phase. With rising levels of PR-Set7 during G2 -phase, H4K20me1 levels reach a maximum before mitosis. In the following G1-phase, H4K20 mono-methyl marks are converted to the di- and tri-methylated state by Suv4-20h enzymes. H4K20me2/me3 levels peak during G1-phase, before the next S-phase dilutes again their concentration (Rice, Nishioka et al. 2002; Jorgensen, Schotta et al. 2013). This implies higher H4K20me2/me3 levels in resting or post-proliferative cells than in cycling cells.

Regarding their distribution, it is striking that H4K20me3 is enriched at pericentromeric and telomeric heterochromatin and imprinted regions, indicating a role in transcriptional silencing. H4K20me2 however is broadly localized, suggesting rather a connection with general chromatin-related processes. Murine double knockout studies *in vitro* and *in vivo* have revealed the essential role of Suv4-20h enzymes during development. Suv4-20h double null (dn) mouse embryonic fibroblasts (MEF) show a delayed S-phase entry, resulting in impaired cell cycle progression and proliferation (Schotta, Sengupta et al. 2008; Jorgensen, Schotta et al. 2013). Similarly, double knockdown of Suv4-20h in mice resulted in genomic instability. Theses mice had delayed growth, impaired lymphoid cell development, lung defects and died perinatally (Schotta, Sengupta et al. 2008). All in all, H4K20 methylation is very likely vital

for processes, such as DNA replication, DNA damage repair and chromatin compaction, to ensure genomic integrity.

Recently, novel analyses in *Xenopus leavis* demonstrated that Suv4-20h enzymes are crucial during non-mammalian embryogenesis as well. In order to differentiate, cells need to silence genes required for pluripotency and to activate lineage-appropriate genes. H4K20me3 levels increase during *Xenopus* embryogenesis (Schneider, Arteaga-Salas et al. 2011) and Suv4-20h1/h2 histone methyltransferases were revealed to have a key role in neuroectodermal differentiation by directly silencing Oct-25, a pluripotency-associated factor (Nicetto, Hahn et al. 2013). XOct-25 normally represses responses to BMP-signaling in ectodermal cells, thus promoting neural differentiation (Takebayashi-Suzuki, Arita et al. 2007). In Suv4-20h double morphants however, Oct-25 was transcriptionally derepressed during neurula stages. As a consequence, genes controlling neural induction and differentiation were specifically downregulated resulting in a block of neuroectoderm differentiation (Nicetto, Hahn et al. 2013).

To summarize, H4K20 methylation by Suv4-20h HMTases is conserved throughout vertebrates, from mammals to frogs. Suv4-20h-mediated H4K20 methylation is important for a normal development and the maintenance of genomic stability. Notably, impaired Suv4-20h expression reduces genomic stability and can result in severe dysfunction, such as growth retardation, neural defects, lung defects and perinatal lethality (Schotta, Sengupta et al. 2008). Suv4-20h histone methyltransferases catalyze the di- and tri-methyl states of lysine 20 on the histone H4 amino terminal tail, which is enriched in transcriptionally repressed heterochromatin. Our lab has recently observed that the relative abundance of the H4K20me3 mark increases in bulk histone during development, suggesting a gradual increase in repressive chromatin quality (Schneider, Arteaga-Salas et al. 2011). Further search for a developmental function for Suv4-20h enzyme production identified a pathway that operates in the neuroectoderm and controls the transition from pluripotent to neural cell states (Nicetto, Hahn et al. 2013). Despite this fact, little is known about the function of Suv4-20h HMTases in other developmental events.

2.5 Objectives

The objectives of the present thesis deal with a novel phenotype observed in Suv4-20h morphant embryos, which affects the process of ciliogenesis. It was previously observed (Nicetto 2012) that Suv4-20 morphants had less and shorter cilia in the *Xenopus* larval skin. In order to understand the connection between Suv4-20h enzymes and ciliogenesis, the presented work aimed to:

1. Establish molecular pathways that link Suv4-20h enzymes to cilia formation. Hereby, the Suv4-20h-mediated ciliary phenotype of the larval Xenopus skin shall be functionally characterized.
2. Study the influence of Suv4-20h enzymes in other multiciliated tissues such as in the forming pronephros.

3. MATERIALS AND METHODS

3.1 Research animals

Mature pigmented *Xenopus laevis* colonies were purchased from Nasco (USA) and Xenopus express (France). Generally, frogs were housed in tanks of still water with a depth of at least 20 cm at a temperature of 17-19°C and were fed three times a week with Pondsticks Premium brittle (Interquell GmbH, Wehringen). Female frogs had a resting period of at least 12 weeks between two HCG injections.

3.2 Technical equipment

Laboratory equipment is listed underneath in alphabetical order.

Equipment	**Supplier and model**
Centrifuges:	Eppendorf: 5417C Stratagene: PicoFuge® Microcentrifuge Thermo Scientific: Haraeus Multifuge 4KR Hettich Zentrifugen: Mikro 22 R
Electrophoresis:	GIBCO BRL: ST 305
Incubator: Waterbath Heatblock	 Dinkelberg: minitherm 2 MTH 232320 Techne: Dri-Block DB-2D
Micro-injection: Glass injection needles Injector Microneedle puller	 World Precision Instruments: Glass 1BBL W/FIL 1.0 mm Digitimer Ltd.: Pli-100 Sutter Instrument: P-87
Microscopes: Stereo microscope Fluorescence stereo microscope	 Zeiss: Stemi SV 6 Leica: M205 FA
Photometry: Spectrophotometer	 PeqLap: Nanodrop ND-1000
PCR:	

Thermocycler	Hybaid: PCR Express
Real-time PCR system	Roche: LightCycler® 480 II
RNA in situ hybridization	
Glass vials	Roland Vetter Laborbedarf OHG: KM-4514HD
Scanning electron microscopy:	
Scanning electron microscope	Jeol: JSM-35 GF
Critical point dryer	BAL-TEC: CPD 030
Sputter coater	Quorum Technologies: Polaron sputter coater

3.3 Reagents

3.3.1 Chemicals

Chemicals from Merck and Sigma were used, except for the following.

Agar, Ampicillin, Streptomycin:	Difco
Agarose, Chicken serum, Lamb serum:	Gibco/BRL
Human Chorionic Gonadotropin Gonasi 5000:	AMSA/ IBSA Lugano
Levamisole:	Vectro Laboratories

3.3.2 Enzymes

Alkaline phosphatase	Roche
BSA fraction V	Roth
Proteinase K	Sigma
Restriction enzymes	New England Bio Labs, Roche, Fermentas
RNase free DNase I	Promega
RNaseA	Sigma
RNasin	Promega
T3, T7, SP6 polymerases	Promega

3.3.3 Kits

DyNAmo cDNA Synthesis Kit	Biozym Scientific GmbH
Plasmid Midi Kit	Qiagen
RNase-Free DNase Set	Qiagen
RNeasy Mini Kit	Qiagen

3.4 Nucleic acids

3.4.1 Morpholino antisense oligonucleotides (MOs)

Control morpholino	5'-cctcttacctcagttacaatttata-3'
Xenopus Suv4-20h1 morpholino	5'-ggattcgcccaaccactt**cat**gcca-3'
Xenopus Suv4-20h2 morpholino	5'-ttgccgtcaaccgatttgaacc**cat**-3'

Xenopus laevis morpholino antisense oligonucleotides (MO) for loss-of-function studies were purchased from Gene Tools, LLC (http://www.gene-tools.com) and kept in aliquots at -20°C. Before usage, morpholino solutions were heated at 65°C for 5 minutes to completely denature secondary structures.

Morpholinos should be about 25 bases in length, with a GC content of 50%, and little or no secondary structure.Translation blocking oligonucleotides bind to the translation initiation complex and should therefore be complementary to the 5'-UTR or the first 25 bases 3' to the translation start site (Heasman 2002; Eisen and Smith 2008).

3.4.2 Oligonucleiotides for RT/qPCR

Primer	**Sequence**	**Manufacturer**
H4 for H4 rev	5'-gaccgcggtcacctacacc-3' 5'-ctggcgcttcagaacataca-3'	Biomers.net, http://www.biomers.net
ODC for ODC rev	5'-acaaagaaacccaaaccga-3' 5'-caaacaacatccagtctccaa-3'	Biomers.net, http://www.biomers.net
dnah9 for dnah9 rev	5'-ctggtgttcggttcacaatg-3' 5'-tccactatcccacgaacctc-3'	Metabion
foxj1 for	5'-atccttttgcagagcagagg-3'	Metabion, http://www.metabion.com

foxj1 rev	5'-tatttgctgcccgttagctc-3'	
foxj1 for foxj1 rev	5'-ccatgggaagagaacaggaa-3' 5'-cggaaatgcctcattgagat-3'	Sigma, http://www.sigmaaldrich.com

3.4.3 Plasmids

3.4.3.1 Plasmids for microinjections

Name	**Restriction enzyme**	**Polymerase**
pCMV-myc mouse *suv4-20h1* N264A, Y299A mutant	PvuI	SP6
pCMV-myc mouse *suv4-20h2* N182A, Y217A mutant	PvuI	SP6
pCS2-n-βGal	NotI	SP6

3.4.3.2 Plasmids for dig-labeled in situ hybridization probes

Name	**Source**	**Restriction enzyme**	**Polymerase**
α-tubulin	L. Kodjacachian, Marseille, France	NotI	T7
dnah9	A. Schweikert, Stuttgart, Germany	ApaI	SP6
foxj1	A. Schweikert, Stuttgart, Germany	HindIII	T7
pax2	T. Hollemann, Halle, Germany	EcoRI	T3
xlim-1	M. Taira, Tokyo, Japan	Xho1	T7
multicilin	C. Kintner, Salk Institute, USA	BamH1	T7

Eurofins MWG Operon (http://www.eurofinsgenomics.eu) did DNA sequencing.

3.5 Antibodies

3.5.1 Primary antibodies

Antibody	Source	Dilution
3G8 4A6	EA Jones, 1995, EXRC University of Portsmouth	ICC 1:50 ICC undiluted
Monoclonal Anti-acetylated α-tubulin	Sigma #T6793	ICC 1:200

3.5.2 Secondary antibodies

Antibody	Source	Dilution
Sheep anti-Digoxigenin Fab fragment conjugated with alkaline phosphatase	Roche #11093274910	In situ hybridization 1:2000
Anti rat-fluorescent antibody Cy3	Jackson Immuno Research #712165153	ICC 1:500
Sheep anti-mouse IgG conjugated with alkaline phosphatase	Chemicon AP303A	ICC 1:1000

3.6 Fertilization and micro-injections

3.6.1 Preparation of embryos

a) Inducing ovulation

On the afternoon prior to microinjection, ovulation was stimulated by injecting 0.25-0.35ml (500-700 units) of human chorionic gonadotropin (HCG) into the dorsal lymph sac of a female *Xenopus laevis*. A fine 27G Sterican needle was used to reduce injury. Kept at 20ºC, frogs started laying eggs 12-16 hours after injection of HCG.

b) Isolating testes

A male *Xenopus laevis* was anaesthetized in a solution of 0.1% 3-Aminobenzoeacid-ethyl-ester for at least 30 minutes and killed through cervical dislocation. Both testes were dissected from the abdominal cavity and immediately transferred into MBS/Chicken serum and preserved at 4°C for a maximum of 10 days.

c) In vitro fertilization and embryo culture

Fertilization was performed by incubation of eggs in 1xMBS with a small amount of crushed testis at room temperature. After 5 minutes, 0.1x MBS was added and fertilized eggs were cultivated in Petri dishes at 16-23°C until the desired stage for microinjections.

d) Removing the egg jelly coat

Before microinjection it is essential to remove the jelly coat, which is a thick protective membrane surrounding the embryos. Removal was achieved by bathing the embryos in a 2% cysteine solution in an Erlenmeyer flask one-hour post fertilization. Dejellying was optimal when eggs started to touch each other, indicating complete removal of the coat. Afterwards, embryos were rinsed three times with 0.1x MBS and cultured in a Petri plate with 0.1x MBS/ Gentamicin at 16-23°C depending on the anticipated growth velocity.

e) Calibrating needles

A glass injection needle (see list in 2.2) was pulled from a capillary with the Microneedle Puller using the settings given below:

Settings				
Microneedle Puller P-87	Heat: 800	Pull: 35	Vel: 140	Time: 139

Next, the needle was fixed in the holder of an injector (Digitimer Ltd.: Pli-100) for calibration and carefully cut with Dumont tweezers to a drop size of 5nl (injection pressure: 30 psi; injection time: 30ms-1s).

3.6.2 Micro-injection

Calibrated needles were filled with 1-2 µl injection solution, containing morpholino oligonucleotides (MO), RNA or both. *In vitro* transcription for sense mRNA was performed as described in 2.9.4.

Embryos were placed onto molded agar plates and injection was made into the animal hemisphere either into one cell at two-cell or into one ventral blastomere at 4-cell stage. For animal cap assay, embryos were injected into all four cells at 4-cell stage. The total amount of injected solution was 5-10nl per embryo. Next, embryos were incubated in 0.1x MBS/ Gentamicin in Petri dishes covered with 2% agarose gel at 23°C. Daily change of buffer provided the best environment for embryo cultivation.

For epidermal cilia phenotype, embryos were injected twice into one blastomere at two-cell stage with Suv4-20h1 or h2 MO (total amount: 40ng per blastomere). For pronephros cilia phenotype, embryos were injected with Suv4-20h1 or h2 MO (30g per one ventral blastomere at 4-cell stage; 40ng per blastomere at two-cell stage) and rescued with 1.5ng mouse Suv4-20h1 RNA. For animal cap assay, embryos were injected with Suv4-20h1 or –h1 and -h2 MO (40ng per embryo; for schemes see Fig. 4.8a). Control embryos were injected with the same total amount of control MO.

3.6.3 Solutions and buffers

Solutions for embryological methods			**Storage**
0.1xMBS/Gentamicin	0.1x 10µg/ml	MBS Gentamicin	RT
1x MBS (Modified Barth's Saline)	0.7mM 5mM 1mM 88mM 2.5mM 1mM	$CaCl_2$ HEPES KCl NaCl $NaHCO_3$ $MgSO_4$	Add $CaCl_2$ before use. pH 7.6 at RT
2% Cysteine solution	2% 0.1x 10M	L-Cysteine MBS NaOH	Sigma pH 7.84 at RT
Agarose gel	0.1x 2%	MBS Agarose	
Anesthetization solution for frogs	0.1%	3-Aminobenzoeacid-ethyl-ester Iced ddH_2O	Freshly made before use;

			powder was kept at -20°C
Human Chorionic Gonadotropin (HCG)	5000 UI/ml	Gonasi HP ddH_2O	AMSA/IBSA Lugano
Testis storage solution	0.8x 20% 200U/ml 200µg/ml	MBS high salt chicken serum Penicillin Streptomycin	Stored at -20°C
MEMFA	0,1M 2mM 1mM 3.7%	MOPS (3-(N-Morpholino)-propanesulfonic acid) EGTA $MgSO4_4$ Formaldehyde	pH 7.4 at RT, freshly made before use

3.7 Micro-dissection

3.7.1 Animal cap explants

Prior to germ layer formation, micro-dissections were carried out from NF 8 to 9 using two sharp Dumont forceps (Switzerland). Embryos were staged according to Nieuwkoop and Faber (Nieuwkoop and Faber 1994). By cutting the pigmented blastocoel roof (animal cap) from the animal hemisphere, we obtained explants derived purely from ectodermal cell populations. Although destined to become epidermis and neuroectoderm *in vivo*, isolated animal cap tissue forms atypical epidermis. This is due to lack of signals promoting neuroectoderm, endoderm and mesoderm induction, such as BMP, FGF and TGF-β (Dale, Matthews et al. 1993; Zhang, Houston et al. 1998; Munoz-Sanjuan and H. Brivanlou 2001).
Embryos were placed in 60mm Petri plates covered with 2% agarose in Ca^2+-enriched solution (0.5x MBS) to avoid dissociation of the tissue. Removal of the vitelline membrane is required before cells and tissues can be dissected. This is achieved by grabbing the vitelline membrane with one pair of forceps in the equatorial region, grasping the membrane with a second pair of forceps and tearing the membrane off. After dissection, caps were transferred to a molded agarose plate. They were cultured in 0.5x MBS until NF 25 and stored in liquid

nitrogen (Results, Fig. 4.8a). To determine the required stage, control whole mount siblings were grown simultaneously.

3.7.2 Dorsal explants

In order to examine the effects of Su(var)4-20 enzymes on monocilium and organ laterality, gastrocoel roof plate explants (GRP/dorsal explants) were created. According to Vick et al. (2009), NF 17 to 18 embryos were collected after they had been injected with 40ng Suv4-20 h1 or control morpholino into both blastomeres at 2-cell stage. After transferring embryos to 0.5xMBS in Petri dishes covered with 2% agarose, the vitelline membrane was removed at the beginning. Disconnected by four cuts with two sharp Dumont forceps (Switzerland), explants for histological tests were immediately moved into MEMFA solution and fixed for one hour at RT. Next, the explants were rinsed twice in 1xPBS for 5 min each and dehydration was performed with 100% Methanol at -20°C over night. For Scanning electron microscopy studies, GRP explants were fixed with 3% Glutaraldehyde for one hour at RT.

3.7.3 Solutions and buffers

			Storage
0.5xMBS	0.5x	MBS	RT
1x MBS (Modified Barth's Saline)	0.7mM 5mM 1mM 88mM 2.5mM 1mM	$CaCl_2$ HEPES KCl NaCl $NaHCO_3$ $MgSO_4$	Add $CaCl_2$ before use. pH 7.6 at RT
2% Cysteine solution	2% 0.1x 10M	L-Cysteine MBS NaOH	Sigma pH 7.8 at RT

3.8 Histological methods

3.8.1 X-Gal staining

Embryos were first fixed in MEMFA for 30 minutes and rinsed with 1xPBS for at least 1 hour. Staining was performed with freshly made X-Gal staining solution and embryos were kept in the dark at RT until the desired blue color was achieved. The amount of time needed for staining was around 15-30 minutes and depended on the amount of β-galactosidase activity in the embryos. To stop the reaction, embryos were rinsed with PBS for 30 minutes, re-fixed with MEMFA for another 30 minutes and washed in PBS three times for 10 minutes each. Last, embryos were stored in 100% ethanol either at RT for 1 hour or at -20°C over night.

3.8.2 Immunocytochemistry (ICC)

Whole mount embryos were fixed in MEMFA for 1-2h at room temperature on a rotating wheel, explants were fixed for 30 minutes. After rinsing with PBS, the embryos were dehydrated in 100% methanol and incubated at -20°C for at least over night. Rehydration in 75%, 50%, 25% methanol in PBSw was performed for 5 min each, followed by a PBT wash for 15 min. To block unspecific antibody binding sites, embryos were incubated in PBT plus 10% heat inactivated goat serum for 1 hour at RT.

After removal of the blocking solution, the primary antibody was added and embryos were incubated in 300µl solution over night at 4°C or 2 hour at RT. Afterwards the embryos were washed 5-6 times in PBT for one hour each at RT. Secondary anti- mouse or anti-rabbit antibodies conjugated to alkaline phosphatase were used in 1:1000 dilution and incubated over night at 4°C. Embryos were rinsed the next morning in PBT six times for one hour each. Prior to staining, endogenous alkaline phosphatases were blocked by adding Levamisole to the AP buffer and incubating for 2x30 min. Staining was conducted in 1ml BCIP/NBT (biomol) staining solution in the dark for 20 to 30 min at RT. Reaction was stopped by rinsing the embryos in PBS and fixating in MEMFA over night. Staining was clearly visible after bleaching ectodermal pigments for 2-4 hours at RT on a light box.

3.8.3 Solutions and buffers

Solutions for Immunocytochemistry			Storage
Alkaline Phosphatase (AP) buffer	100mM 50mM 100mM 0.1% 5mM	Tris/HCl (pH 9.5) $MgCl_2$ NaCl Tween 20 Levamisole	Freshly made before use
AP staining solution	4.5µl 3.5µl 1ml	NBT (Nitro blue tetrazolium) 75mg/ml in 70% dimethylformamide BCIP (5-bromo-4-chloro-3-indolyl-phosphate) 50mg/ml in 100% dimethylformamide AP buffer	Kept at -20°C Kept at -20°C
Bleaching solution	1% 5% 0.5x	H_2O_2 Formamide SSC H_2O_{dest}	Freshly made before use
Blocking buffer	1x 10%	PBT heat inactivated serum	
Lamb Serum		heat-inactivated lamb serum (30 min at 56°C)	Stored at -20°C
MEMFA	0,1M 2mM 1mM 3.7%	MOPS (3-(N-Morpholino)-propanesulfonic acid) EGTA $MgSO_4$ Formaldehyde	pH 7.4 at RT, freshly made before use
PBS	103mM 2.7mM 1.7mM 0.7mM	NaCl KCL KH_2PO_4 Na_2HPO_4	pH 7.2 at RT
PBSw	1x 0.1%	PBS Tween 20	

PBT	1x 2mg/ml 0.1%	PBS BSA Triton-X-100	
X-Gal staining solution	0,25M 0,25M 25µl/ml 1M	$K_3Fe(CN)_6$ K4Fe(CN)6 Xgal (40mg/ml) 2µl/ml MgCl2 in 1x PBS	

3.9 RNA *in situ* hybridization

3.9.1 Bacterial transformation

Transformation was performed according to standard protocols (Sambrook et al., 1989) using XL1 Blue E. coli strains.

XL1 Blue	recA1 endA1 gyrA96 thi-1 hsdR17 supE44 relA1lac [FcproABlacIqZDM15 Tn10 (Tetr)]	Stratagene

Plasmid DNA was purified with Plasmid Midi Kit (Qiagen) according to the manufacturer's protocol.

DNA and *in vitro* synthesized RNA respectively were analyzed by agarose gel electrophoresis. Each sample was mixed with a loading dye and pipetted to a well in a 1% TBE agarose gel containing ethidium bromide. DNA ladders of 1kb or 100bp were used as size standard. Electrophoresis gels were recorded with the Gel documentation System G:BOX (Syngene).

3.9.2 *In vitro* transcription of digoxigenin-labeled antisense RNA probes

Linearization

To allow run-off transcription, plasmid templates were linearized with the following set up:

10µg	DNA template
4µl	Buffer B (Roche, Mannheim, Germany)
3µl	Restriction enzyme
Add to 40µl	DEPC H_2O

Reactions were conducted for two hours in an incubator at 37°C. Complete linearization was controlled by 1% TBE agarose gel electrophoresis as described above. Linearized plasmids were stored in aliquots at -20°C.

In vitro transcription

The following transcription reactions were set up to generate antisense RNA:

2µg	Linearized plasmid
10µl	5x Transcription buffer
5µl	10mM Dig-NTPs mix
5µl	100mM DTT
0.5µl	40U/µl RNasin
2µl	RNA-Polymerase
Add to 50µl	DEPC H_2O

The reactions were carried out for two hours at 37°C. After that another µl of RNA-Polymerase was mixed to the set up mixture. Next, reactions were incubated over night at 37°C, after which 1µl of DNase was added and incubated for 30 min at 37°C.
According to the RNeasy Mini Kit (Qiagen) manufacturer's protocol, the dig-labeled RNA probes were separated from unincorporated mononucleotides and stored in 50% formamide at -20°C.

3.9.3 *In vitro* transcription of messenger RNA for microinjections

The following transcription reactions were set up to generate capped sense mRNA for microinjections:

2µg	Linearized plasmid
10µl	5x Transcription buffer
5µl	25mM G(5´)pppGcap analog
10µl	10mM NTPs mix
5µl	100mM DTT
0.5µl	40U/µl RNasin
Add to 50µl	DEPC H_2O
2µl	RNA polymerase

The reactions were carried out for two hours at 37°C. Another µl of RNA-Polymerase was mixed to the set up and reactions were incubated for another two hours at 37°C. Finally the mRNA probes were cleaned up according to the Qiagen RNeasy Mini Kit manufacturer's protocol and messenger RNA quality was tested by gel electrophoresis. Aliquots were stored at -80°C.

3.9.4 RNA in situ hybridization (ISH)

Whole mount embryos for ISH were collected in 5ml screw-cap storage vials and fixed in freshly made MEMFA for 1.5-2h (30 min for animal caps) at RT on a rotating wheel. Prior to fixation, the vitelline membrane had been removed manually. MEMFA was removed by washing 3 x 5 min in 1x PBS, followed by a quick rinse with 100% ethanol and dehydration with fresh ethanol at least over night at -20°C to support probe penetration.

In situ hybridization was performed according to the protocols by (Sive, Grainger et al. 2000) with minor modifications:
First, samples were removed from storage and rehydrated stepwise to 75%, 50%, 25% ethanol by adding 1x PBSw, followed by 3 x 5min washes in 1x PBSw. To increase dig-labeled probe staining, the embryos were permeabilized by incubating in 10µg/ml Proteinase K for 15min (5min for explants) at RT. Because of Proteinase K usage, embryos need to be refixed in PBSw containing 4% paraformaldehyde for 20 min. Next, embryos were washed 5 x 5min in PBSw at RT. PBSw was exchanged with 50% hybridization solution in the first wash and with 100% hybridization solution in the second wash, each step taking 3 min at RT. The

entire buffer was removed and 0.5ml of fresh hybridization solution was added per vial. Thereafter, samples were incubated in a water-bath and kept for one hour at 65°C to inactivate endogenous phosphatases. Subsequently, prehybridization followed for about 6h at 60°C to reduce nonspecific sticking of probes. 30-50ng of digoxigenin-labeled RNA probe was mixed with 100µl of hybridization solution, heated at 90°C for 5min and added to the prehybridization solution. Hybridization was performed over night at 60°C in a water bath.
Next, non-hybridized probes were removed in several 20x SSC washes. The first steps occurred at 60°C: embryos were rinsed for 10 min in fresh hybridization solution and then washed 3 x 20 min in 2x SSC buffer, embryos were then washed 2 x 30min in 0.2X SSC, followed by one 10min wash in MAB solution at RT. The solution was replaced with 1ml of MAB containing 2% BMB blocking solution (Boehringher Mannheim) and vials were placed vertically on a rocking table for one hour at RT. Afterwards the solution was replaced with fresh MAB containing 2% BMB blocking solution and a 1/2000 dilution of the anti-digoxigenin antibody coupled to alkaline phosphatase. Samples were agitated vertically for 4h at RT. Excess antibodies were removed by rinsing the samples in MAB and replacing with fresh MAB over night at 4°C. Washes in MAB were continued 5 x 1 hour the next day. For the chromogenic reaction, embryos were incubated in alkaline phosphatase buffer 2 x 5 min at RT and replaced with 0.5ml freshly prepared staining solution. Samples were kept in the dark and staining was quickly stopped by 2 x 10 min washes in 1X PBS at RT, once staining reached deep saturation. If overnight staining was required, samples were placed at 4°C. After fixation in MEMFA for at least 1.5 hour at RT on a rotator embryos were then washed 3 x 20 min in 1X PBS containing 75% ethanol to prepare samples for bleaching. To better visualize in particular weak expression signals, epidermal and melanocyte-derived pigment granules were dissolved by performing a bleaching reaction for 2-4 hours at RT on a light box.

3.9.5 Solutions and buffers

Solutions for RNA In situ hybridization			**Storage**
Hybridization Solution	5X 50% 1% 0.1% 0.01%	SSC Formamide Boeheringer blocking solution Torula RNA Heparin	-20°C

	0.1% 0.1% 5mM	Tween-20 CHAPS EDTA	
1% TBE agarose gel	50ml 1x 1% 5µl	TBE buffer (Tris/Borate/EDTA) Agarose Ethidium bromide	
MAB (Maleic Acid Buffer), pH 7.5	100mM 150mM	maleic acid NaCl	
MEMFA	0,1M 2mM 1mM 3.7%	MOPS (3-(N-Morpholino)-propanesulfonic acid) EGTA $MgSO_4$ Formaldehyde	pH 7.4 at RT, freshly made before use
Paraformaldehyde	4%	Paraformaldehyde in PBSw	
PBS	103mM 2.7mM 1.7mM 0.7mM	NaCl KCL KH_2PO_4 Na_2HPO_4	pH 7.2 at RT
PBSw	1x 0.1%	PBS Tween 20	
Proteinase K	10µg/ml	Proteinase K in PBSw	
SSC 20x	3M 0.3M	NaCl sodium citrate	pH 7.0 at RT

3.10 Real time polymerase chain reaction

3.10.1 RNA purification from Xenopus leavis explants

10-15 animal cap explants were harvested at NF 25 in 1.5ml Eppendorf tubes and directly processed, or frozen in liquid nitrogen and kept in the -80°C freezer. RNA purification was conducted using the RNeasy Mini Kit (Qiagen) in line with the manufacturer's protocol, including the on-column DNA digestion using the RNase-Free

DNase Set. RNA concentration was determined photometrically using the nanodrop ND-1000 (PeqLab). Finally samples were stored in aliquots of 5-10µl at -80°C.

3.10.2 Reverse transcription for RT/qPCR

After RNA purification, reverse transcription was carried out according to the DyNAmo cDNA Synthesis Kit protocol (Biozym).

3.10.3 Quantitative real-time PCR (RT/qPCR)

The following set up was prepared:

1µl	cDNA template
5µl	SYBR Green Master Mix
1µl	3,0µM primer for and rev
3µl	H_2O

PCR was performed using a LightCycler® Multiwell plate 384, white from Roche. Each sample was amplified in triplicates. The plate was sealed with a foil and centrifuged at 3000rpm for 1 min to eliminate bubbles in the reactions.

After the run, results were analyzed using the $2^{-\Delta\Delta}C_T$ method according to Livak and Schmittgen, 2001. To diminish inhomogeneity in RNA quality and amount, C_t (cycle threshold) levels of target genes were normalized to the two housekeeping genes ODC and H4. Next, mRNA amounts in control MO injected ACs were set as one. Further, a ratio of mRNA levels in Suv4-20h MO injected and Co MO injected ACs was calculated.
Settings for reactions were as following:

Steps	Cycles	Temperature in °C	Time in sec
1. Denaturation	1	95	60
2. Amplification	45	95	10
		60	20
		72	10
3. Melting	1	95	5
		65	60
4. Cooling	1	40	30

3.11 Scanning electron microscopy (SEM)

3.11.1 Preparation of explants

All gastrocoel roofplate explants (GRP) were dissected at NF 17 to 18 and transferred to 3% Glutaraldehyde fixation solution as soon as possible to avoid rolling up of the explants. GRPs were fixed in glass vials at RT for one hour, while gently moved on a rotator. To obtain clean explants for good SEM pictures, it was important to thoroughly and carefully free the GRPs from cell debris by washing with 1xPBS several times, at least 3x20 min. At the end samples were immediately delivered to the Institute for Anatomy, University of Munich, for further treatment according to their protocol. This included secondary fixation in Osmium tetroxide, 1% OsO_4 and a stepwise dehydration in 30%, 50%, 70%, 90%, 96% and 100% ethanol for 3 x 5-15 min each step. Samples were then completely dehydrated by removing liquid with the critical point drying method. All samples were attached on a specimen stub and sputter-coated with gold to confer electrical conductivity to the specimen that is required for SEM.

3.11.2 SEM

The scanning electron microscope images were kindly taken by Mrs. Beate Aschauer (Laboratory of Professor Ulrich Welsch, Institute of Anatomy, Medical Faculty, LMU, Munich) using the Jeol: JSM-35 GF scanning electron microscope.

3.11.3 Solutions and buffers

Solutions for Scanning electron microscopy			
3% Glutaraldehyde solution	25% 0.1M	Glutaraldehyde, 4°C Sorensen's Phosphate buffer	
Sorensen's Phosphate buffer	0.1M 0.1M	KH_2PO_4 Na_2HPO_4 x 2 H_2O	pH 7.4

3.12 LNA *in situ* hybridisation

3.12.1 Preparations

Embryos for LNA *in situ* hybridization were injected at two-cell stage into one animal blastomere. 30-40ng morpholino or 1.5ng of Suv4-20h1 mRNA were injected together with Alexa 488 as lineage tracer and tested for microRNA miR-449 expression. Wild type, control MO, Suv4-20h1 MO, Suv4-20h2 MO and Suv4-20h1 MO+Suv4-20h1 mRNA injected embryos were studied at the following stages: NF 25 and NF 32-35. To analyze epidermal multiciliated cells, NF 25 embryos were collected, which gave a robust expression in the epidermis. In the pronephros, strong signals were observed from NF 32 onward hence NF 32-35 embryos were used to investigate miR-449 pronephric expression,. Fixation of embryos was performed in 4% PFA over night at 4°C. Next, samples were washed 2x10 minutes in PBS kept in 100% methanol at -20°C. Penetrance of acetylated α-tubulin and Dnah9 depletion in immunostainings were used to assess ciliogenic phenotypes. Only batches with highly depleted epidermal cilia were used for LNA *in situ* tests.

LNA *in situ* hybridization experiments were kindly performed by Mrs. Virginie Thomé (Laboratory of Dr. Laurent Kodjabachian, Institut de Biologie du Développement de Marseille-Luminy, France).

3.12.2 Solutions and buffers

Solutions for LNA In situ hybridization			**Storage**
4%	4%	PFA	pH 7.4, stored at
Paraformaldehyde	1x	PBS	-20°C

3.13 Video-tracking

For fluid flow analysis on the larval epidermis, NF 33/34 Suv4-20h1 morphant and control morphant embryos were anaesthetized with Tricaine in petri dishes covered with agarose. A microinjection needle was filled with a red dye (Phenol Red, Sigma-Aldrich), which we used to visualize the fluid flow. As embryos rest on their sides, the fluid flow of either side was tested individually. The tip of the needle was placed near to the embryo's skin surface and the dye was released in a pulsed manner. It was made sure to eliminate factors

that could disturb the fluid flow, e.g. ventilation by air condition and unidirectional injection. The fluid flow was recorded using the Leica Application Suite V3 3.0.

3.14 Statistical tests

A two-tailed Fischer's exact test was performed to analyse the significance of morphological and molecular phenotypes. Quantitative real-time PCR studies were validated by two-tailed Student's t-test.

4. RESULTS

4.1 Morpholino induced analysis of Suv4-20h enzymes in *Xenopus leavis* epidermal multiciliogenesis

An increasing number of studies have pointed out the importance of cilia in signaling processes, early embryonic development, as well as pathological conditions of the respiratory tract, kidneys and carcinogenesis (Fliegauf, Benzing et al. 2007). In order to treat such diseases it is essential to learn as much as possible about the development of the affected organ. The embryonic epidermis of *Xenopus laevis* has become a highly suited model to study cilia development as well as mucociliary epithelia and mucociliary diseases. The larval skin is quite similar to the human respiratory epithelium. Among other cell types, mucus-secreting goblet and mucus clearing multiciliated cells (MCC) are pivotal for a proper functioning of the epithelium (Billett and Gould 1971; Morrisey and Hogan 2010; Dubaissi and Papalopulu 2011). Additionally, genes and molecular mechanisms required for ciliogenesis are similar in *Xenopus* and human showing that this relatively simple model can translate to human development. Furthermore, *Xenopus laevis* has many assets, which have established it as a favored model for research on mucociliary epithelium and cilia development. *Xenopus* grows quickly, a great variety of molecular tools can be used for analysis and due to its external location, the embryonic skin is easier to access for treatments and analysis compared to mammal respiratory epithelia (Werner and Mitchell 2012).

Our laboratory has been studying the effects of the di- and tri-methylation catalyzing Suv4-20h1 and -h2 histone methyltransferases in the early development of *X. laevis*. Nicetto (2012) discovered that Suv4-20h1/h2 enzymes were required for formation of the neuroectoderm and the expression of neuronal markers Delta-like 1, Neurogenin and N-tubulin. Intriguingly, RNA *in situ* hybridization analysis showed that while Delta-like1 was downregulated in the neurogenic stripes of the forming brain, expression levels were upregulated in the skin of Suv4-20h double morphants (Nicetto 2012).

The expression of non-neuroectodermal Delta-like 1 is associated to cilia formation in the frog larval skin (Deblandre, Wettstein et al. 1999) and further investigations in Suv4-20h double morphants revealed that the expression of the axonemal marker acetylated α-tubulin was reduced. Moreover, confocal analysis showed shorter and less cilia per ciliated cell in the epidermis. Co-injection of xSuv4-20h1/2 morpholinos and murine Suv4-20h1/h2 mRNA was

able to restore both Delta-like 1 and acetylated α-tubulin expression in the epidermis. These results led to the asumption that Suv4-20h enzymes-mediated H4K20 di- and tri-methylation was required for ciliogenesis (Nicetto 2012). The genetic background in cilia formation has been characterized in depth, however there is little knowledge about epigenetic regulatory mechanisms of cilia development, leading us to characterize the functions of the Suv4-20h enzymes in the formation of these vital cell organelles.

For the following studies, "loss-of-function" experiments were performed in order to analyze Suv4-20h HMT function in ciliogenesis. Therefore, anti-sense morpholino oligonucleotide assays were used (Materials and Methods, 3.5.1) to inhibit endogenous Suv4-20h protein synthesis (Fig. 4.1b). Morpholino oligonucleotides (MO) are currently the leading tools to achieve protein knockdown in *Xenopus laevis*. Some of the advantages to other gene knockdown approaches, e.g. S-DNA and siRNA, include high sequence specificity, low off-target effects and high affinity to RNA (Summerton 2007). Suv4-20h MOs (Fig. 4.1c) were designed by Gene Tools and tested for specificity before use. Suv4-20h MO specific translation blocking of the targeted template has previously been proven by *in vitro* TNT assay. Additionally, western blot analysis significantly showed that Suv4-20h1/h2 depletion causes a decrease of H4K20me2 and H4K20me3 marks, whereas H4K20me1 increased. Suv4-20h enzyme data from preliminary work was achieved by double protein knockdown with 60ng of each Suv4-20h1 and Suv4-20h2 morpholino (Nicetto 2012).

In my experiments, 30-50ng of Suv4-20h1 morpholino was injected. These concentrations achieved a ciliary phenotype with comparable strength and penetrance to the Suv4-20h double morphants. Furthermore, Suv4-20h1 and Suv4-20h2 morpholino injection generated the same phenotype. Nonetheless, the phenotype was stronger and occurred with higher penetrance in Suv4-20h1 morphants than in Suv4-20h2 morphants at older stages (own data and personal correspondence). These observations supported the results of Nicetto et al., according to which the temporal expression patterns of the two Suv4-20h enzymes are opposing. While Suv4-20h1 mRNA levels increase, Suv4-20h2 levels decrease from midgastrula onwards (Nicetto, Hahn et al. 2013). Reviewing the molecular and phenotypic findings suggested that Suv4-20h1 enzyme was more important than Suv4-20h2 in later stages of embryogenesis. Thus, subsequent analyses were mainly performed by Suv4-20h1 protein knockdown.
Experiments were conducted according to the following principles. Embryos from outbred *Xenopus* adults were used to obtain individual microinjected cohorts. Basically, Suv4-20h1 or

-h2 depleted morphant cohorts were compared to control embryo cohorts, which served as an external control for microinjection and subsequent statistical analysis of penetrance. Control cohorts were uninjected wild type embryos or control morpholino injected embryos. Additonally, the injected versus the uninjected side of each embryo was compared within a morphant cohort (internal control). This method enabled to minimize the non-specific developmental differences that occur in cohorts injected with different morpholinos. The internal control was established by the mode of microinjection itself. Morphant embryos were usually generated by unilateral microinjection of morpholino (Fig. 4.1a). Thereby, Suv4-20h1, -h2 or control morpholino was injected twice into the animal pole of one blastomere at two-cell stage (NF 2). To assess the injected side, a lineage tracer such as lacZ RNA or fluorescent Alexa Fluor-488 was co-injected. In this way, all specimens were completely uninjected on the one side and morpholino-injected on the other side. Noteworthy, injection of control MO produced phenotypes comparable to that of wild type embryos and uninjected side of morphants.

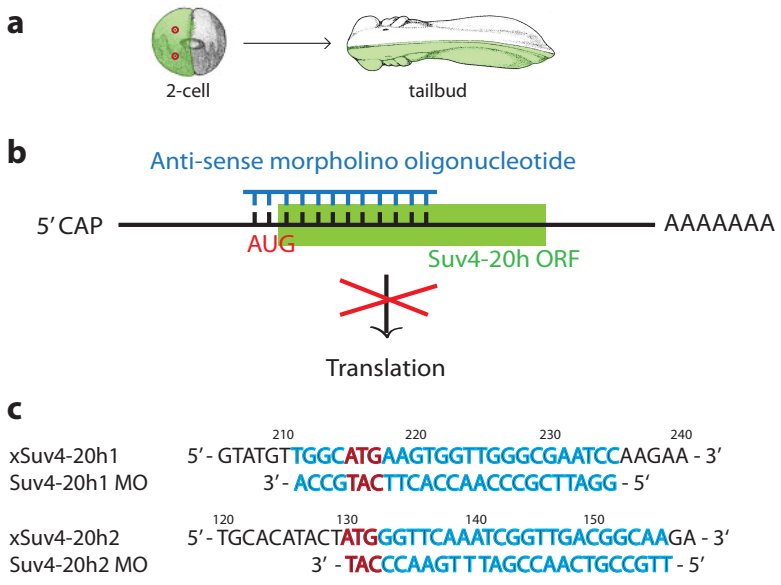

Fig. 4.1: Morpholino oligonucleotides
a) Unilateral injection mode. **b)** Protein knockdown by translation blocking morpholinos. MO binds to the complementary region of the target mRNA and inhibits progression of the initiation complex (Eisen and Smith 2008). **c)** From top to bottom: sequence of xSuv4-20h1 target region (NM_001092308) and Suv4-20h1 MO. Sequence of xSuv4-20h2 mRNA (NM_001097050) and Suv4-20h2 MO and Suv4-20h target region. The region of morpholino base pairing is displayed in blue; the start codon is labeled in red.

4.1.1 Abrogation of Suv4-20 h1 HMT reduces expression of acetylated α-tubulin

Acetylation of α-tubulin is correlated with stabilized microtubules, for example those located in ciliary axonemes and neuronal processes. On the surface of the embryo, acetylated α-tubulin is found in the apical cilia tufts of MCCs (Chu and Klymkowsky 1989). In the following analyses, the cilia tufts were visualized by whole mount ICC using anti-acetylated α-tubulin antibody to elucidate the ciliary phenotype in control cohorts and morphants.
Figure 4.2 shows acetylated α-tubulin expression of a wild type embryo via immunocytochemistry. Cilia tufts were normally arranged in dorso-ventral stripes consisting of single multiciliated cells with gaps between the MCCs (Fig. 4.2).

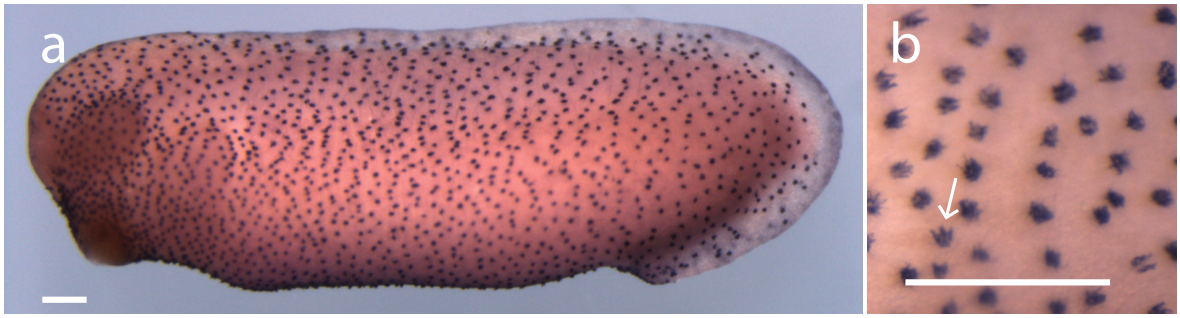

Fig. 4.2: Acetylated α-tubulin marks ciliary axonemes. a: Whole-mount immunocytochemistry of a NF 27 WT embryo with acetylated α-tubulin expressed in evenly scattered multiciliated cells in the epidermis; alkaline phosphatase (ap)-staining. **b**: high magnification image of cilia tufts (arrow). Scale bars: 200 µm.

To investigate the Suv4-20h1-related cilia changes, I analyzed the expression of acetylated α-tubulin in wild type, control MO injected and Suv4-20h1 MO injected cohorts. Images in Fig. 4.3 and 4.4 were achieved using fluorescent whole mount ICC with anti-acetylated α-tubulin antibodies. Morphants were generated by microinjection of 40ng *Xenopus* Suv4-20h1 morpholino with fluorescent Alexa Fluor-488 and the same amount of a standard control morpholino plus Alexa respectively. As ciliated cells are fully differentiated by NF 23 (Deblandre, Wettstein et al. 1999), acetylated α-tubulin expression was studied from NF 25 onwards. Therefore, embryos were staged according to Nieuwkoop and Faber (Nieuwkoop and Faber 1994) and divided into groups of left side and right side injected embryos before fixation. Fig. 4.3 shows an image taken from a representative wild type sample after immunostaining. The “speckled” red fluorescent signal indicated expression of acetylated α-

tubulin and each bright red spot represents hundreds of cilia in the apical surface of a multiciliated cell. Ciliary tufts are displayed via scanning electron microscopy (Fig. 4.3b).

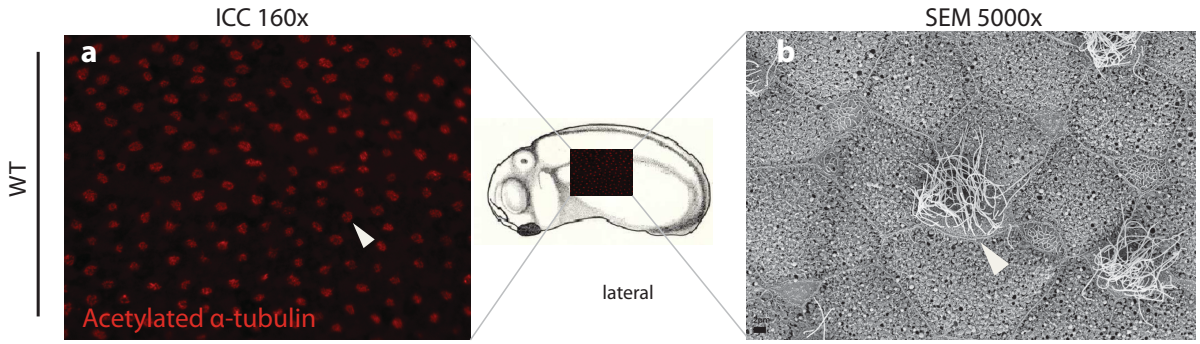

Fig. 4.3: Immunohistochemistry with anti-acetylated α-tubulin antibodies showing a salt-and-pepper pattern of NF 25 Xenopus epidermis. a: lateral view of an WT embryo. Bright red spots indicate cilia tufts as seen in Fig 4.2. Illustration of an embryo shows region of magnification. b: scanning electron microscopy image, where multiciliated cells are surrounded by goblet cells and ionocytes. Arrowhead indicates a multiciliated cell in the ICC and SEM images.

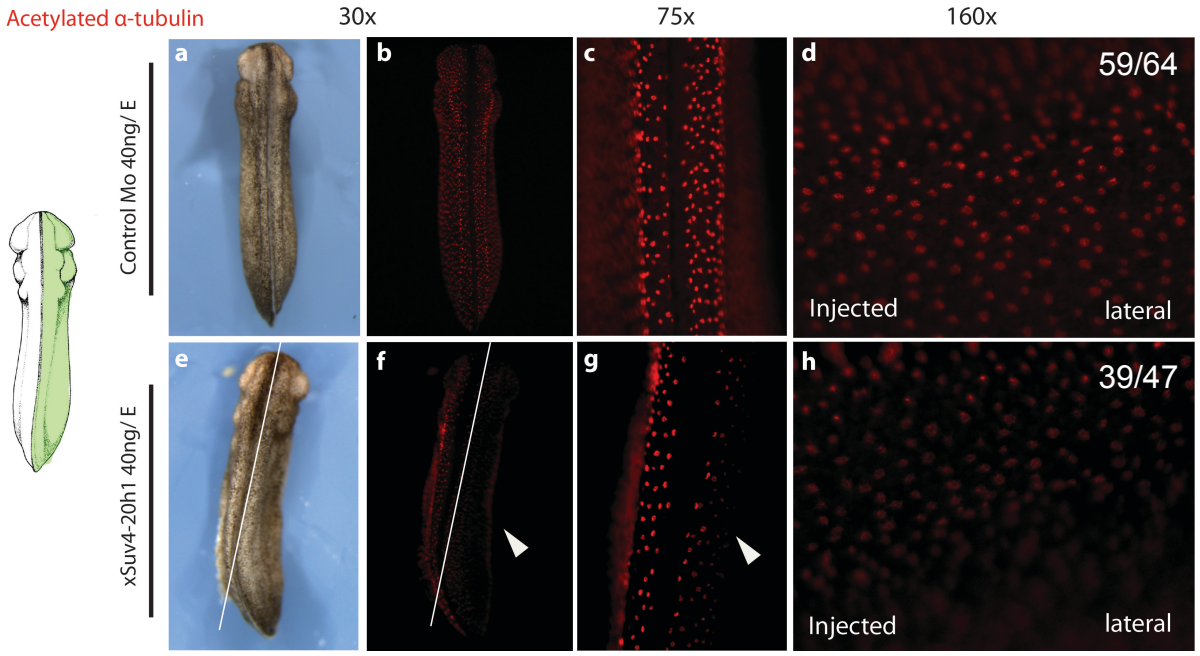

Fig. 4.4: Acetylated α-tubulin is reduced in Suv4-20h1 MO injected embryos. Immunocytochemistry against acetylated α-tubulin in right side injected NF 26 embryos. The first three columns represent dorsal views of embryos. The fourth colum shows lateral view of the injected side. **a-d:** acetylated α-tubulin expression in Co-MO injected embryos is similar in injected and uninjected side. **e-h:** acetylated α-tubulin is reduced in the injected side of Suv4-20h1 morphants (arrowhead) (n=4 independent experiments).

As can be seen in Fig. 4.4 the acetylated α-tubulin fluorescent signal is noticeably weakened in the injected side of Suv4-20h1 morphants (Sh1-MO); Fig 4.4e-h). Additionally, cilia tufts ("red spots") appeared smaller. In contrast, acetylated α-tubulin signal was equally strong in both sides of control morpholino (Co-MO) injected samples (Fig. 4.4a-d). This showed that

multiciliogenesis was defective in Suv4-20h1 morphants similar to Suv4-20h double morphants.

4.1.2 Depletion of Suv4-20h1 HMT perturbs directional fluid flow

Airway multicilia beat in a so-called metachronous wave in order to establish a unidirectional fluid flow to transport debris, noxious agents and infectious organisms from the respiratory epithelium (Chilvers and O'Callaghan 2000). *X. laevis* epidermal multicilia work similarly. The fluid flow keeps the larval skin clean and sufficiently provided with oxygen (Werner and Mitchell 2012). A strong fluid flow requires cilia motility and cilia organization in two planar polarities: the rotational and tissue-level polarity. Cilia need to be polarized to each other within a ciliated cell and ciliated cells in turn need to be polarized to each other within a tissue respectively (Wallingford 2010). The epidermal fluid flow is established as early as NF 23 when differentiated cilia are on the skin surface (Deblandre, Wettstein et al. 1999). Cilia can generate a powerful stroke, which is sufficient to propel the resting embryo in the buffer solution over the smooth surface of the agarose gel.

Given the decreased acetylated α-tubulin signal in the Suv4-20h1 morphants, it was further investigated, whether the epidermal fluid flow was affected. Unilaterally injected embryos showed strong phenotypic changes such as lack of eye and melanophores (melanocytes), neurologic defects and a curved anterior-posterior axis in the injected side, similar to Suv4-20h double morphants (Nicetto, Hahn et al. 2013). Control morphants showed a directed and fast fluid flow on each uninjected and injected side (Fig. 4.5a,b). The red dye was transported quickly from the head region to the tail region forming a y-shaped flow pattern. In contrast to the control, Suv4-20h1 morphants had a disturbed fluid flow on the skin surface (Fig. 4.5c,d). Here, the red dye was removed more slowly and without a visible flow pattern, indicating a perturbation in fluid flow, which might be caused by cilia motility defects or by planar polarity defects.

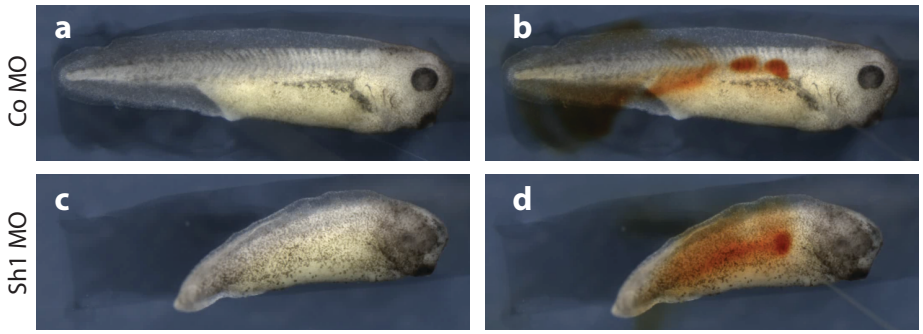

Fig. 4.5: Cilia-driven fluid flow is perturbed in Suv4-20h1 morphants. Unidirectional cilia-driven fluid flow generated by hundreds of beating cilia was observed in anesthetized tadpoles. Xenopus laevis embryos were injected with control morpholino and Suv4-20 h1 morpholino respectively. Here, injected sides are shown. In the beginning, a dye was injected on the surface of the embryos in an area close to the head. **a,b:** in control embryos, the dye was quickly washed away towards the tail of the embryo, thus creating a y-shaped flow pattern **(b)**. **c,d:** flow pattern in injected side of Suv4-20h1 morphants was perturbed. The flow is slowed down, which was indicated by accumulation of dye on the skin. Note the eye defect and shortened body axis. Movie in Supplement.

4.1.3 Suv4-20h HMTases are required for ciliogenesis by promoting expression of ciliogenic genes

To gain more insight into the mechanisms underlying the Suv4-20h ciliary phenotype, multiciliogenic genes such as *foxj1* and *dnah9* were investigated using RNA *in situ* hybridization. In its function as a transcription factor, FoxJ1 (forkhead box J1) promotes activation of genes required for apical docking of basal bodies, cilia extension and cilia motility. Interestingly, it is a key regulator of motile cilia only, but not of non-motile primary cilia. Mice, which lacked foxj1/Hfh-4, had missing 9+2-type (motile) cilia formation and organ patterning, whereas 9+0-type (primary) cilia formation was unaffected. Motile cilia were dose-dependently reduced in number and shortened in length by Foxj1 MO injection (Pohl and Knochel 2004; Stubbs, Oishi et al. 2008; Neugebauer, Amack et al. 2009). *Dnah9* (dynein axonemal heavy chain 9) is one of the genes induced by FoxJ1 and is critical for cilia motility. Motile cilia require dynein arms to generate a wave-like bending of the axonemes that collectively produce a fluid flow along surfaces. Dynein motor function of the nine outer doublet microtubules is essential for initiation and propagation of motility, which in fact is due to microtubule sliding powered by ATP hydrolysis. Interestingly, doublet microtubules slide asynchronously and thus generate an effective and a recovery stroke (Satir 1980; Kramer-Zucker, Olale et al. 2005; Stubbs, Oishi et al. 2008).

First of all, two-cell stage embryos were unilaterally injected into the animal region of one blastomere. Only precisely injected embryos were collected for succeeding analysis.

In figure 4.6, representative embryos from tadpole stages (NF 25), when MCCs are differentiated, are stained for *foxj1* mRNA. Via RNA *in situ* hybridization, messenger RNAs of genes of interest are detected. The first two columns display the right side of wild type, Co MO and Suv4-20h1 MO injected specimen. The last two columns represent the left side, which is injected, where indicated.

As expected, *foxj1* was expressed in ciliated cells of the epidermis, creating a regular polka dot like pattern of stained cells. Notably, *foxj1* was also detectable in the central nervous system, especially in the most caudal part of the spinal cord central canal, the ciliated ampulla terminalis (Hagenlocher, Walentek et al. 2013). In Suv4-20h1 morphant embryos, expression was still visible in the epidermis. Furthermore, Suv4-20h1 MO injected specimen at tadpole stages appeared to have more MCCs. This phenotype was scored at high penetrance (Fig. 4.6k,l, $p<0.001$, Fisher's exact test, two-tailed). Among others, it was striking that the density of MCCs was higher in the head region. More clearly than in control morphants and in the uninjected side of each embryo, *foxj1*-labeled cells were adjacent to each other.

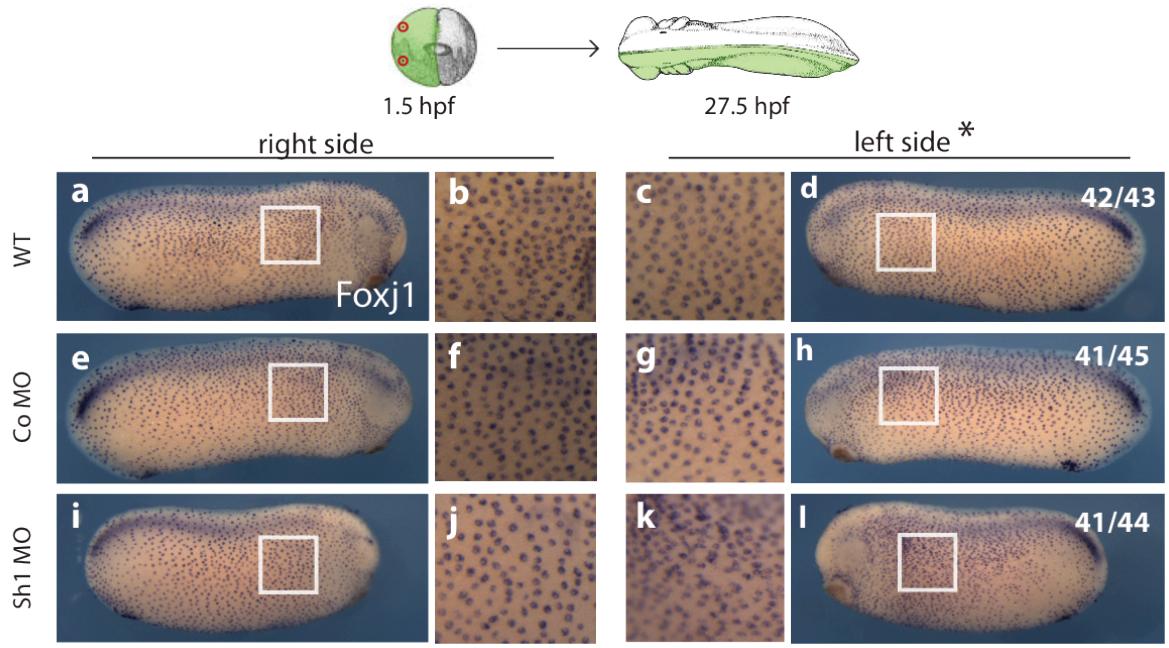

Fig. 4.6: Suv4-20h1 HMT depletion increases the number of *foxj1* positive cells in the non-neural ectoderm. RNA *in situ* hybridization (ISH). Graphic shows unilateral injection mode: two red spots mark site of microinjection. Images show lateral views of NF 25 wild type, control MO injected and Suv4-20h1 MO injected embryos. The right side is uninjected, whereas the left side is injected, where it is indicated (*). White boxes in the head region mark regions of higher magnification displayed in

b,c,f,g,j and k. Numbers of embryos showing the displayed type of staining are compared to the total number of analyzed embryos (n=3 independent experiments). hpf: hours post fertilization.

Figure 4.7 shows immunostaining for *dnah9*, which has a comparable spacial expression (e.g. expression in MCC and CNS) to *foxj1*. Similar to *foxj1*, each purple stained dot represents a ciliated epidermal cell, which is positive for *dnah9* mRNA. Both control embryos (Fig. 4.7a-h) and morphants (Fig. 4.7k,l) display analogous results to *foxj1* mRNA expression. The amount of *dnah9*+ cells in Suv4-20h1 morphants also appeared to be increased, whereas it was normal in control embryos and in the uninjected halves.

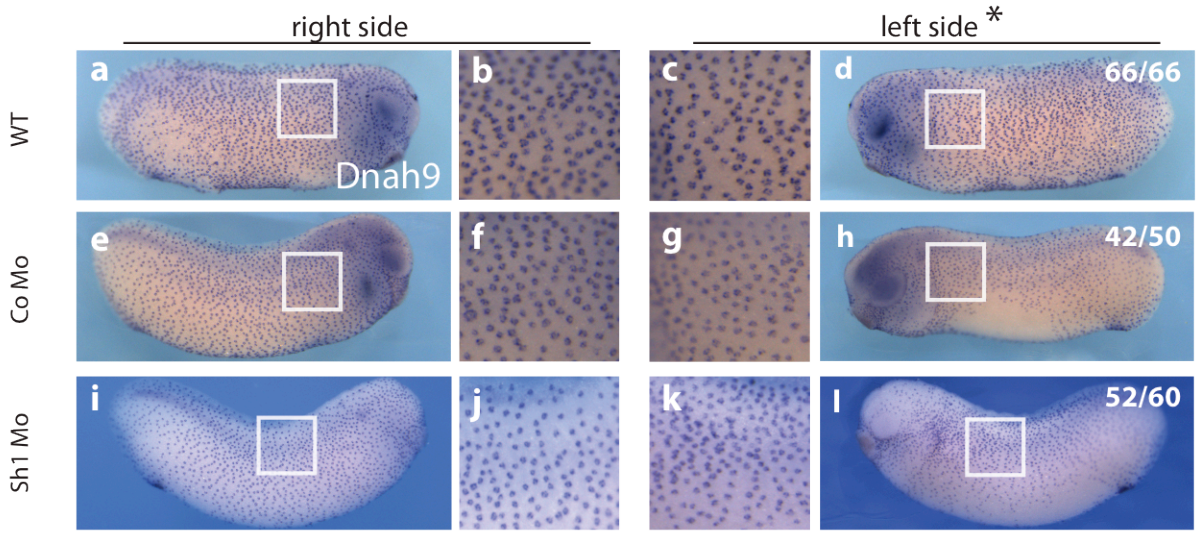

Fig. 4.7: Suv4-20h1 depletion increases the number of *dnah9* mRNA positive cells in the non-neural ectoderm
ISH with unilaterally injected embryos. Lateral views of uninjected (a-d, e-f, i-j) and MO injected (g-h, k-l) sides of NF 25 embryos. White boxes in the head region mark areas of higher magnification. *dnah9* expression pattern of Suv4-20h1-morphant embryos resembled *foxj1* expression; *dnah9*+ multiciliated cells were upregulated, especially in the anterior region (k,l). The penetrance of affected embryos was high ($p<0.001$, Fisher's exact test); *: injected side, where indicated (n=3 independent experiments).

To further address, if mRNA levels of ciliary genes were affected, a relative quantification via real-time PCR was performed. Thereby, mRNA levels of genes in morphant and wild type ectodermal explants (animal caps) were detected relative to the mRNA levels of two reference ('housekeeping') genes, e.g. ODC and H4. To analyze epidermal expression levels of genes of interest, animal cap (AC) assay was chosen. Animal caps represent isolated epidermal tissue. Thus, it was expected that MO-related changes in expression levels of each cohort would be free from meso-endodermal signals.

Fig. 4.8a demonstrates the sequential steps in the preparation of animal caps. Relative quantification was performed for above-mentioned genes *foxj1* and *dnah9*. Morphant embryos

as well as control and wild type embryos were analyzed at tadpole stage NF 25 when ciliated cells are differentiated. *ODC* and *H4* were used as reference genes to normalize mRNA levels of the studied genes.

The total amount of *foxj1*+ cells, which represent ciliated cells, were significantly increased in conditions injected with Suv4-20h1 MO (p=0.002). Cells were increased by 45% relative to control MO injected caps. *Foxj1*+ cells were increased by 24% in Suv4-20h1/h2 morphants (p=0.021). Thus, to assess relative quantification of *foxj1* and *dnah9* per each multiciliated cell, mRNA expression levels were calculated with the increased number of *foxj1*+ cells. Results identify significant lower levels for *foxj1* and *dnah9* in Suv4-20h1 and double morphants relative to control morphants by about 50%, (p=0.05, p=0.01 respectively, Fig. 4.8c). The difference in the results (more MCCs, but reduced mRNA levels) might be explained by the two different methods that I have used, where quantitative (RT/qPCR) and non-quantitative (ISH) methods were compared. These results indicate, that reduced *foxj1* expression levels might result in less cilia and shorter cilia length, a phenotype, which has been observed in *Xenopus* (Stubbs, Oishi et al. 2008). Additionally, *dnah9* expression levels were lower indicating that this caused defects in cilia motility and therefore affected fluid flow. However, there is a second phenotype: Suv4-20h1 depletion apparently increases the number of MCCs, leading to more *foxj1* and *dnah9* positive cells.

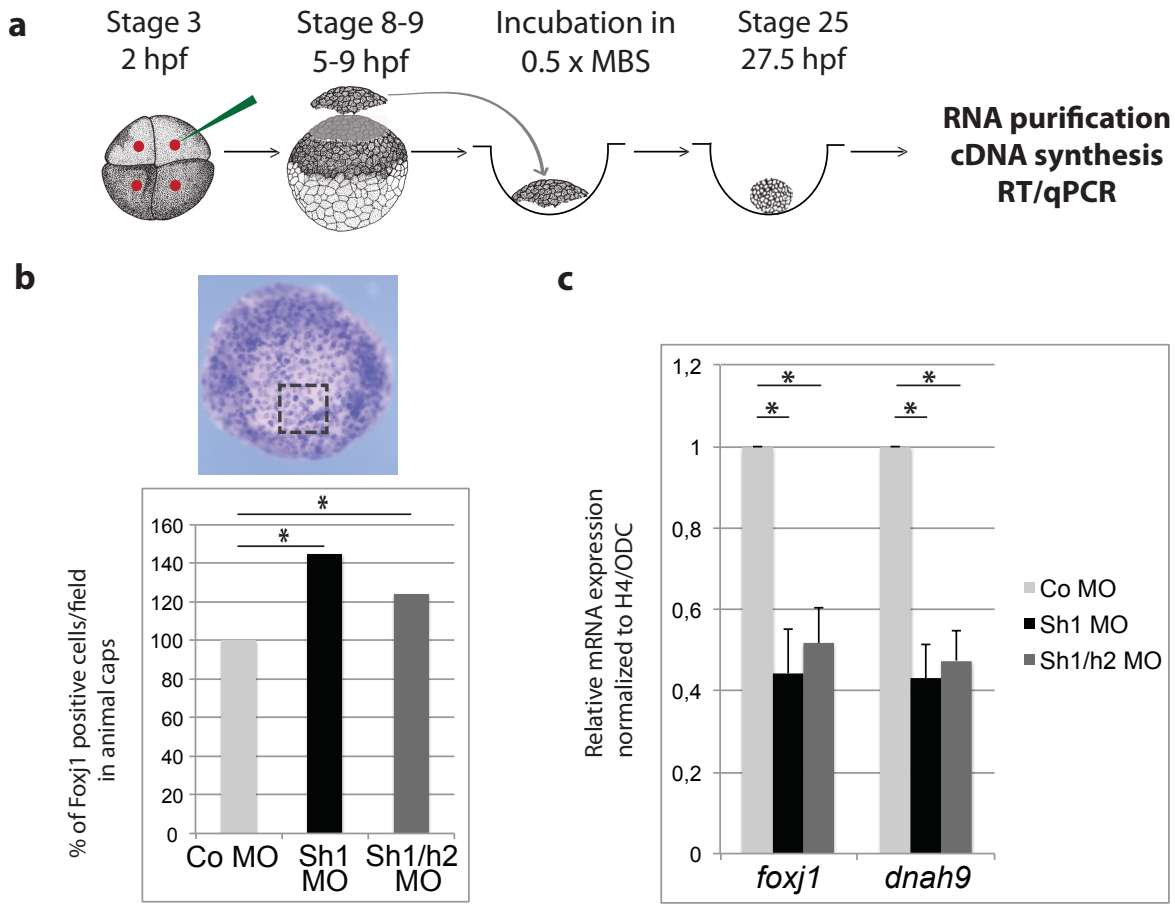

Fig. 4.8: Depletion of Suv4-20h1 or h1/h2 enzymes decreases mRNA levels of *foxj1* and *dnah9*. RT/qPCR in animal caps. **a:** illustration of animal cap preparation: injection of 40ng of control, Suv4-20h1 or h1/h2 MOs. Isolation of ACs, culture in a saline solution until NF 25. **b:** three fields of 100x100px were counted per cap of which a mean value was calculated. The grey box marks a representative field. Significant increase of *foxj*1+ cells in 40ng Suv4-20h1 MO (p=0.002) injected caps by 45% relative to control MO caps. 24% increase of *foxj1*+ cells in 40ng Suv4-20h1/h2 MO (p=0.02). n=7 caps per condition, cells absolute n=697 (Co MO), n=1154 (Sh1 MO), n=979 (Sh1/h2 MO), n=2 independent experiments. **c:** Relative quantification of *foxj1* and *dnah9* expression levels were normalized to ODC/H4. The mRNA expression levels of morphants were calculated with the increase in *foxj1*+ cells. *Foxj1* and *dnah9* levels were significantly two-fold reduced in Suv4-20h1 and double morphants relative to control morphants (*foxj1*: p=0.03 and p=0.01 respectively, *dnah9*: p=0.01 and p=0.01), error bars indicate SEM (n=3 independent experiments).

4.1.4 Depletion of Suv4-20h HMTases perturbs multiciliated cell fate specification

On the cellular level, cilia formation was compromised and the cilia-driven fluid flow was perturbed. Paradoxically, more *foxj1*+ and *dnah9*+ cells were observed in the larval epidermis, which could imply that Suv4-20h specific processes interfered with multiciliated cell fate specification leading to more MCCs in the mucociliary epithelium of the skin. To

address this question, Suv4-20h1 and Suv4-20h2 MO effects on multiciliated cell specification were studied.

In the absence of Suv4-20h1/h2 HMTs, Delta-like 1 (Dll1) mRNA was increased in the non-neural ectoderm (Nicetto 2012). The Delta/Notch pathway has a crucial role in cell determination. Therefore, we investigated if multiciliated cell precursor (MCP) selection was affected. According to Deblandre et al. (1999), two steps are required to form differentiated MCCs on the epidermal surface. First, during gastrulation, a subset of cells is selected to become a MCC by expressing Delta-like 1. Second, during neurulation, these cells express α-tubulin as a prerequisite of cilia formation.

As *dll1* overexpression was detected at late gastrula, a time when precursors are chosen, embryos from a stage immediately afterwards were analyzed. α-tubulin and Foxj1 were used as markers for ciliated cell precursors and motile ciliated cells respectively (Deblandre, Wettstein et al. 1999). Furthermore, Multicilin (mci) was investigated as a hallmark of multiciliated cells (Stubbs, Vladar et al. 2012). At NF 14, all three markers appear within multiciliated cell precursors of the inner layer in a regularly spaced pattern. Results obtained from RNA *in situ* hybridization analyses with these markers indicate that reduced Suv4-20h1 or -h2 enzyme function results in an overproduction of MCC precursors, i.e. *α-tubulin+, mci+ and foxj1+* cells.

Fig. 4.9 shows *in situ* hybridization for the ciliated cell marker *α-tubulin* on neurula stage (NF 14) embryos. Accordingly, the uninjected side of the embryo could be distinguished from the injected side, which stained indigo after treatment with X-Gal. Control MO injected specimen showed the typical spotted pattern of *α-tubulin*-probe containing MCPs. In between them are unstained, MCP-free areas (Fig 4.9a-c). In contrast, there were clearly more *α-tubulin+* cells in the Suv4-20h MO treated embryos (Fig. 4.9d-l), which led to densely packed *α-tubulin+* cells in the inner skin layer. Sections of embryos showed a thickening of the *α-tubulin+* inner layer in the Suv4-20h MO injected side (Fig. 4.9j).

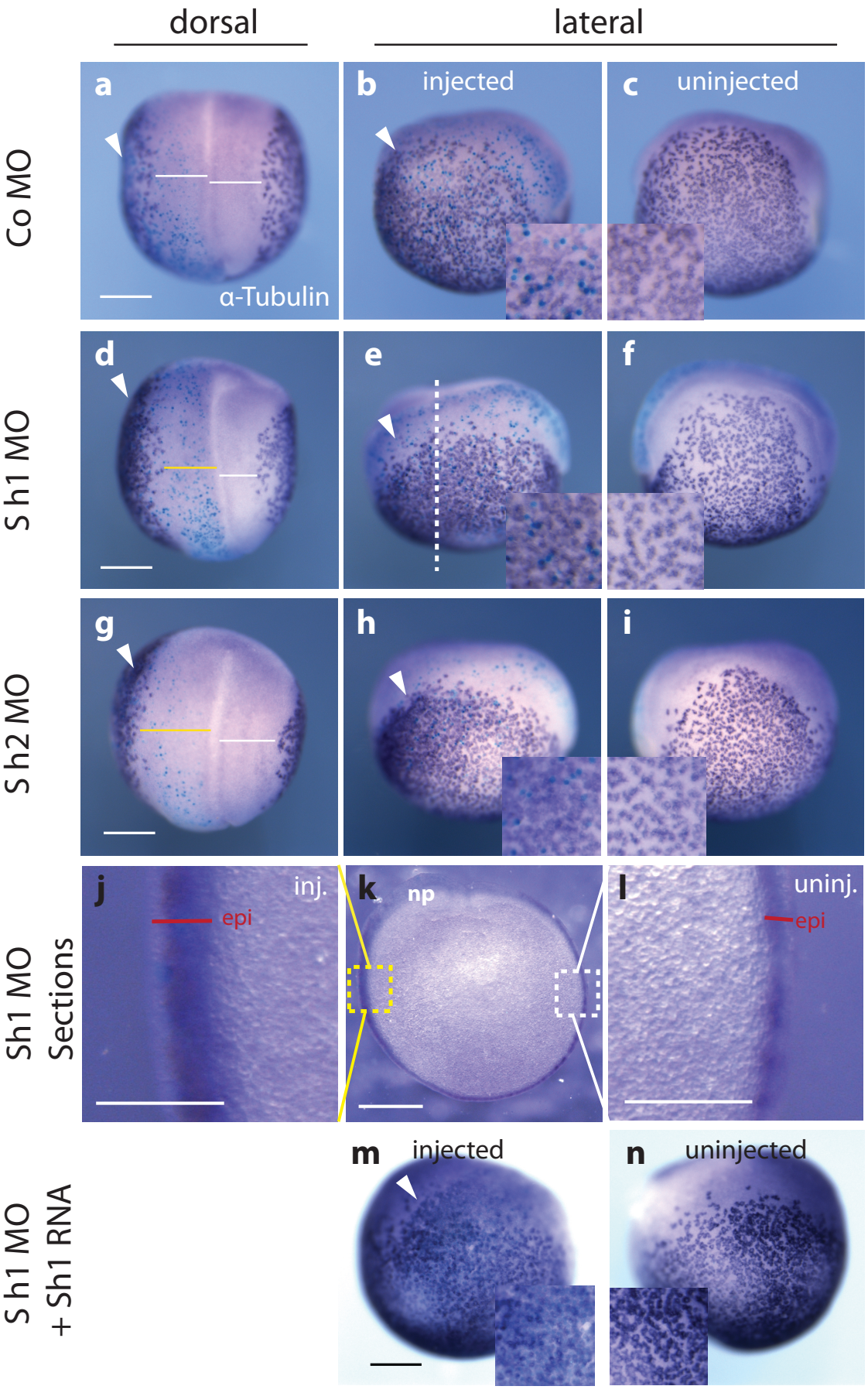
dorsal
lateral
Co MO
Sh1 MO
Sh2 MO
Sh1 MO Sections
Sh1 MO + Sh1 RNA
a
α-Tubulin
b
injected
c
uninjected
d
e
f
g
h
i
j
inj.
epi
k
np
l
uninj.
epi
m
injected
n
uninjected

Fig. 4.9: Suv4-20h1 or -h2 knockdown increases the density of *α-tubulin*-labeled ciliated cell precursors. *In situ* hybridization. First column shows dorsal view of samples, second column the injected half and the third the uninjected half. **a-c:** control morpholino injected embryos showing a normal phenotype. **d-i:** Suv4-20h1 ($p<0.001$) and Suv4-20h2 ($p<0.001$) morphants showing an increased population of ciliated cell progenitors in the injected region. Displayed are a lower power view of the whole embryo and an insert of higher power. **d,g:** Note the wide neural plate due to delayed neural tube formation in the injected side (marked by yellow line). **k:** section through a Suv4-20h1 morphant (as indicated by white dashed line in e) illustrates *α-tubulin* stained cells in the epidermis. Yellow box: injected side, White box: uninjected side. The injected side had more *α-tubulin*+ MCPs **(j)** and the inner layer of the epidermis was thicker in the injected side compared to the uninjected side **(l)**. **m,n:** Rescue decreased the number of *α-tubulin*+ cells compared to uninjected side and Suv4-20h1 MO injected regions ($p=0.001$) . Scale bars, 200µm. White arrowhead: injected side and anterior region, epi: epidermis, np: neural plate (n=3 independent experiments).

The upregulation of *α-tubulin*+ cells was evident with high penetrance in three individual experiments (Fig. 4.10). Some wild type and control MO injected embryos that were affected were presumably due to non-specific effects. The specificity of the Suv4-20h-related *α-tubulin* upregulation was tested by a so-called rescue experiment. Phenotypes that were caused by effective Suv4-20h1 translation blocking can be rescued by adding Suv4-20h1 RNA, which cannot be targeted by the used Suv4-20h1 morpholino. For this purpose, alongside to Suv4-20h1 MO, murine Suv4-20h1 RNA was injected, which encodes a well-characterized protein with similar function. Upon rescue, the amount of *α-tubulin*+ cells was comparable in injected and uninjected regions (Fig. 4.9m,n), demonstrating a Suv4-20h1-specific effect.

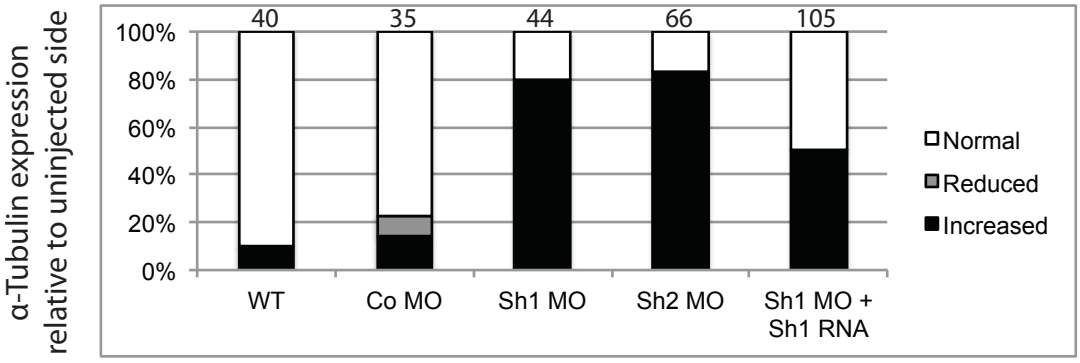

Fig. 4.10: Statistical analysis of Suv4-20h MO effects on *α-tubulin* expression in MCPs (Related to Fig. 4.9). Embryos were examined for *α-tubulin* at NF 14 by ISH. The absolute number of embryos is indicated in the top row of the diagram (n=three independent experiments).

Furthermore, the upregulation of *foxj1*+ (Fig. 4.11) and *mci*+ (Fig.4.12) cells in RNA *in situ* hybridization analysis at NF 14 supports the idea that MCPs are increased.

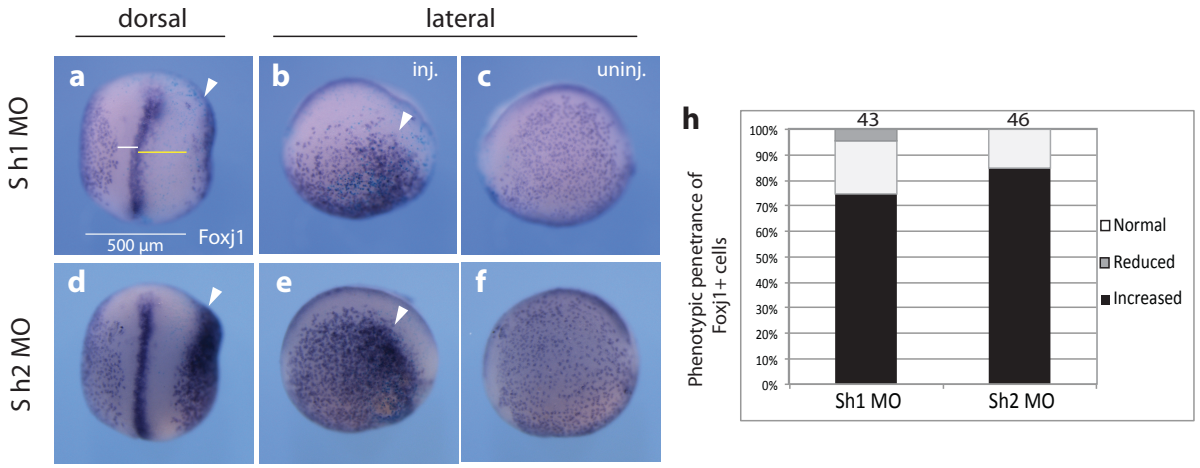

Fig. 4.11: Suv4-20h1 or -h2 ablation increases number of *foxj1*+ multiciliated cell precursors. *In situ* hybridization. LacZ RNA and Suv4-20h1 or Suv4-20h2 MO were injected into one blastomere at two-cell stage. At NF 14/15, embryos were fixed and X-Gal staining (light blue color) was performed to trace the injected side (arrow heads). The *foxj1* probe was detected with NBT/ BCIP (purple color). Note again the delayed neural fold formation of the Suv(ar) depleted side **(a,b,d,e)**. *Foxj1* positive cells mark the putative multiciliated cells. Increased density of *foxj*1-positive cells correlates with higher density of *α-tubulin*+ cells. **h:** As shown in the diagram, injection of both Sh1 MO ($p<0.001$, two-tailed) or Sh2 MO ($p<0.001$) increased the density of *foxj1*+ cells (n=three independent experiments).

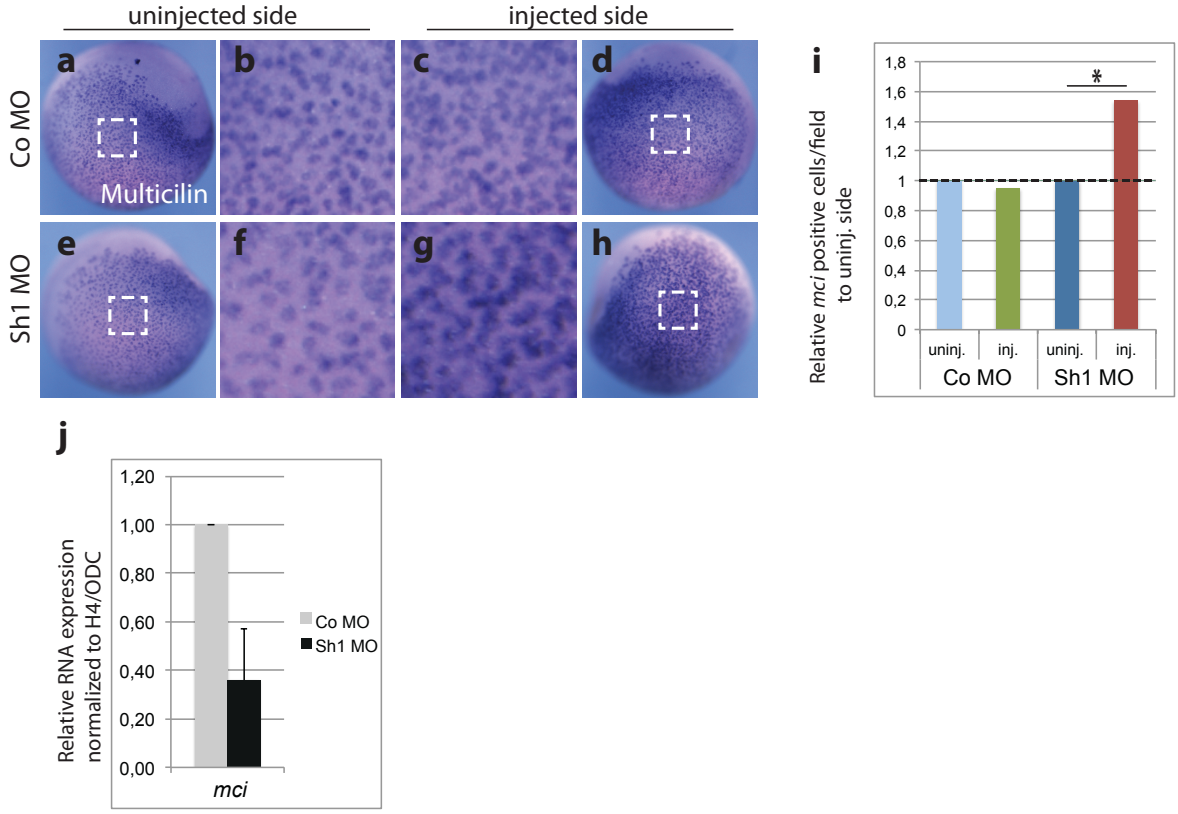

Fig. 4.12: Suv4-20h1 knockdown causes an increase of multicilin-positive MCPs.
a-d: RNA *in situ* hybridization of NF 14 embryos. The number of MCPs, which were detected by *mci* probes, was upregulated in the Suv4-20h1 depleted cohort. **i**: Precursor counts were relatively increased in the Suv4-20h1MO injected side by 50% compared to the uninjected side ($p<0.0001$). **j**: Suv4-20h1 ablation strongly reduced *mci* mRNA levels by over 60% relative to control MO injected skin explants ($p=0.15$). White boxes: region of higher magnification (n=three individual experiments).

Fig. 4.12 displays the expression of *mci* mRNA in multiciliated cell precursors. MCPs were significantly increased in the injected sides (n=987) of Suv4-20h1 MO compared to the uninjected sides (n=658) by about 50% ($p<0.0001$, e-i). The numbers were assessed by the following method. From each side (injected/uninjected) of an embryo, one field of a fixed size was selected at a comparable region (see white boxes in Fig. 4.12) and *mci*+ cells were counted. In the control MO injected cohort, MCP counts were similar in injected (n=1107) and uninjected sides (n=1168).
The ciliogenic genes, *foxj1* and *dnah9* were downregulated in tailbud stages. To test whether this is also valid for *mci* mRNA levels in MCPs, relative quantification was conducted with NF 14 skin explants. *ODC* and *H4* were again used as reference genes to normalize mRNA levels of the gene of interest and mRNA amount in the control MO injected cohort was set as one. Given that Suv4-20h1 morphants generated more MCPs, the *mci* mRNA levels were adjusted to the 50% increase in *mci*+ cells. *Mci* mRNA levels were lower in Suv4-20h1 morphants relative to control morphants by more than 60%, ($p=0.15$, Fig. 4.12j).

The results show a clear rise in the amount of multiciliated cell progenitors that are positive for *α-tubulin, foxj1* and *mci* after Suv4-20h protein ablation. According to Deblandre et al. (1999), the number of MCPs is restricted by lateral inhibition through the Delta/Notch pathway. Overexpression of *dll1* was reported to increase the number of specified MCPs (Deblandre, Wettstein et al. 1999). Consequently, the most obvious interpretation from our data together with previous findings of *dll1* upregulation during the gastrula stages would be that Suv4-20h HMTs are necessary to restrict the multiciliated cell fate specification via Delta/Notch.

4.1.5 Depletion of Suv4-20h HMTases perturbs multiciliated cell spacing pattern

In the process of multiciliated cell development, MCPs move by intercalation from the inner deep layer to the outer layer of the skin. As a result of this, two differentiated MCCs hardly ever touch each other. Additionally, multiciliated cells of the *Xenopus* larval skin adopt an evenly spaced pattern with goblet cells, small secretory cells and ionocytes separating the MCCs (Deblandre, Wettstein et al. 1999).
It was interesting to know if the increase of MCPs results in patterning changes in the *Xenopus* mucociliary epithelium. Immunohistochemistry for acetylated α-tubulin, which is a

stable form of *α-tubulin* found in microtubules, was carried out in order to detect MCCs on the skin surface. Subsequently, the injected and uninjected side of each embryo was pictured and compared to each other. On each side, a standardized region was selected and the number of multiciliated cells per field was counted. In morphant embryos, the numbers of mature MCCs was significantly increased (p=0.0184) by 30% compared to the non-injected (Fig. 4.13). The spacing pattern seemed more random, although big clusters of MCCs in contact with each other were missing. This suggests that the mechanism of intercalation of progenitor cells was still operating. Therefore, the increase in the number of progenitors and multiciliated cells might be explained by a shift in cell determination towards the MCC fate, an over-proliferation of committed multiciliated cell precursors or both.

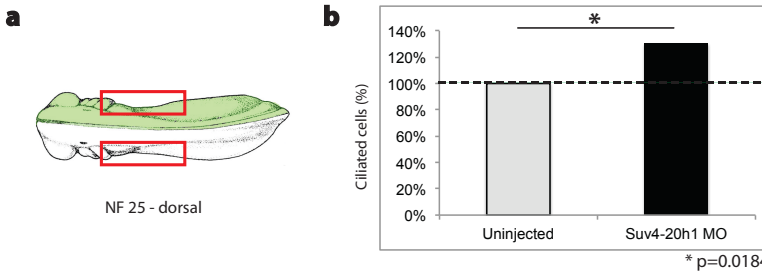

Fig. 4.13: Increased number of MCPs gives rise to more MCCs in Suv4-20h1 morphants. a: graphic of the selected regions for MCC counting.
b: increased multiciliated cell counts upon Suv4-20h1 MO injection (p=0.018), marked by acetylated α-tubulin staining. Cells absolute n=1339 (uninj.), n=1744 (inj.);
(n=7 independent experiments).

4.2 Suv4-20h enzymes are required for ciliogenesis during pronephric development

4.2.1 Expression levels of genes required for multiciliogenesis are reduced in the nephrostomes

Motile multiciliated cells not only exist in the epidermis, but also in the pronephros. The amphibian embryonic kidney, which is derived from intermediate mesoderm, has three ciliated nephrostomes. The ultrafiltrate from the glomus is thought to be streamed into the adjacent tubules via the nephrostomes by a swirling beating of the many cilia (Mobjerg, Larsen et al. 2000; Wessely and Tran 2011). This raises the question whether Suv4-20h HMTs promote ciliogenesis in a general manner.

To address this issue, embryos were injected into one ventral blastomere at 4-cell stage to specifically target nephrostomes and epidermis and were collected at different time points after NF 28. *In situ* hybridization for *dnah9* in NF 32/ 33 tadpoles shows expression in three organs: pronephros, otic vesicle and epidermis. In the pronephros, *dnah9* is expressed in three defined structures, called nephrostomes. In Suv4-20h1 morphants, ciliogenesis was blocked in the nephrostomes given that *dnah9* expression was highly affected in the Suv4-20h1 MO injected half ($p<0.001$). 80% showed a strong phenotype with an absent expression (Fig. 4.14g,h) and 10% showed a reduced phenotype in the nephrostomes. The specificity of the observed pronephric phenotype was demonstrated by a rescue experiment with Suv4-20h1 MO and murine Suv4-20h1 mRNA coinjection. Succeeding analysis showed that the absent *dnah9* expression in the nephrostomes was reduced by 30% in rescue embryos relative to the Suv4-20h1 MO condition ($p=0.0006$, Fig. 4.14k,l,m). Furthermore, the fraction of embryos with one/two or three (normal) *dnah9*+ nephrostomes was larger. Interestingly, 7 out of 99 embryos from the rescue cohort appeared to have 4 *dnah9*+ nephrostomes. Consequently, the added RNA compensated for the reduced Suv4-20h1 protein levels and loss of *dnah9* expression recovered partially in rescued embryos. This recovery of *dnah9* expression, although incomplete, testifies to the specific nature of the ciliogenic defect in Suv4-20h1 morphants.

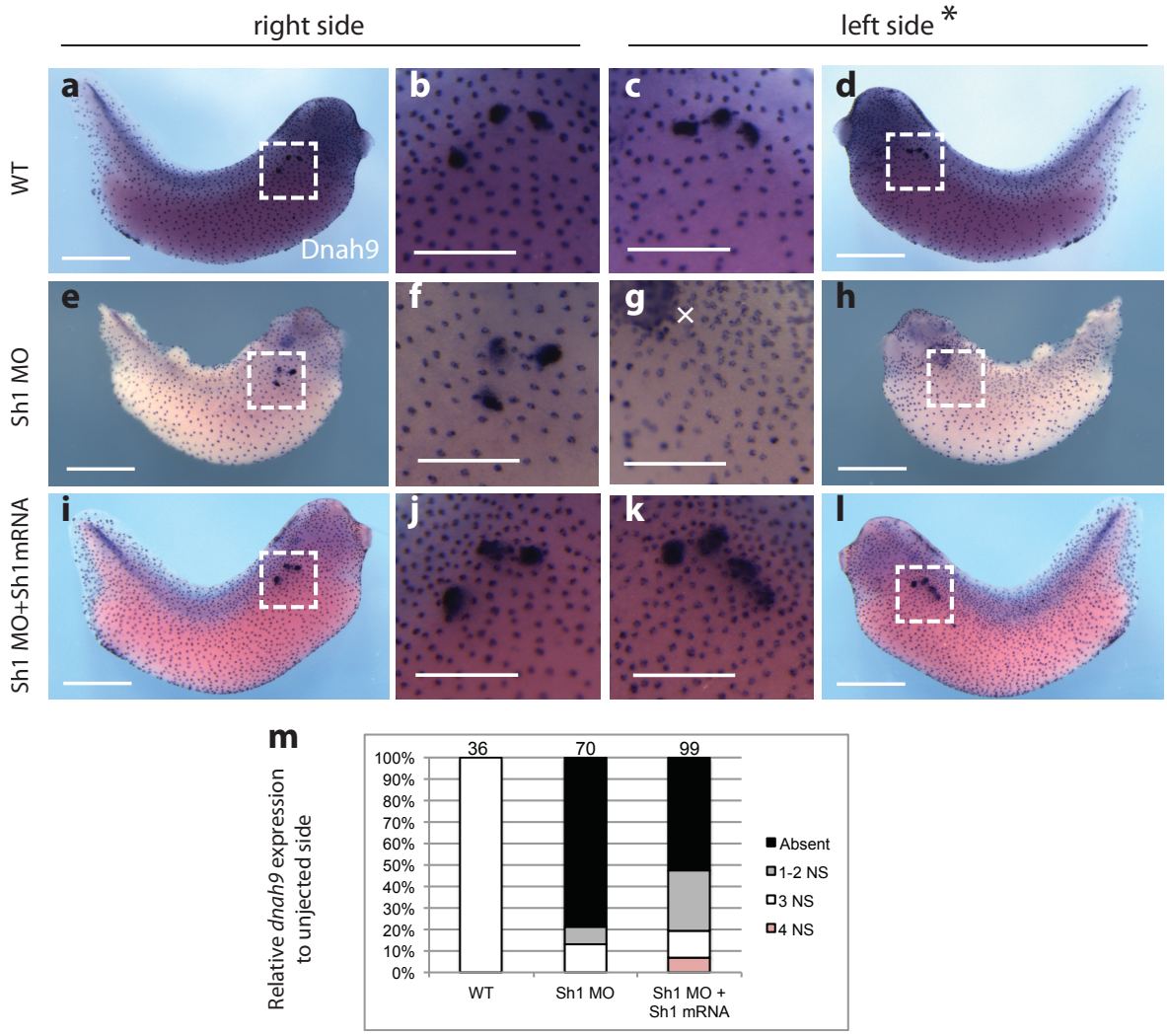

Fig. 4.14: Suv4-20h1 enzyme depletion abolishes dynein axonemal heavy chain 9 in the embryonic kidney. Expression was detected by RNA *in situ* hybridization. **a-d:** wild type embryos with three nephrostomes, shown in higher magnifications **(b,c)**. **e-h:** half-injected Suv4-20h1 morphants showed loss of *dnah9* expression in the nephrostomes **(g,h)**. Furthermore, an increase of MCCs was seen compared to the uninjected half. **i-l:** Rescued phenotypes displayed *dnah9* expression in the nephrostomes **(k,l,m)** indicating that phenotypic changes were Suv4-20h1 morpholino specific and co-injection of mouse Suv4-20 RNA was able to compensate for Suv4-20h1 knockdown. **m:** 30% increase of embryos showing a normal or reduced phenotype with one to three nephrostome in the rescued region. Uninjected halves were used as internal control. **n:** illustration of a sectioned amphibian pronephric kidney with ciliated nephrostome. Scale bar, 200µm for a,d,e,h,i,l, 100µm for b,c,f,g,j,k. White boxes mark regions of magnification. NS: nephrostome, *: injected side, where indicated, ×: abnormal skin with dense patch of MCCs. (n=three independent experiments).

To address the question of how Suv4-20h1 MO affects the pathway upstream of *dnah9*, we assessed key regulatory genes of the multiciliogenic program, such as *foxj1* and *mci*. *FoxJ1* is a known master regulatory factor for motile ciliogenesis (Pohl and Knochel 2004; Stubbs, Oishi et al. 2008; Yu, Ng et al. 2008) and *mci* is required for the exit from cell cycle and for centriole assembly in MCCs (Stubbs, Vladar et al. 2012). Again, similar to *dnah9* expression,

foxj1 was induced in ciliated nephrostomes. In unilaterally injected, NF 32/33 Suv4-20h1 morphants, *foxj1* expression in the nephrostomes was weaker (Fig. 4.15c,d) and diffuse in contrast to uninjected and control MO injected sides ($p<0.001$, Fig 4.15a,b). Nevertheless, the amount of embryos with an absent *foxj1* expression was lower than those with an absent *dnah9* expression. This might indicate that in nephrostomes FoxJ1 function is dependent on dosage in inducing ciliary proteins, such as Dnah9.

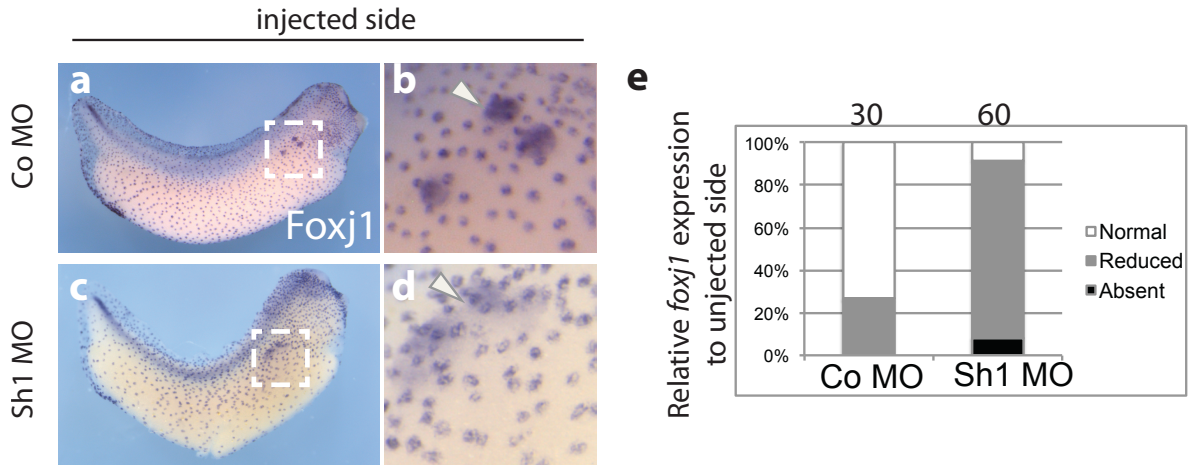

Fig. 4.15: Depletion of Suv4-20h1 HMT reduces *foxj1* expression in the nephrostomes. Expression was detected by RNA *in situ* hybridization in NF 32/33 embryos. **a-b:** *foxj1* staining in the nephrostomes showed a distinct pattern in uninjected and control morphants (white arrow head). **c-e:** *foxj1* is downregulated and diffusely stained in Suv4-20h1 morphants (n= three independent experiments).

While FoxJ1 is sufficient for motile cilia formation, multicilin, a transcriptional regulatory factor upstream of FoxJ1, is specifically required for multiciliogenesis. For this purpose, *mci* promotes centriole assembly and induces *foxj1* expression (Stubbs, Vladar et al. 2012). *Mci* was normally transiently expressed in the nephrostomes and the overlaying skin around NF 28. It vanished in later stages after multiciliated cells were differentiated in the nephrostomes. At NF 28, shortly before *foxj1* and *dnah9* expressions were downregulated, *mci* expression was massively perturbed by Suv4-20h1 MO injection. For almost all Suv4-20h1 morphants, MCC formation in the pronephric nephrostomes seemed to be blocked according to loss or reduction of *mci* expression (Fig. 4.16g-i). Note that the epidermal expression at NF 28 was absent as well. Thus, this might indicate that Suv4-20h1 enzyme is required for both epidermal and kidney multiciliogenesis (Marcet, Chevalier et al. 2011) by stimulating *mci* expression.

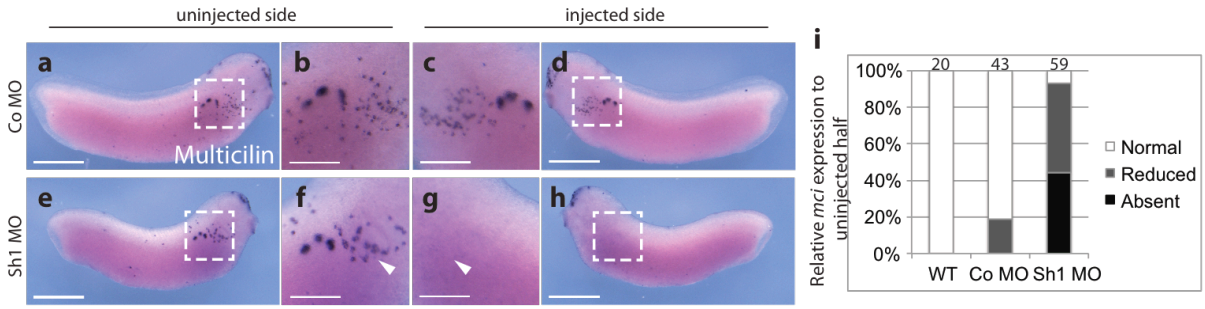

Fig. 4.16: Suv4-20h1 protein knockdown leads to loss of multicilin. Expression was detected using RNA *in situ* hybridization. Uninjected and injected sides of embryos were compared. Injected side was traced with fluorescent Alexa 488. White box in lower magnification view of whole embryo marks region of high magnification. **a-d:** Representative specimen of control condition. Epidermal *mci* expression was in the skin around the gills (arrowhead). **e-h:** Loss of *mci* RNA in nephrostomes and skin of the injected region. **i:** high penetrance of *mci* nephrostome phenotype in Suv4-20h1 MO condition compared to wild type and control MO. Scale bar: 200µm for a,d,e,h and 100µm for b-c,f-g (n=three individual experiments).

4.2.2 Suv4-20h1 protein knockdown represses microRNA miR-449 expression in the nephrostomes

Recent work has identified the microRNA miR-449 as a promoter of multiciliogenesis in both human and frog by directly inhibiting the Delta/Notch pathway (Marcet, Chevalier et al. 2011). *Mci*, *foxj1* and *dnah9* are genes downstream of Notch and were repressed in Suv4-20h1 morphants. Since Notch represses *mci* expression (Stubbs, Vladar et al. 2012), we assumed that Delta/Notch was activated in Suv4-20h morphants. Towards this goal, miR-449 expression was examined in wild type and half-injected Suv4-20h1 and control morphants older than NF 32. MiR-449 co-localizes with *acetylated α-tubulin* mRNA indicating that it functions in MCCs. A locked nucleic acid (LNA) *in situ* hybridization approach was used to detect microRNAs.

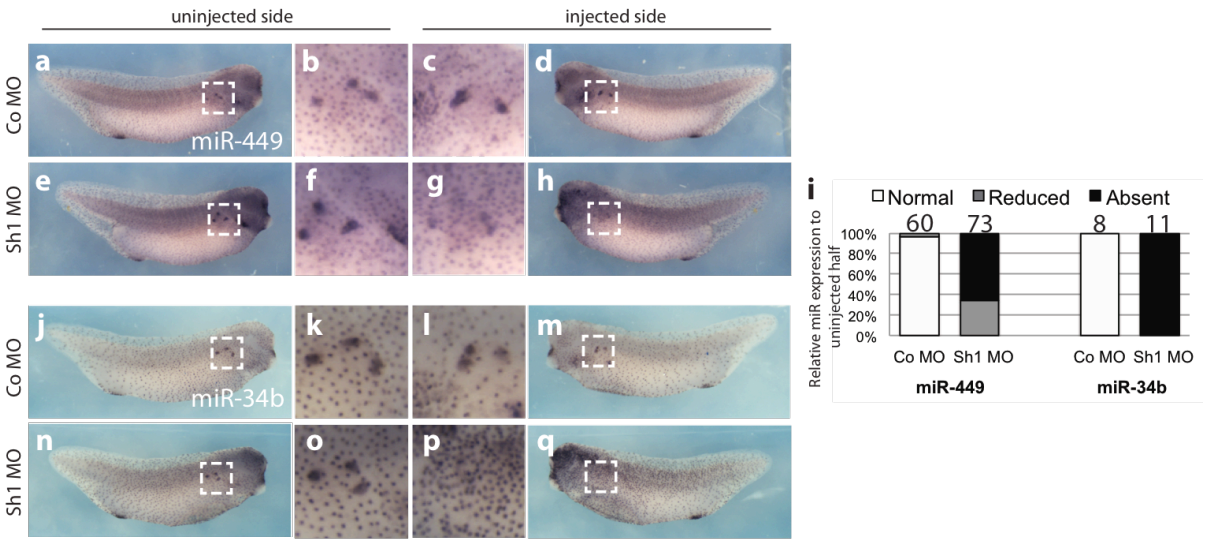

Fig. 4.17: Suv4-20h1 protein knockdown represses microRNA miR-449 expression in nephrostomes. Half-injected embryos with Co MO, Suv4-20h1 MO and Alexa 488 as lineage marker, LNA *in situ* hybridization of NF 32-35 embryos. **a-d:** the control cohort showed similar expression for miR-449 in the skin and nephrostomes of the uninjected and injected side. **e-i:** Injection of Suv4-20h1 MO dramatically reduced miR-449 ($p<0.001$) in the nephrostomes by almost 70% (n=three individual experiments). Likewise, miR-34b, which belongs to the same superfamily of microRNAs, seemed to be affected (**n-q**) (n=one individual experiment). White boxes mark regions of higher magnification. LNA ISH was kindly performed by V. Thomé, IBSM Marseille.

LNA *in situ* hybridization was performed on Suv4-20h1 morphant cohorts, which were validated for the ciliogenic phenotype. Fig. 4.17 shows the injected and uninjected sides of control morphants (a-d) and Suv4-20h1 morphants (e-h). In nephrostomes, miR-449 expression was present in both sides of control embryos, whereas it was absent in the injected side of Suv4-20h1 morphant cohort ($p<0.001$). This experiment was repeated three times and showed a loss of miR-449 in as many as 70% (Fig. 4.17g,i). Noteworthy, miR-449 expression was visible in the epidermis. Furthermore, there were clearly more miR-449+ cells in the skin. This observation supports previous findings that the number of MCCs was upregulated in the Suv4-20h1 depleted skin. The simplest explanation for the loss of miR-449 expression is that Suv4-20h1 enzyme acts upstream of miR-449 to promote multiciliogenesis. Furthermore, this also implies that the shift in cell fate specification toward the MCC fate is due to miR-449.

MiR-34b is another microRNA, which shares the seed region with miR-449 and which is enriched in MCCs (Marcet, Chevalier et al. 2011). Like miR-449, miR-34b is absent after Suv4-20h1 knockdown ($p<0.001$; Fig. 4.17n-q). Although only tested in a restricted number of embryos, the results were steady (11 out of 11 embryos; Fig. 4.17i).

4.2.3 Suv4-20h1 knockdown does not repress pronephric anlage markers

The observed changes in ciliogenesis gene expression may be caused by defects in cilia formation or in pronephric kidney development. To distinguish between theses causes, the pronephric anlage marker x*lim-1* (Taira, Otani et al. 1994) and *pax2* were analyzed. Pax2 is a well-characterized transcriptional factor of specific functional importance for the pronephric development (Heller and Brandli 1997). Fig. 4.18 shows the *pax2* expression pattern both in nephrostomes, as well as in proximal and distal (*) tubules of NF 32 embryos (Fig. 4.18a,b). In Suv4-20h1 depleted embryos, *pax2* expression was clearly present, and seemed to be rather ectopic in the pronephric structures. *Xlim-1* expression was unaltered in both control MO injected and Suv4-20h1 MO injected embryos. The *xlim-1* expression of injected versus uninjected sides was similar in intensity and pattern. Fig. 4.18e,h shows dorsal views, where injected and uninjected sides can be compared to each other. Fig. 4.18f,i demonstrate the injected side indicated by blue X-Gal staining.

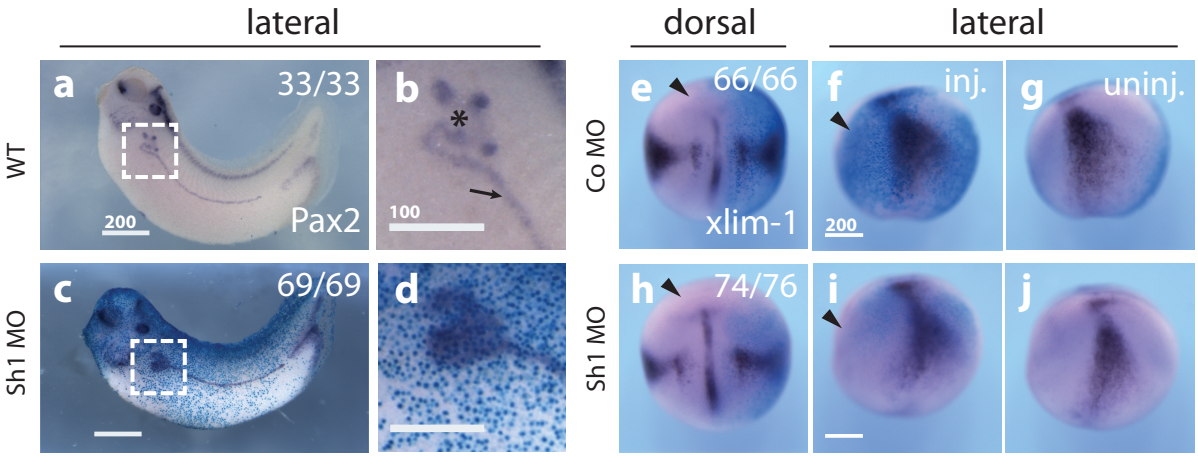

Fig. 4.18: Pronephric anlage markers *pax2* and *xlim-1* are expressed in Suv4-20h1 morphants. RNA *in situ* hybridization on NF 32/33 embryos. X-Gal staining was used as lineage tracer (blue staining). **a-b:** wild type *pax2* expression in tubules (*) and duct (arrow). **c-d:** protein knockdown of Suv4-20h1 does not eliminate *pax2* expression in nephrostomes and tubules, although the expression seems to be less distinct in these structures (n=3 independent experiments). **e-j:** NF 20, *xlim-1* is unperturbed in Suv4-20h1 morphant and control morphant cohorts; anterior is marked by arrowhead. Scale bar: 200µm; 100µm for b,d. (n=three independent experiments).

4.2.4 Suv4-20h1 depletion inhibits tubule formation

According to *xlim-1* and *pax2* expressions in neurula and tadpole stages, induction of the pronephros was not blocked. However, in order to detect defects in pronephric development, two well-characterized antibodies for proximal tubules (3G8) and distal tubules/duct (4A6) were used in immunostainings. 3G8 recognizes a luminal antigen in proximal tubules, whereas 4A6 stains the entire cell surface of distal tubules and duct. Both antibodies stain tubular antigens regardless of the tubular morphology (Vize, Jones et al. 1995; Brennan, Nijjar et al. 1998). The structures that were stained in the uninjected side of Suv4-20h1 morphants corresponded to those found in control morphants (data not shown). In contrast, the signal for both antibodies was lost in the injected side of Suv4-20h1 morphants compared to the control cohort ($p<0.001$). Transversal sections through these Suv4-20h1 morphant embryos demonstrated a clear staining for both 3G8 and 4A6 in tubules of the uninjected side (Fig. 4.19i,j,l,m). However, no staining was detectable in the injected side (k,n). Additionally, tubule structures could not be identified in the injected side where the staining was missing. The most obvious explanation is that the antigens are missing due to differentiation problems. This can be caused by defects in epithelial differentiation or the lack of tubule formation.

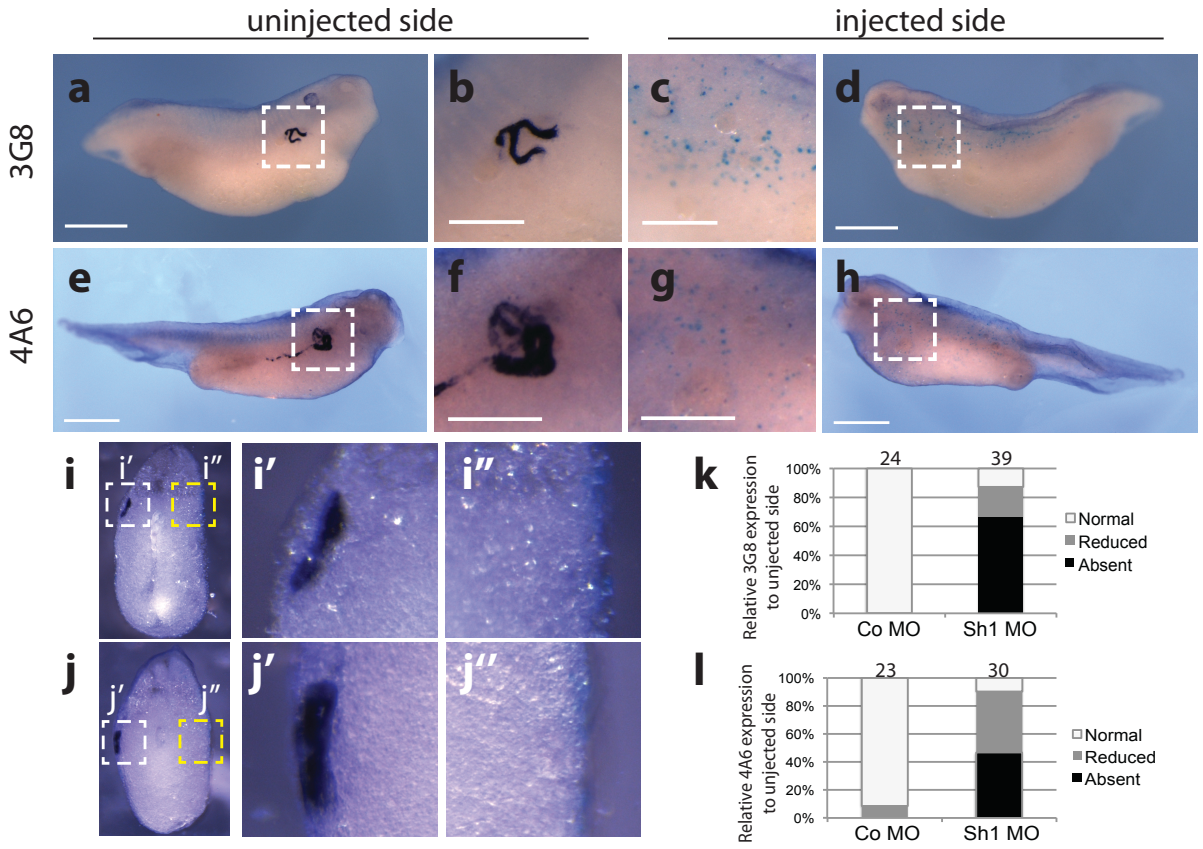

Fig. 4.19: Suv4-20h1 protein knockdown inhibits tubule differentiation. 3G8 and 4A6 were detected by immunocytochemistry at NF 33 (3G8) and NF 37/38 (4A6). X-Gal staining was used as lineage marker. **a-d:** Loss of 3G8 antigen in proximal tubules of Suv4-20h1 MO injected regions ($p<0.001$). **e-h:** morphants lacked 4A6 staining in distal tubules and duct of the injected region (g.h). White box in lower magnification view of whole embryo marks region of high magnification. **i-j:** transversal sections. **i':** 3G8 immunostaining showing expression in the uninjected side (white box in i) versus absent expression in the injected region ($p<0.001$; **i'', k**). **j':** 4A6 is expressed in the uninjected half of Suv4-20h1 morphants, but is missing in the injected side (**j'', l**). (n=two individual experiments for each antibody).

4.2.5 Knockdown of Suv4-20h1 leads to edema formation

Studies in four days old (>NF 45) embryos demonstrated that the tubule system was developed in Suv4-20h1 MO injected cohorts. These embryos were generated by injection at 4-cell stage into all cells and were subsequently analyzed for morphological changes. Since *Xenopus* embryos are transparent at these developmental stages, this approach is well suited to evaluate internal organs, such as the kidney. In comparison to uninjected and control MO injected embryos, Suv4-20h1 depleted morphants were massively deformed. Embryos did not swim around in the petri dish like the control cohorts and had striking abnormalities of the eyes and melanophores, which supports prior findings by our lab in embryos at earlier stages (Nicetto 2012). The eyecups were not fully bisected and seemed to lack the lens.

In addition to these phenotypic changes, all Suv4-20h1 morphant tadpoles were severely edematous. The edema was found in a generalized manner (Fig. 4.20c) reminiscent of embryos with impaired pronephros differentiation (Tran, Pickney et al. 2007). Suv4-20h1 morphant tadpoles showed dilated tubules on higher power magnification, whereas wild type and control siblings formed compactly organized tubules with a comparatively small diameter (Fig. 4.20a',b'). The results represent a limited number of specimens, but the observed phenotype is consistent (11/11 embryos; $p<0.001$)

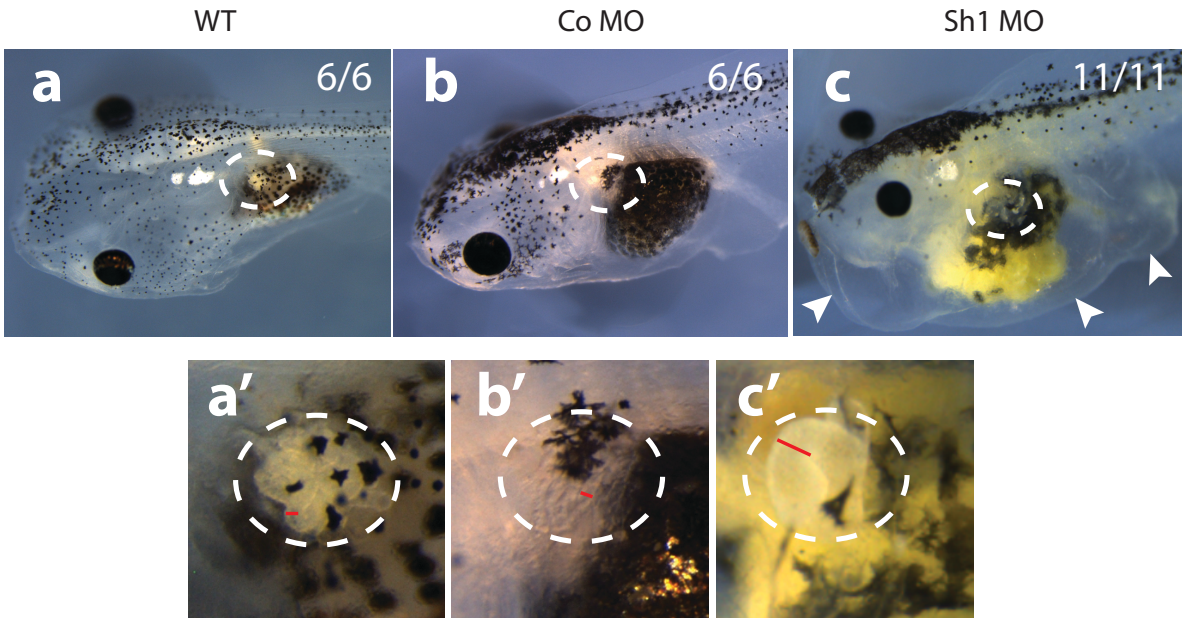

Fig. 4.20: Knockdown of Suv4-20h1 HMT leads to edema formation.
Embryos >NF 45. **a-b:** control conditions showing well developed embryos. **c:** edema in Suv4-20h1 morphants occurs in a generalized manner (arrowheads). **a'-c':** higher maginification of pronephric tubules, highlighted with white circles. Red lines mark tubule width. WT and control MO injected embryos **(a',b')** are normal, whereas Suv4-20h1 morphants show dilated tubules ($p<0.001$) **(c')**. Numbers indicate embryos showing the above phenotype compared to the total amount of analyzed embryos (n=one individual experiment).

5. DISCUSSION

During the transition from pluripotent to a differentiated state, cells need an exact temporal and spatial organization of gene expression to drive cell fate specification. Cells possess the same genome, but establish individual cellular identities with specialized cellular functions. This is mainly achieved by epigenetic mechanisms, since genes remain mostly unaltered. Epigenetic mechanisms are known to play a vital role in early development of embryos by regulating cell-lineage appropriate gene expression. For instance, histone lysine methylation marks, such as H4K20me3 and H3K9me3, are involved in transcriptional gene repression and mark pericentromeric and telometric heterochromatin (Schotta, Lachner et al. 2004; Li, Liu et al. 2012; Nicetto, Hahn et al. 2013).

This thesis addresses the role of the H4K20me2/me3 catalyzing histone methyltransferases Suv4-20h1 and Suv4-20h2 in multiciliated cell development. During embryogenesis, the abundance of H4K20me3 increases approximately five-fold as demonstrated by western blot analysis in frog embryos (Schneider, Arteaga-Salas et al. 2011), which implies an important role for the Suv4-20h HMTases during development (Nicetto, Hahn et al. 2013). Moreover, down-regulation of Suv4-20h enzymes by morpholino approach can impair the formation of a specific cell organelle, the cilium. Cilia formation was affected in the *Xenopus* embryonic skin and additionally in another multiciliated tissue, the embryonic kidneys.

Analysis of the Suv4-20h-ablated ciliary phenotype in the *Xenopus* skin demonstrated two specific results in single morphants. Since Suv4-20h1 or –h2 enzymes both increase di- as well as tri-methylated H4K20 in *Xenopus* (Nicetto, Hahn et al. 2013), it is thought that there is no functional subdivision of Suv4-20h1 or –h2, but rather a general reduction in H4K20me3 levels, which result in defective cilia formation. First of all, the specification of multiciliated cell precursors (MCP) is affected subsequently leading to an increase in multiciliated cell (MCC) numbers. Secondly, on the level of the individual multiciliated cell, expression levels of multiciliogenic genes are reduced leading to a defective ciliary phenotype.

5.1 Suv4-20h enzymes impact epidermal cilia formation

5.1.1 Suv4-20h HMTases effects on multiciliated cell specification

The skin in *Xenopus laevis* develops after gastrulation in two distinct cell layers of the non-neural ectoderm: the inner sensorial and outer superficial layer. In general, ciliated cells are committed in the inner layer via Delta/Notch signaling (Drysdale and Elinson 1992). A subset of cells with high expression levels of Delta-like 1 (*dll1*) inhibits neighboring notch-presenting cells from taking on the multiciliated cells fate. This mechanism is referred to as lateral inhibition and helps cells to become different from surrounding cells. During early neurula stages (NF 12-14) cells with high *dll1* levels give rise to committed ciliated cell precursors, which intercalate into the outer layer during neurulation and finally form a cilia tuft (NF 20-22) (Deblandre, Wettstein et al. 1999). The radial intercalation is important to create a regularly spaced pattern of MCCs in the larval skin (Stubbs, Davidson et al. 2006).

The prominent upregulation of multiciliated cells in Suv4-20h morphants proposes a contribution of Suv4-20h enzymes to the fate specification process of MCPs. Indeed, investigation of *mci*, *α-tubulin* and *foxj1* expression in multiciliated precursor cells in Suv4-20h1 and –h2 morphants confirmed that the increase in cell number already occurred in neurula (NF 14), i.e. during the period when MCPs arise. Multicilin-expressing cells during this stage represent MCPs. As expected, *mci*+ precursor counts were significantly raised by about 50% in Suv4-20h1 morphants compared to controls. Most control morphants on the contrary presented similar MCP numbers in the injected and uninjected side of each specimen. Consistent with this key finding, *α-tubulin*- and *foxj1* mRNA-expressing MCPs are elevated with high penetrance (≈ 80%) in Suv4-20h1 and -h2 morphants. Since embryos were rescued by coinjection of Suv4-20h1 MO and murine Suv4-20h1 mRNA, the increase in the *α-tubulin*+ MCP number is caused by the morpholino-mediated downregulation of H4K20 tri-methylation. This result establishes another biological function of Suv4-20h enzymes in skin, in addition to their impact on neural differentiation (Nicetto, Hahn et al. 2013).

These findings in whole embryos are supported by analysis in animal caps at tailbud stage (NF 25). The ciliogenic marker *foxj1* was investigated as a hallmark for multiciliated cells. In RNA *in situ* hybridization, foxj1 was, similarly to *α-tubulin* and *mci,* expressed in more cells. The number of *foxj1* mRNA-positive MCCs increased relatively (45%) at equal proportions to

mci mRNA-positive MCCs (50%). This suggests that Suv4-20h1-mediated effects on MCP specification are comparable in whole embryos and animal caps.

At tailbud stages, ciliary axonemes can be visualized by immunostaining for the structural marker acetylated α-tubulin. These immunostainings presented an evenly spaced, "spotty" arrangement of cilia tufts in wild type and control embryos. The ciliated cells appeared to be aligned in rows along the dorsoventral axis of the embryo, leaving gaps of unciliated areas between the rows. In Suv4-20h morphants on the contrary, the regular alignment of acetylated α-tubulin expressing cells was perturbed compared to the uninjected side of the specimen, as well as to the control morphants. Furthermore, acetylated *α-tubulin*-labeled cells were significantly increased (30%) in the skin of Suv4-20h1 morphants. This result indicates that more MCPs give rise to more MCCs. Noteworthy, the increase in acetylated α-tubulin+ cells (MCC) is smaller compared to the increase in MCPs. A robust inhibition of ciliation can explain this difference, since only MCCs with visible cilia tuft are scored. Possible mechanisms underlying the inhibited ciliary phenotype will be discussed in the next chapter.

The results presented here provide support to the hypothesis that Suv4-20h enzymes are important for the specification of MCPs. Data from this work show that Suv4-20h enzyme depletion leads to more MCPs suggesting a repressive function in ciliated cell precursor specification. Deblandre et al. (1999) states that *dll1* expression regulates the number of MCPs and that *dll1* overexpression leads to an increase of MCPs. The underlying mechanism may be explained by the so-called *cis*-inhibition of Notch. This proposed mechanism describes that ligands can *trans*-activate Notch receptors of neighboring cells or *cis*-inhibit Notch within the same cell, causing Notch inhibitory effects (Jacobsen, Brennan et al. 1998; Deblandre, Wettstein et al. 1999; Marcet, Chevalier et al. 2011b). In other words, sufficient high levels of *dll1* within the cells could prevent the cell from lateral inhibition and thus more MCPs could be specified. Indeed, a previous report by Nicetto et al. showed that *dll1* mRNA+ cells of double Suv4-20h morphants was specifically and strongly upregulated in the epidermis (Nicetto, Hahn et al. 2013). Consistent with this finding, the delta like-1 upregulation was reproducible in Suv4-20h1 single morphants (data not shown). The most straightforward conclusion is that the Suv4-20h protein knockdown causes an upregulation of non-neural ectodermal *dll1*, which interferes with ciliated cell specification leading to an increase of precursor cells.

Several reports have demonstrated the importance of Delta/Notch signaling for the specification of lineage-restricted precursor cells (Deblandre, Wettstein et al. 1999; Dubaissi and Papalopulu 2011; Morimoto, Nishinakamura et al. 2012). In the *Xenopus* mucociliary epithelium, the Delta/Notch pathway regulates specification of both precursors for ciliated cells and ionocytes (Deblandre, Wettstein et al. 1999; Hsiao, You et al. 2007). Ionocytes express many ion channels and are thought to play a role in ionic regulation, which is vital for the function of specialized epithelia. Both precursor types are committed in the inner layer and intercalate to the surface of the epidermis (Dubaissi and Papalopulu 2011). Stubbs et al. (2006) suggested that MCCs and ionocytes are "regulated in tandem by Notch signaling" instead of a reciprocal manner (Stubbs, Davidson et al. 2006). Since Suv4-20h protein depletion increased *dll1* positive cells, this implies that Suv4-20h enzymes also impact other cell types in the skin, i.e. ionocytes. In other words, epidermal *dll1* upregulation in morphants may increase, apart from MCC numbers, also ionocyte numbers, which potentially leads to a perturbation of the normal skin homeostasis. Thus, further investigations would illuminate the role that Suv4-20h enzymes have in the differentiation of the mucociliary epithelium.

5.1.2 Suv4-20h HMTases promote multiciliogenesis

Previous studies, mainly in *Xenopus laevis*, have identified several transcription factors that coordinate ciliogenesis. The transcription regulatory factor X2 (rfx2) is broadly required for all types of ciliogenesis. The forkhead-box transcription factor FoxJ1 is necessary for motile cilia formation. For example, cells with a high *foxj1* level establish a single motile cilium (Stubbs, Oishi et al. 2008).

What distinguishes multiciliated from monociliated cells? MCCs involve a large number of cilia on the apical cell surface and therefore need hundreds of centrioles. Centriole formation is normally coupled to the cell cycle, when multiple daughter centrioles are formed orthogonally to a mother centriole at G1/S transition. Since MCCs are postmitotic and require massive centriole amplification, these cells need at least one additional factor to *foxj1* in order to exit from the cell cycle and to start *de novo* centriole assembly (Dirksen 1991; Klos Dehring, Vladar et al. 2013). Recently, a factor called multicilin (mci) was identified, which is specifically needed and sufficient for the formation of multiciliated cells (Stubbs, Vladar et al. 2012). Multicilin is thought to act at the start of the multiciliogenic pathway, downstream of Notch and upstream of FoxJ1 (Stubbs, Vladar et al. 2012), Dnah9 and Rfx2 (Yu, Ng et al. 2008; Chung, Peyrot et al. 2012; Stubbs, Vladar et al. 2012). Preliminary observations in

Suv4-20h double morphants showed defective cilia formation in the skin with less abundant and shorter cilia (Nicetto 2012), a condition that for example is also observed in the airways of smokers (Leopold, O'Mahony et al. 2009). The observed Suv4-20h ciliary phenotype suggests that the transcriptional regulation of multiciliogenic genes is changed in the Suv4-20h morphants.

In this thesis, specific ciliary genes, including *mci*, *foxj1* and *dnah9* were analyzed via RT/qPCR at two time points. The first time point is during neurulation (NF 14), when progenitor cells are specified. The second one is during tailbud stage (NF 25), when ciliated cells are differentiated and exhibit cilia tufts on their cell surface as reported by Deblandre et al. (1999). Knockdown of Suv4-20h1 protein levels shows a significant increase of *mci* mRNA positive precursor cells by 50% compared to the uninjected side of the same embryo. Notably, the increase in multicilin positive cells is accompanied by a decline in mRNA levels of *mci. Mci* mRNAs were decreased strongly by 60% in MCPs, although this result was not significant ($p=0.15$, student t-test). The data was collected from three independent experiments and the strength of the reduction was variable between them. Nevertheless, expression levels were downregulated in all three experiments when compared to controls. Additional experiments will be required to validate this difference statistically. This suggests that Suv4-20h1 drives multiciliogenesis by promoting *mci* expression. The results are compatible with a prior report by Stubbs et al. (2012) who states that multicilin knockdown leads to inhibition of multiciliated cell formation. Similar to their result, Suv4-20h morphant embryos show reduced levels of *mci* and *foxj1* mRNA levels (Stubbs, Vladar et al. 2012). The data from *mci* expression studies are in good agreement with quantitative analyses performed for *foxj1* and *dnah9* at the tailbud stage. Both *foxj1* and *dnah9* mRNA levels are significantly decreased by two-fold in Suv4-20h1 and Suv4-20h1/h2 depleted specimen. These results can explain the initially mentioned Suv4-20h ciliary phenotype, which shows less and shorter cilia. According to Stubbs et al., FoxJ1 protein knockdown also produces fewer and shorter cilia in the skin (Stubbs, Oishi et al. 2008).

The consistent transcriptional inhibition of ciliary genes in Suv4-20h1 morphants indicates that Suv4-20h enzymes regulate multiciliogenesis via the promotion of the multiciliogenic pathway. Suv4-20h1 ablation compromises the expression of multiciliogenic factors and consequently, MCPs lack factors needed to differentiate and generate normal cilia tufts.

Independent studies have recently indicated a cross talk between non-ciliated and multiciliated cells in the skin of Xenopus. Similar to MCC formation, Ionocytes, also known as proton-secreting cells, differentiate by intercalating into the outer layer. It has been shown that Ionocytes have a non-cell autonomous effect on MCC differentiation. Ionocytes express the trynscription factor *foxi1e*, which is required for both epidermal and neural ectoderm formation (Mir, Kofron et al. 2007). Foxi1e knockdown diminishes ionocytes and can harm the development of multiciliated cells. Although ciliated cell specification and intercalation is unaffected, MCCs presented fewer, shorter and abnormal beating cilia (Deblandre, Wettstein et al. 1999; Dubaissi and Papalopulu 2011). Future studies should therefore analyze the interconnection between H4K20 tri-methylation and Ionocyte formation in the multiciliated epithelium to wholly understand the Suv4-20h morphant ciliary phenotype.

Another interesting point concerns the Suv4-20h role in cell cycle regulation. Schotta et al. showed that loss of H4K20me3 marks is associated with a delay in G1/S-phase transition and impaired cell cycle progression (Schotta, Sengupta et al. 2008). This fact could be an important link to the observation that Suv4-20h morphants assemble less cilia in MCCs. Delayed S-phase entry after Suv4-20h depletion might hinder centriole assembly and therefore result in fewer cilia. In addition to promotion of the ciliogenic pathway, Suv4-20h enzymes could regulate multiciliogenesis by coordination of the cell cycle progression. However, this remains to be investigated. For example, cilia formation can be assessed by immunostaining after acceleration or inhibition of the cell cycle. Comparing these ciliary phenotypes with the Suv4-20h1 depleted morphants can expose whether an impaired cell cycle progression impacts ciliogenesis.

5.1.3 Contribution to cilia-driven fluid flow across the epidermis

Motile cilia are found throughout the body and establish a directional fluid flow across tissue surfaces or lumina. The cilia-driven fluid flow is involved in the breakage of body symmetry in embryos and is also needed for the development of organs, including the central nervous system and inner ear (Kramer-Zucker, Olale et al. 2005; Blum, Beyer et al. 2009; Colantonio, Vermot et al. 2009). Further functions are to move an ovum toward the uterus, provide sperm motility and to drive cerebrospinal fluid flow in brain ventricles (Fawcett 1954; Lyons, Saridogan et al. 2006; Fliegauf, Benzing et al. 2007; Hagenlocher, Walentek et al. 2013). Airway cilia-driven flow of extracellular mucus keeps the respiratory epithelium

clean. In *Xenopus*, embryos respire through their skin. Thereby the fluid flow is required to provide the larval skin with oxygen and ions. Moreover, cilia-driven flow is linked to the protection of the epidermal mucociliary epithelium against infections as very recently reported by Dubaissi et al. (Werner and Mitchell 2012; Dubaissi, Rousseau et al. 2014).

Cilia-driven fluid flow on the skin of Suv4-20h1 depleted larval embryos was abnormal. The Suv4-20h1MO-mediated reduced flow velocity could be due to the following hypotheses. A defect in multiciliogenesis, for example, can result in stumpy or less cilia with a weaker stroke power (Neugebauer, Amack et al. 2009; Dubaissi and Papalopulu 2011). Furthermore, defects in ciliary motility due to lack of dynein, which is a key component of motile cilia, can cause impaired fluid flow (Satir 1980; Colantonio, Vermot et al. 2009; Vick, Schweickert et al. 2009). The decline in *dnah9* mRNA levels of Suv4-20h morphants together with the compromised fluid flow is in good agreement with studies by Vick et al. (2009). This report has demonstrated that *dnah9* depletion reduced motility of epidermal cilia without affecting the ciliation (Vick, Schweickert et al. 2009). Furthermore, molecular results (*foxj1, mci*) from the present loss-of-function studies explain the observed ciliary phenotype in a consistent manner. Taken together, my findings implicate that Suv4-20h-depletion inhibits the expression of multiciliogenic genes required for normal cilia length, number and motility resulting in reduced fluid flow on the knockdown side. This is also supported by electron microscopy pictures of the larval epidermis showing the compromised cilia tufts (Nicetto 2012).

However, contributions from other signaling pathways cannot be excluded yet. Recent work by Walentek et al. has linked serotonin-secreting cells (SSC) in the frog epidermis to cilia motility. Serotonin has effects on non-motile and motile cilia (Brailov, Bancila et al. 2000; Whitfield 2004). It induces the ciliogenesis of motile cilia and regulates the beating frequency (Beyer, Danilchik et al. 2012; Walentek, Bogusch et al. 2014). Inhibition of serotonin synthesis impaired cilia motility and weakened flow rate in the frog skin (Walentek, Bogusch et al. 2014). If epidermal cilia motility is stimulated also by serotonin, the ciliogenic defect in Suv4-20h morphants could also be indirect, for instance, due to reduced serotonin production or reduced SSC specification.

Furthermore, fluid flow is dependent on the orientation of cilia, which is regulated by the planar cell polarity pathway (PCP). Cilia are polarized in a sequential fluid flow-mediated

manner: PCP signaling sets the initial orientation that is followed by a refining flow-mediated step (positive feedback loop) provided that cilia are motile (Mitchell, Jacobs et al. 2007). Defects of the PCP pathway and cilia polarization can impair cilia-driven fluid flow (Konig and Hausen 1993; Park, Mitchell et al. 2008). Cilia orientation can be assessed by microinjection of mRNA encoding two proteins fused to fluorescent tag that localize either to the basal body (Centrin-RFP) or to the striated rootlet (Clamp-GFP). The trajectory of the straight line between the rootlet and BB of each cilium provides the direction of effective stroke. It is hereby important to investigate whether all trajectories are properly aligned within one cell (Mitchell, Stubbs et al. 2009). In this way, epidermal cilia orientation of Suv4-20h1 morphants can be visualized.

5.2 Are Suv4-20h enzymes obligatory regulators of ciliogenesis?

Multicilia are generated in vertebrates in the brain ventricles, airways, kidneys, the reproductive system and the epidermis. Monocilia on the contrary are found in the auditory organ and the gastrocoel roof plate (GRP) (Choksi, Lauter et al. 2014). In the following, my data from other ciliated tissues, such as the GRP, otic vesicle and pronephric kidney will be discussed.

Cilia in the GRP are transiently assembled and produce a fluid flow by rotational ciliary beating that induces organ laterality (Vick, Schweickert et al. 2009). There is yet no significant evidence that Suv4-20h enzymes perturb ciliogenesis of single motile cilia, for example in the *Xenopus* GRP. Suv4-20h1 morpholino injected embryos showed non-significant ($p=0.15$) reduction of cilia length (2.86±0.7µm, n=87) compared to uninjected (3.8±0.04µm, n=70) and control morpholino injected (3.8±0.9µm, n=97) embryos (Appendix Fig. S1). Although there was no major disturbance in organ arrangement, Suv4-20h1 morphants showed an abnormal leftward pointing of the gut coil compatible with a weak situs defect. Unfortunately, the analysis of GRP cilia could not be continued due to technical problems with the electron microscope used.

Another monociliated tissue is the inner ear. According to a recent report in zebrafish both motile cilia and immotile kinocilia are present in the auditory vesicles, also known as otic vesicles (Stooke-Vaughan, Huang et al. 2012). It was demonstrated that ciliary motility contributes to a normal otholith biogenesis and localization. Otholiths are mineralized

structures inside the inner ear and are necessary for sensation of gravity and linear acceleration (Colantonio, Vermot et al. 2009; Stooke-Vaughan, Huang et al. 2012). Tests in zebrafish have demonstrated that the knockdown of *dnah9* disrupts cilia motility causing defects in otolith assembly (Colantonio, Vermot et al. 2009). Motile cilia are also present in the *Xenopus* otic vesicles demonstrated by the expression of motile cilia-components, such as *dnah9* and *radial spoke protein 3* (*RSP3*) (Zhang, Zhao et al. 2013). Preliminary data from injection of Suv4-20h1 mopholino also suggest ciliogenic defects in the otic vesicles where *rfx2* and *dnah9* expression was diminished or even eliminated in the knockdown side (data not shown). Further tests with molecular markers and histological analysis of sections would clarify the role of Suv4-20h enzymes in inner ear ciliogenesis and otolith formation.

5.2.1 Suv4-20h1 HMT regulates ciliogenesis in the embryonic kidney

In the course of my work, I have observed that ciliogenic genes are misregulated in the forming pronephros, in addition to the epidermis. Ciliary genes are usually expressed in MCCs in three multiciliated funnels, called nephrostomes. Similar to epidermis, candidate genes, such as *mci*, *foxj1* and *dnah9* were investigated for their possible involvement in pronephric ciliogenesis.

All genes of interest were strongly compromised in the pronephric nephrostomes. *Mci* is transiently expressed in the *Xenopus* larval skin from gastrulation until late neurula, when MCCs differentiate (Stubbs, Vladar et al. 2012). It then disappears from the skin, except in the gill and forehead areas. At early tailbud stage (NF 28), *mci* is re-expressed in the nephrostomes until the late tailbud stage (NF 32). In RNA *in situ* hybridization, the *mci* expression in the Suv4-20h1-MO injected cohort was highly affected (≥90%). In half of the affected embryos, the expression in the nephrostomes and the skin was even lost.
Foxj1 and *dnah9* mRNA expression was similarly affected (90%). These observations are comparable to reports by Yu et al. (2008), where the pronephros of Foxj1a deficient zebrafish embryos lacked the expression of motile ciliogenic genes, including *dnah9* (Yu, Ng et al. 2008). Consequently, loss of *foxj1* and *dnah9* compromises the formation of motile cilia (Stubbs, Oishi et al. 2008; Yu, Ng et al. 2008; Vick, Schweickert et al. 2009; Hagenlocher, Walentek et al. 2013). It is noteworthy that in this thesis, *foxj1* showed a weaker phenotype than *dnah9* supporting the dose-dependent function of *foxj1*. Stubbs et al. pointed out that

epidermal cilia were lost upon a strong reduction of *foxj1* protein levels, while cilia were only impaired in length and number upon a weak reduction at medium to low doses (Stubbs, Oishi et al. 2008). In most of the Suv4-20h1 morphants, *foxj1* was downregulated, whereas *dnah9* was robustly eliminated (80%). The evidence for a specific effect of Suv4-20h enzymes was provided, when the epidermal cilia phenotype could be rescued by coinjection of Suv4-20h1/h2 MO and murine Suv4-20h1/h2 mRNA (Nicetto 2012). The Suv4-20h1-depleted pronephric phenotype was also rescued by co-injection of Suv4-20h1 morpholino with murine Suv4-20h1 mRNA. *Dnah9* expression in the rescue cohort clearly recovered compared to the Suv4-20h1 knockdown cohort showing that the Suv4-20h MO works specifically for more than one phenotype. In this context, the prominent downregulation of ciliary genes in the pronephric nephrostomes of the Suv4-20h1 depleted cohort suggests a general requirement of Suv4-20h1 HMT for multiciliogenesis (Fig. 4.14).

Kidney development depends critically on the transcription factors *xlim-1* and *pax2*, which control specification of the organ anlage and tubule formation, respectively. The transcription factor *xlim-1* is first detected in the pronephric anlagen of late gastrula embryos and is therefore the earliest marker with nephrogenic potential (Taira, Otani et al. 1994). During neurula stages, the pronephric anlage will give rise to the capsule, tubule and duct primordiae, which in turn will differentiate into the epithelial lining of the tubules and duct. Around early tailbud stage, tubules are differentiated (Brandli 1999). *Pax2* is a transcription factor expressed in the pronephric tubules and duct and controls the transition from mesenchyme to epithelium (Taira, Otani et al. 1994; Heller and Brandli 1997; Brandli 1999). Moreover, analysis in mice has revealed that *pax2* is required for the differentiation of intermediate mesoderm and that *pax2* deficiency prevents kidney formation (Torres, Gomez-Pardo et al. 1995). It was shown in zebrafish that *pax2* is additionally necessary to maintain the pronephric cell fate. Loss of *pax2* resulted in the absence of pronephric tubules suggesting a role for *pax2* in tubule differentiation as well (Majumdar, Lun et al. 2000).

It is important to exclude possible failure of kidney specification and differentiation as a modifying cause for the dysregulation of the above studied ciliary genes. If pronephic development was impaired, nephrostome formation could be inhibited and ciliary markers would be absent. *Xlim-1* and *pax2* were examined at two time points during kidney development (neurula and late tailbud stage). Suv4-20h1 MO injection clearly did not alter *xlim-1* expression suggesting that kidney specification was unaffected. Additionally, despite

the downregulation of the ciliary genes in the nephrostomes, the pronephric and ductal *pax2* expression was present. This indicates that kidney specification and differentiation is not compromised and that the downregulation of pronephric multiciliogenesis is rather due to the specific inhibition of ciliogenesis by Suv4-20h1 MO, comparable to the cilia phenotype in the skin.

5.2.2 Cilia and pronephric tubule formation

The nephron, the functional unit of the pronephros, is segmented into glomus, coelom, nephrostome, proximal tubule, intermediate tubule, distal tubule and duct from anterior to porterior (Wessely and Tran 2011). Pronephric tubule epithelia undergo maturation and terminal differentiation around NF 30. Pronephros maturation involves formation of the lumina, cell proliferation and functional maturation, including the appearance of ion channels and transporters. The embryonic kidney is fully functional after NF 37/38 when blood supply of the nephron has started (Brandli 1999; Wessely and Tran 2011). The frog kidney contains two types of cilia, which are spatially separated. As mentioned before, multiciliated cells are located in the nephrostomes and transport urinary filtrate into the tubules. Primary cilia, on the contrary, line up the tubule and duct and are credited with sensory functions (Mobjerg, Larsen et al. 2000; Tran, Pickney et al. 2007).

There are two monoclonal antibodies (mab), where antigens are differentially expressed in the pronephric kidney. The mab 3G8 recognizes an antigen on the luminal membrane of nephrostomes and proximal tubules from NF 31 onwards, while 4A6 binds to an epitope that localizes to the entire cell surface of the distal tubules and duct from NF 37/38 onwards (Vize, Jones et al. 1995; Brennan, Nijjar et al. 1998). As shown in Fig. 4.19, 3G8 and 4A6 staining was strongly reduced, whereas *xlim-1* and *pax2* were expressed both in controls as well as in morpholino treated specimen. Taken together, these data suggest that Suv4-20h1 is critical for the formation of the pronephric tubules and duct. The specification of the pronephros anlage is not affected *per se*, since the tubule differentiation marker *pax2* is expressed in its normal location. However, in the Suv4-20h1 injected side cells fail to undergo proper terminal tubule differentiation displayed by the 3G8 and 4A6 staining.

Although Suv4-20h morphants show higher rate of apoptosis and reduced cell proliferation (Nicetto, Hahn et al. 2013), the remaining *pax2* expression argues strongly against a complete suppression of pronephric kidney.

Another and more likely explanation is based on a report of Vasilyev and co-workers. According to Vasilyev, cilia-driven fluid flow is needed for the proximal-directed collective cell migration in zebrafish pronephros development (Vasilyev, Liu et al. 2009). In *Xenopus* kidney development, a posterior to anterior morphogenetic cell movement also shapes the proximal tubule (Nieuwkoop and Faber 1994). Similar to zebrafish, cilia-dependent fluid flow may be linked to the extension and differentiation of the proximal pronephros in *Xenopus*. The slower fluid flow on the skin surface of Suv4-20h1 depleted morphants suggests that pronephric fluid flow may be impaired as well given that multiciliogenesis is inhibited. Since nephrostome formation (NF 28) precedes the onset of tubule differentiation (NF30) (Heller and Brandli 1997), inhibition of multiciliogenesis may weaken fluid flow and thus cause defects in tubular differentiation.

Indeed, observation of dilated tubules in Suv4-20h1 morphants indicates that cilia-driven fluid flow is affected. Additionally, these morphant embryos developed dramatic edema (Fig. 4.20). These data are comparable to a report by Tran et al. (2007) who demonstrated that *Xenopus* Bicaudal-C depleted embryos developed a phenotype similar to PKD (polycystic kidney disease) with expanded tubules and large edema due to defects in pronephric differentiation (Tran, Pickney et al. 2007). PKD is a common disease affecting one in 1000 humans. Cysts are caused by extremely dilated tubule lumina and patients with PKD develop multiple cysts, which can drastically interfere with kidney function, eventually leading to organ failure. Recent work has linked cilia and cystic diseases. Furthermore, a variety of genes mutated in cystic diseases, such as polycystin 1, polycystin 2, inversin, polaris and pkd2, are localized to cilia or associated to ciliogenesis (Drummond 2005). Kramer-Zucker et al. (2005) reported that cilia-driven fluid flow is necessary for a normal kidney development in zebrafish. Knockdown of *dhc9* (dynein heavy chain 9) homologous to *Xenopus dnah9* led to impaired cilia motility, reduced fluid flow, tubule distention and cysts formation (Kramer-Zucker, Olale et al. 2005). Interestingly, these zebrafish cysts mutants also revealed a curved body axis comparable to Suv4-20h1 morphants. The related pronephric phenotype to zebrafish *dhc9* depleted embryos implies that the enlarged tubules and severe edema of Suv4-20h1 morphants are due to downregulation of *dnah9. Dnah9* deficiency disturbed cilia

motility and hence fluid flow generated in the nephrostomes was impaired. This in turn resulted in fluid accumulation and edema.

General mesodermal (Xbra, VegT) and skeletal muscle (MyoD) genes were normally expressed in Suv4-20h-double morphants (Nicetto, Hahn et al. 2013). However, kidney markers have not been assessed. My data shows, there is a defect in pronephros implicating that Suv4-20h functions are not germlayer restricted and confer additional aspects than exit from pluripotency.

5.3 Suv4-20h HMTases impact microRNA miR-449 production

As reported by multiple studies, Notch signaling is important for both pronephros formation and multiciliogenesis (McLaughlin, Rones et al. 2000; Liu, Pathak et al. 2007; Marcet, Chevalier et al. 2011; Wang, Fu et al. 2013). Very recently, a direct inhibitor of the Delta/Notch signaling has been shown to be an essential factor that induces multiciliogenesis. This factor is the microRNA miR-449 (Marcet, Chevalier et al. 2011). MicroRNAs are small (23 nucleotides) non-coding RNAs, which silence protein expression by complementary base pairing between the seed region of the miRNA and the target mRNA at the 3'-UTR. Thereby, translational blocking, mRNA destabilization or a combination of both mechanisms occurs (Bartel 2009). Interestingly, the host gene for miR-449, which is CDC20B, is located next to a region, where *mci* is encoded (Lize, Klimke et al. 2011; Stubbs, Vladar et al. 2012).

MiR-449 and ciliogenic genes are co-localized in the multiciliated cells of the nephrostomes and the larval skin. Depletion of miR-449 blocks multiciliogenesis in both the nephrostomes and the epidermis (Marcet, Chevalier et al. 2011). In this thesis, the effects upon Suv4-20h1 ablation were identical to those observed after miR-449 knockdown suggesting a link between them. Indeed, miR-449 expression was abolished in the nephrostomes of Suv4-20h1 depleted embryos (Fig. 4.17). The absent miR-449 expression is in line with the above-mentioned increase in *dll1* levels after Suv4-20h1 ablation in MCPs and pronephros respectively (see Appendix Fig. S2). Since *dll1* downregulation is necessary for the normal MCC differentiation, multiciliogenesis was impaired in both the epidermis and the nephrostomes of Suv4-20h1 morphants. These results argue strongly that multiciliogenesis depends on the induction of miR-449 by Suv4-20h enzymes.

The epidermal miR-449 phenotype of Suv4-20h1 deficient embryos was weaker compared to the pronephric phenotype. MCPs increased in the epidermis, which is comparable to findings by Marcet et al. (2011), but quantitative analysis of miR-449 levels remains to be performed. It is expected that miR-449 mRNA levels will decline since *dll1* is elevated in the skin of Suv4-20h1 morphants. As mentioned before, MCPs are increased, presumably, because more cells are committed by the *cis*-inhibition of Notch (Jacobsen, Brennan et al. 1998; Deblandre, Wettstein et al. 1999; Marcet, Chevalier et al. 2011b).

MiR-449 and miR-34 belong to the same family of microRNAs and share the seed sequence. Thus, they are predicted to target similar mRNAs, since the seed region is central for the interaction between miRNA and the mRNA target (Cardinaud, Moreilhon et al. 2009; Marcet, Chevalier et al. 2011). The miR-34 family of microRNAs is an important component of the p53 tumor suppressor network (He, He et al. 2007). Furthermore, it has been described as regulator of multiciliogenesis through *cmyb* in the zebrafish pronephros (Wang, Fu et al. 2013). The miR-34 family of microRNAs is also enriched in the ciliated epidermis of *Xenopus* (Marcet, Chevalier et al. 2011). In my experiments, Suv4-20h1 protein knockdown results in downregulation of miR-34b in the nephrostomes. This cohort is also *mci, foxj1* and *dnah9* deficient. Taken together, this leads to the assumption that Suv4-20h1 HMT also regulates other microRNAs, e.g. miR-34b, during MCC formation in the *Xenopus* pronephros.

Together, these observations lead us to a model for how Suv4-20h might be involved in multiciliogenesis (see Fig. 5.1). In this model, Suv4-20h enzymes regulate ciliated cell fate specification during gastrula and neurula stages via the Delta/Notch pathway. MicroRNA miR-449 appears to be the major link between Suv4-20h and the Delta/Notch signaling. Suv4-20h enzymes are thought to provide high levels of miR-449. If embryos are Suv4-20h deficient, miR-449 is strongly repressed. Since Suv4-20h HMTases catalyze repressive methylation marks (Schotta, Lachner et al. 2004), the enzymes cannot promote miR-449 production directly, but rather indirectly through one or more yet unknown factor(s) (Fig. 5.1b).

While miR-449 is ablated in the nephrostomes, it is not ablated in the epidermis. Therefore, two factors are postulated, which are termed as “X” and “Y” to avoid that there is only one single factor/pathway in which Suv4-20h enyzmes may regulate multiciliogenesis. These factors could be the same, but they do not have to be the same, since they are acting in two

different tissues. Possible factors for "X" are genes that might regulate miR-449/CDC20B induction. To date, no activator of miR-449/CDC20B in the mucociliary epithelium has been reported. Those factors might be Sox7, Sox17, FoxJ1 and other Fox-factors (FoxA1, FoxA2, FoxM1, FoxF1) (Maeda, Dave et al. 2007; Lize, Klimke et al. 2011). Oct-25 may be a possible factor connecting the Suv4-20h enzymes to the compromised ciliogenesis and may represent "Y". Oct-25 mRNA is normally restricted to pluripotent cells, but it is sustained throughout the ectoderm in Suv4-20h double morphants beyond its physiological temporal expression (Nicetto, Hahn et al. 2013). Therefore, persistent *oct-25* levels may interfere with cilia differentiation.

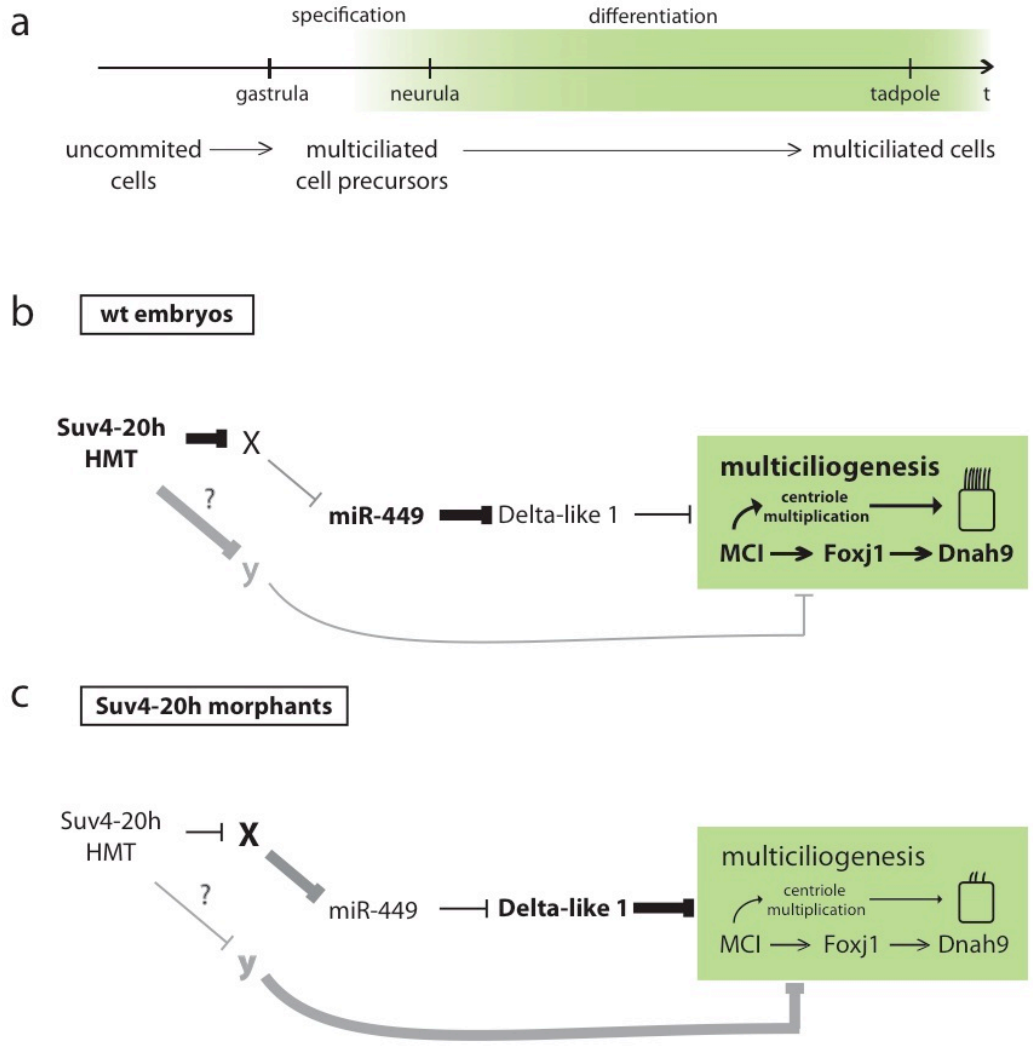

Fig 5.1: Model of the Suv4-20h HMTases function. a: timeline for the formation of multiciliated cells in the *Xenopus* epidermis. **b:** proposed function of Suv4-20h HMTases in wildtype embryos. **c:** Suv4-20h HMTases function in Suv4-20h morpholino injected embryos. Grey color depicts pathways that have yet to be identified. "Y" indicates an auxiliary pathway that can inhibit multiciliogenesis. Thickness of lines depicts effect power.

This rise in miR-449 secures low *dll1* levels after fate specification. This is important for a normal MCC differentiation and high levels of *dll1* inhibit ciliogenesis as demonstrated by *mci*, *foxj1, dnah9* and acetylated α–tubulin downregulation. It is not clear why suppressed levels of *dll1* mRNA are necessary in MCPs to promote ciliogenesis, but one explanation could be that *dll1* may act cell-autonomously and block multiciliogenesis within the same cell by yet unknown mechanisms (Deblandre, Wettstein et al. 1999; Marcet, Chevalier et al. 2011).

Other studies have revealed a role for miR-449 in various significant events, including cell cycle progression, differentiation and apoptosis (Lize, Klimke et al. 2011). MiR-449 is thought to be a tumor-suppressive miRNA and was also related to prostate and gastric cancer (Lize, Herr et al. 2010). Interestingly, H4K20me3 is also correlated to cancer progression (Fraga, Ballestar et al. 2005).

Data in this thesis collectively suggest for the first time a link between Suv4-20h HMTases, H4K20me2/me3 and microRNAs. This model can be validated by analysis of the global H4K20me3 distribution and identifying direct target genes of the Suv4-20h enzymes. Afterwards, target genes could be further tested to infer effects on the miR-449 host gene *cdc20b*. Via miR-449, Suv4-20h HMTases might regulate a whole series of events, including cancer development. This important finding opens up new future directions for the analysis of Suv4-20h enzymes function.

5.4 Conclusions and future directions

Cilia-related disorders can affect many organ systems and underlie a broad spectrum of human diseases. It is therefore a primary concern to understand how cilia formation is regulated. In this dissertation, I have investigated the role of the Suv4-20h histone methyltransferases in ciliogenesis in various tissues. The following are the main research contributions of this dissertation.

The data presented here demonstrate a specific requirement for Suv4-20h enzymes in ciliogenesis, especially in multiciliogenesis, for epidermis and kidney. In the epidermis, two different phenotypes are observed. First, Suv4-20h morphants display an increased MCP fate

selection suggesting that Suv4-20h HMTases restrict MCP numbers via the Delta/Notch pathway. Second, on the level of the individual cell, multiciliogenic and axonemal genes - *mci*, *foxj1*, *dnah9* and *acetylated α–tubulin* - are reduced indicating problems with centriole amplification and/or axoneme formation.
In the kidney, similarly to the epidermis, Suv4-20h enzymes are required to drive multiciliogenesis. Markers for multiciliogenesis, such as miR-449, *mci*, *foxj1* and *dnah9* are strongly compromised in the nephrostomes and tubular markers 3G8 and 4A6 reveal a problem with proximal and distal tubulogenesis.

Suv4-20h-related ciliary phenotypes are functionally relevant as demonstrated by the strong impairment of the cilia-driven fluid flow on the epidermal surface and the development of a massive general edema consistent with compromised pronephric cilia function. The embryonic skin of *Xenopus* is similar to the human airway epithelium indicating that the Suv4-20h phenotypes could also be clinically relevant.

My data place Suv4-20h HMTases upstream of both miR-449 and Dll1 in the genetic cascade of multiciliogenesis. This work provides the first evidence that cilia formation, specifically multiciliogenesis, is connected to the epigenome.

Future research will be needed to fully understand the mechanisms that convey the Suv4-20h activity. A focus in future studies should be a genome-wide analysis of candidate target genes that link Suv4-20h enzymes to ciliogenesis. Particularly, direct and indirect interactions between Suv4-20h and miR-449 will be important. The search for a direct target gene using the methods in this work had limitations, since only a restricted number of genes could be tested. Nevertheless, this approach was important, since the genes that were identified here can guide genome-wide studies to establish an epistatic network ranging from Suv4-20h activity, enrichment of H4K20me2/me3 marks to misregulation of cilia structural genes or factors that regulate the ciliogenic pathway. RNA sequencing (RNA-Seq) on control and morphant animal caps, which form epidermis in isolation, would be important to investigate the Suv4-20h contribution to ciliogenesis. Additionally, ChIP-Seq for H4K20me3 would help to examine whether specific regions/genes involved in ciliogenesis and/or ciliopathies are decorated by this modification and detect changes upon Suv4-20h depletion.

Genome-wide analyses, such as RNA-Seq or ChIP techniques, are available for the related *Xenopus tropicalis*, because its genome has been almost fully sequenced. Genes that are down- or upregulated in response to Suv4-20h protein depletion will be of special attention as possible direct target genes and interaction partners of the Suv4-20h enzymes.

It would be useful to raise antibodies for *Xenopus* Suv4-20h HMTases for future research. They could be used to perform both genome wide analysis (ChIP-Seq) and biochemical approaches (mass spectrometry), e.g. to study whether Suv4-20h1 and -h2 interact with specific factors in the ciliogenic program. Such questions could be addressed in both animal caps and whole embryo samples by immunoprecipitation with Suv4-20h1 or –h2 antibody and mass spectrometry analysis on immunoprecipitated proteins.

Studies in the epidermis and kidney have given first clues of Suv4-20h enzymes' impact on ciliogenesis. It would be important to further investigate whether Suv4-20h enzymes have a role during monocilium formation (GRP, otic vesicles) beside their role during multiciliogenesis. Also in the context of cilia-related disorders, it might be helpful to investigate the Suv4-20h effects in these tissues, which are often associated with ciliopathies (GRP, otic vesicles, brain ventricles, kidneys and lungs).

An important aspect of future investigations regards the study of the ciliogenic potential of Suv4-20h enzymes in mammalian models, including the human airway epithelial cells, where ciliogenesis can be studied *in vitro* at the air-liquid interface. The mouse model can also be considered to study the Suv4-20h enyzme role within the formation of the mucociliary epithelium, especially, since Suv4-20 dn mice displayed lung defects (Schotta, Sengupta et al. 2008).

The results of my thesis define Suv4-20h enzymes as relevant and specific regulators of the multiciliogenic differentiation program. They contribute a level of epigenetic control that works upstream of known ciliogenic regulatory proteins. Given the broad impact of epigenetic mechanisms on normal and pathological physiology, it is conceivable that this finding may have a profound impact on our understanding of why a growing number of human diseases show defects in cilia formation.

APPENDIX

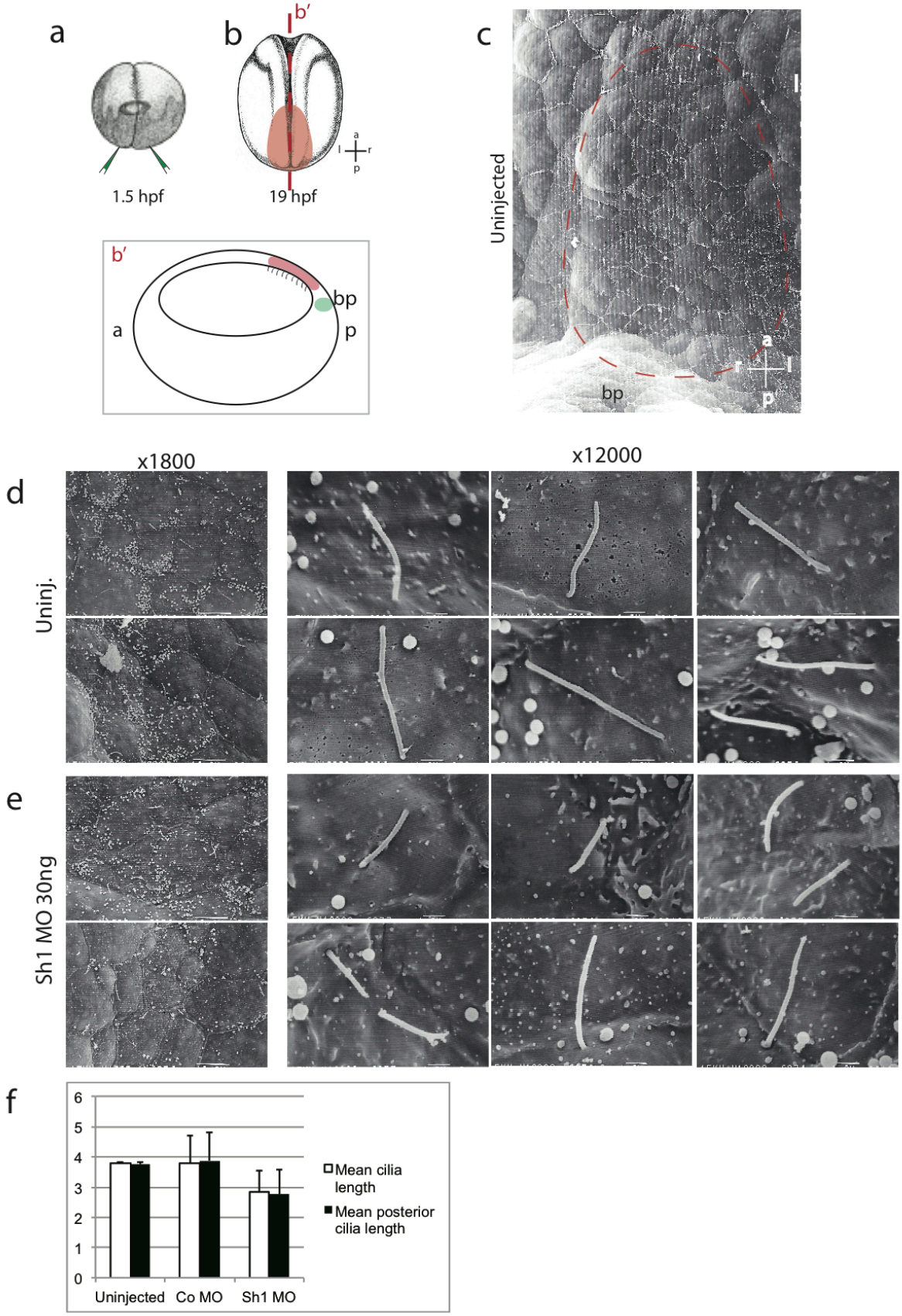
a
b
b′
1.5 hpf
19 hpf
a
p
l
r
b′
bp
a
p
c
Uninjected
bp
a
p
l
r
x1800
x12000
d
Uninj.
e
Sh1 MO 30ng
f
6
5
4
3
2
1
0
Uninjected
Co MO
Sh1 MO
Mean cilia length
Mean posterior cilia length

Fig. S1 Analysis of GRP cilia after Suv4-20h1 depletion
a: injection into the dorsal marginal zone of both blastomeres at two-cell stage. **b:** Graphic depicting the ciliated area of the gastrocoel roof plate (GRP) in red. Sagittal section as marked by red dashed line (**b'**). **c:** SEM picture of a GRP explant at neurula stage (NF 17/18), GRP is marked in red. **d,e:** SEM pictures of GRP monocilia in uninjected and Suv4-20h1 MO injected embryos. **f:** mean cilia length of all GRP cilia and mean cilia length of cilia that are located at the posterior part of the cell. Uninjected (70/2; total number of cilia counted in number of embryos), Co MO (97/4), Suv4-20h1 MO (87/4). Lengths in µm. Error bars represent SD. a: anterior, p: posterior, l: left, r: right, bp: blastoporus. Scale bars in x1800, 10µm. Scale bars in x12000, 1µm.

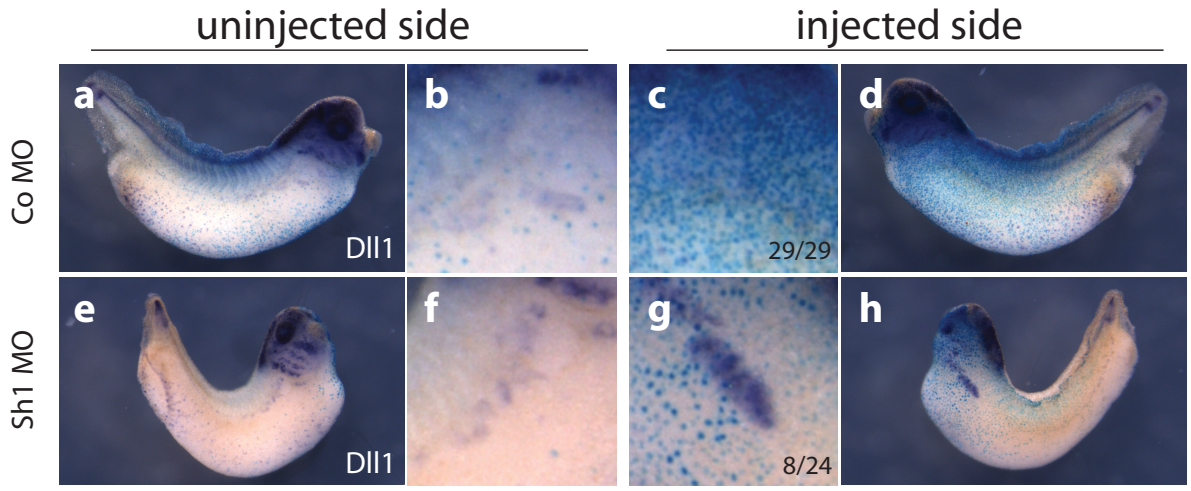

Fig. S2 Suv4-20h1 depletion upregulates delta-like 1 expression in the pronephros. RNA *in situ* hybridization of NF 33 embryos. First two columns represent uninjected sides of embryos. Last two columns show the injected sides visualized by lacZ staining. **a-d:** *Dll1* expression in the pronephros is physiologically lost at NF 33. **e-h:** *Dll1* expression in the injected side of Suv4-20h1 depleted embryos is sustained (n=two independent experiments).

REFERENCES

Afzelius, B. A. (1976). "A human syndrome caused by immotile cilia." Science **193**(4250): 317-319.

Allfrey, V. G., R. Faulkner, et al. (1964). "Acetylation and Methylation of Histones and Their Possible Role in the Regulation of Rna Synthesis." Proc Natl Acad Sci U S A **51**: 786-794.

Bartel, D. P. (2009). "MicroRNAs: target recognition and regulatory functions." Cell **136**(2): 215-233.

Beyer, T., M. Danilchik, et al. (2012). "Serotonin signaling is required for Wnt-dependent GRP specification and leftward flow in Xenopus." Curr Biol **22**(1): 33-39.

Billett, F. and R. Gould (1971). "Fine structural changes in the differentiating epidermis of Xenopus laevis embryos." J Anat **108**(Pt 3): 465-480.

Bloodgood, R. A. (2010). "Sensory reception is an attribute of both primary cilia and motile cilia." J. Cell Sci. **123**(4): 505-509.

Blum, M., T. Beyer, et al. (2009). "Xenopus, an ideal model system to study vertebrate left-right asymmetry." Dev Dyn **238**(6): 1215-1225.

Boisvieux-Ulrich, E. and D. Sandoz (1991). "Determination of ciliary polarity precedes differentiation in the epithelial cells of quail oviduct." Biol Cell **72**(1-2): 3-14.

Brailov, I., M. Bancila, et al. (2000). "Localization of 5-HT(6) receptors at the plasma membrane of neuronal cilia in the rat brain." Brain Res **872**(1-2): 271-275.

Brandli, A. W. (1999). "Towards a molecular anatomy of the Xenopus pronephric kidney." Int J Dev Biol **43**(5): 381-395.

Brennan, H. C., S. Nijjar, et al. (1998). "The specification of the pronephric tubules and duct in Xenopus laevis." Mech Dev **75**(1-2): 127-137.

Cardinaud, B., C. Moreilhon, et al. (2009). "miR-34b/miR-34c: a regulator of TCL1 expression in 11q- chronic lymphocytic leukaemia?" Leukemia **23**(11): 2174-2177.

Chilvers, M. A. and C. O'Callaghan (2000). "Local mucociliary defence mechanisms." Paediatr Respir Rev **1**(1): 27-34.

Choksi, S. P., G. Lauter, et al. (2014). "Switching on cilia: transcriptional networks regulating ciliogenesis." Development **141**(7): 1427-1441.

Chu, D. and M. Klymkowsky (1989). "The appearance of acetylated alpha-tubulin during early development and cellular differentiation in Xenopus." Dev Biol **136**(1): 104-117.

Chung, M. I., S. M. Peyrot, et al. (2012). "RFX2 is broadly required for ciliogenesis during vertebrate development." Dev Biol **363**(1): 155-165.

Colantonio, J. R., J. Vermot, et al. (2009). "The dynein regulatory complex is required for ciliary motility and otolith biogenesis in the inner ear." Nature **457**(7226): 205-209.

Dale, L., G. Matthews, et al. (1993). "Secretion and mesoderm-inducing activity of the TGF-beta-related domain of Xenopus Vg1." EMBO J **12**(12): 4471-4480.

Dambacher, S., M. Hahn, et al. (2010). "Epigenetic regulation of development by histone lysine methylation." Heredity (Edinb) **105**(1): 24-37.

Davey, C. A., D. F. Sargent, et al. (2002). "Solvent mediated interactions in the structure of the nucleosome core particle at 1.9 a resolution." J Mol Biol **319**(5): 1097-1113.

Deblandre, G., D. Wettstein, et al. (1999). "A two-step mechanism generates the spacing pattern of the ciliated cells in the skin of Xenopus embryos." Development **126**(21): 4715-4728.

Dirksen, E. R. (1991). "Centriole and basal body formation during ciliogenesis revisited." Biol Cell **72**(1-2): 31-38.

Drummond, I. A. (2005). "Kidney development and disease in the zebrafish." J Am Soc Nephrol **16**(2): 299-304.

Drysdale, T. A. and R. P. Elinson (1992). "Cell Migration and Induction in the Development of the Surface Ectodermal Pattern of the Xenopus laevis Tadpole." Development, Growth & Differentiation **Volume 34**(Issue 1): 51–59.

Dubaissi, E. and N. Papalopulu (2011). "Embryonic frog epidermis: a model for the study of cell-cell interactions in the development of mucociliary disease." Dis. Model. Mech. **4**(2): 179-192.

Dubaissi, E., K. Rousseau, et al. (2014). "A secretory cell type develops alongside multiciliated cells, ionocytes and goblet cells, and provides a protective, anti-infective function in the frog embryonic mucociliary epidermis." Development **141**(7): 1514-1525.

Eisen, J. S. and J. C. Smith (2008). "Controlling morpholino experiments: don't stop making antisense." Development **135**(10): 1735-1743.

Ezratty, E. J., N. Stokes, et al. (2011). "A role for the primary cilium in Notch signaling and epidermal differentiation during skin development." Cell **145**(7): 1129-1141.

Fawcett, D. W. (1954). "The study of epithelial cilia and sperm flagella with the electron microscope." Laryngoscope **64**(7): 557-567.

Feng, Q., H. Wang, et al. (2002). "Methylation of H3-lysine 79 is mediated by a new family of HMTases without a SET domain." Curr Biol **12**(12): 1052-1058.

Fliegauf, M., T. Benzing, et al. (2007). "When cilia go bad: cilia defects and ciliopathies." Nat Rev Mol Cell Biol **8**(11): 880-893.

Fortini, M. E. (2009). "Notch signaling: the core pathway and its posttranslational regulation." Dev Cell **16**(5): 633-647.

Fraga, M. F., E. Ballestar, et al. (2005). "Loss of acetylation at Lys16 and trimethylation at Lys20 of histone H4 is a common hallmark of human cancer." Nat Genet **37**(4): 391-400.

Gardner, K. E., C. D. Allis, et al. (2011). "Operating on chromatin, a colorful language where context matters." J Mol Biol **409**(1): 36-46.

Goldberg, A. D., C. D. Allis, et al. (2007). "Epigenetics: a landscape takes shape." Cell **128**(4): 635-638.

Gurdon, J. B. and N. Hopwood (2000). "The introduction of Xenopus laevis into developmental biology: of empire, pregnancy testing and ribosomal genes." Int J Dev Biol **44**(1): 43-50.

Gurdon, J. B., T. J. Mohun, et al. (1985). "All components required for the eventual activation of muscle-specific actin genes are localized in the subequatorial region of an uncleaved amphibian egg." Proc Natl Acad Sci U S A **82**(1): 139-143.

Hagenlocher, C., P. Walentek, et al. (2013). "Ciliogenesis and cerebrospinal fluid flow in the developing Xenopus brain are regulated by foxj1." Cilia **2**(1): 12.

Hansen, J. C. (2012). "Human mitotic chromosome structure: what happened to the 30-nm fibre?" EMBO J **31**(7): 1621-1623.

Hayes, J. M., S. K. Kim, et al. (2007). "Identification of novel ciliogenesis factors using a new in vivo model for mucociliary epithelial development." Dev Biol **312**(1): 115-130.

He, L., X. He, et al. (2007). "microRNAs join the p53 network--another piece in the tumour-suppression puzzle." Nat Rev Cancer **7**(11): 819-822.

Heasman, J. (2002). "Morpholino oligos: making sense of antisense?" Dev Biol **243**(2): 209-214.

Heller, N. and A. W. Brandli (1997). "Xenopus Pax-2 displays multiple splice forms during embryogenesis and pronephric kidney development." Mech Dev **69**(1-2): 83-104.

Hsiao, C. D., M. S. You, et al. (2007). "A positive regulatory loop between foxi3a and foxi3b is essential for specification and differentiation of zebrafish epidermal ionocytes." PLoS One **2**(3): e302.

http://www.omim.org/entry/209900. Retrieved April 11, 2014.

Ibanez-Tallon, I., A. Pagenstecher, et al. (2004). "Dysfunction of axonemal dynein heavy chain Mdnah5 inhibits ependymal flow and reveals a novel mechanism for hydrocephalus formation." Hum Mol Genet **13**(18): 2133-2141.

Jacobsen, T. L., K. Brennan, et al. (1998). "Cis-interactions between Delta and Notch modulate neurogenic signalling in Drosophila." Development **125**(22): 4531-4540.

Jones, C. M., M. R. Kuehn, et al. (1995). "Nodal-related signals induce axial mesoderm and dorsalize mesoderm during gastrulation." Development **121**(11): 3651-3662.

Jorgensen, S., G. Schotta, et al. (2013). "Histone H4 lysine 20 methylation: key player in epigenetic regulation of genomic integrity." Nucleic Acids Res **41**(5): 2797-2806.

Kasuya, K. and M. Miyoshi (2001). Fine Structure of Cilia and Basal Bodies, with Reference to the Mouse Trachea. Med. Bull. Fukuoka Univ. **28(1):** 29-36.

Klos Dehring, D. A., E. K. Vladar, et al. (2013). "Deuterosome-mediated centriole biogenesis." Dev Cell **27**(1): 103-112.

Knowles, M. R. and R. C. Boucher (2002). "Mucus clearance as a primary innate defense mechanism for mammalian airways." J Clin Invest **109**(5): 571-577.

Konig, G. and P. Hausen (1993). "Planar polarity in the ciliated epidermis of Xenopus embryos." Dev Biol **160**(2): 355-368.

Kouzarides, T. (2007). "Chromatin modifications and their function." Cell **128**(4): 693-705.

Kramer-Zucker, A. G., F. Olale, et al. (2005). "Cilia-driven fluid flow in the zebrafish pronephros, brain and Kupffer's vesicle is required for normal organogenesis." Development **132**(8): 1907-1921.

Kühl, M. and S. Gessert (2010). Entwicklungsbiologie. Stuttgart, UTB basics Ulmer.

Leopold, P. L., M. J. O'Mahony, et al. (2009). "Smoking is associated with shortened airway cilia." PLoS One **4**(12): e8157.

Lewis Wolpert, C. T. (2011). Principles of Development, Oxford University Press.

Li, M., G. H. Liu, et al. (2012). "Navigating the epigenetic landscape of pluripotent stem cells." Nat Rev Mol Cell Biol **13**(8): 524-535.

Liu, Y., N. Pathak, et al. (2007). "Notch signaling controls the differentiation of transporting epithelia and multiciliated cells in the zebrafish pronephros." Development **134**(6): 1111-1122.

Lize, M., C. Herr, et al. (2010). "MicroRNA-449a levels increase by several orders of magnitude during mucociliary differentiation of airway epithelia." Cell Cycle **9**(22): 4579-4583.

Lize, M., A. Klimke, et al. (2011). "MicroRNA-449 in cell fate determination." Cell Cycle **10**(17): 2874-2882.

Luger, K., M. L. Dechassa, et al. (2012). "New insights into nucleosome and chromatin structure: an ordered state or a disordered affair?" Nat Rev Mol Cell Biol **13**(7): 436-447.

Lyons, R. A., E. Saridogan, et al. (2006). "The reproductive significance of human Fallopian tube cilia." Hum Reprod Update **12**(4): 363-372.

Ma, M. and Y. J. Jiang (2007). "Jagged2a-notch signaling mediates cell fate choice in the zebrafish pronephric duct." PLoS Genet **3**(1): e18.

Maeda, Y., V. Dave, et al. (2007). "Transcriptional control of lung morphogenesis." Physiol Rev **87**(1): 219-244.

Majumdar, A., K. Lun, et al. (2000). "Zebrafish no isthmus reveals a role for pax2.1 in tubule differentiation and patterning events in the pronephric primordia." Development **127**(10): 2089-2098.

Marcet, B., B. Chevalier, et al. (2011b). "MicroRNA-based silencing of Delta/Notch signaling promotes multiple cilia formation." Cell Cycle **10**(17): 2858-2864.

Marcet, B., B. Chevalier, et al. (2011). "Control of vertebrate multiciliogenesis by miR-449 through direct repression of the Delta/Notch pathway." Nat Cell Biol **13**(6): 693-699.

Marshall, J. D., R. T. Bronson, et al. (2005). "New Alstrom syndrome phenotypes based on the evaluation of 182 cases." Arch Intern Med **165**(6): 675-683.

McLaughlin, K. A., M. S. Rones, et al. (2000). "Notch regulates cell fate in the developing pronephros." Dev Biol **227**(2): 567-580.

Mikkelsen, T. S., M. Ku, et al. (2007). "Genome-wide maps of chromatin state in pluripotent and lineage-committed cells." Nature **448**(7153): 553-560.

Mir, A., M. Kofron, et al. (2007). "FoxI1e activates ectoderm formation and controls cell position in the Xenopus blastula." Development **134**(4): 779-788.

Mitchell, B., R. Jacobs, et al. (2007). "A positive feedback mechanism governs the polarity and motion of motile cilia." Nature **447**(7140): 97-101.

Mitchell, B., J. L. Stubbs, et al. (2009). "The PCP pathway instructs the planar orientation of ciliated cells in the Xenopus larval skin." Curr Biol **19**(11): 924-929.

Mobjerg, N., E. H. Larsen, et al. (2000). "Morphology of the kidney in larvae of Bufo viridis (Amphibia, Anura, Bufonidae)." J Morphol **245**(3): 177-195.

Morimoto, M., R. Nishinakamura, et al. (2012). "Different assemblies of Notch receptors coordinate the distribution of the major bronchial Clara, ciliated and neuroendocrine cells." Development **139**(23): 4365-4373.

Morrisey, E. and B. Hogan (2010). "Preparing for the first breath: genetic and cellular mechanisms in lung development." Dev Cell **18**(1): 8-23.

Munoz-Sanjuan, I. and A. H. Brivanlou (2001). "Early posterior/ventral fate specification in the vertebrate embryo." Dev Biol **237**(1): 1-17.

Neugebauer, J. M., J. D. Amack, et al. (2009). "FGF signalling during embryo development regulates cilia length in diverse epithelia." Nature **458**(7238): 651-654.

Nicetto, D. (2012). On the Way to Differentiation: Xenopus Suv4-20h Histone Methyltransferases Regulate the Transition from the Pluripotent to the Ectoderm Cell State. Fakultät für Biologie. München, Ludwig-Maximilians-Universität München. **PhD**.

Nicetto, D., M. Hahn, et al. (2013). "Suv4-20h histone methyltransferases promote neuroectodermal differentiation by silencing the pluripotency-associated Oct-25 gene." PLoS Genet **9**(1): e1003188.

Nieuwkoop, P. and J. Faber (1994). Normal Table of Xenopus laevis (Daudin). New York, Garland Publishing Inc.

Nieuwkoop, P. D. and J. Faber (1967). Normal table of Xenopus Laevis Amsterdam, The Netherlands, North Holland Publishing Co.

Nishino, Y., M. Eltsov, et al. (2012). "Human mitotic chromosomes consist predominantly of irregularly folded nucleosome fibres without a 30-nm chromatin structure." EMBO J **31**(7): 1644-1653.

Oh, E. C. and N. Katsanis (2012). "Cilia in vertebrate development and disease." Development **139**(3): 443-448.

Park, T. J., B. J. Mitchell, et al. (2008). "Dishevelled controls apical docking and planar polarization of basal bodies in ciliated epithelial cells." Nat Genet **40**(7): 871-879.

Pelletier, G. J., S. L. Brody, et al. (1998). "A human forkhead/winged-helix transcription factor expressed in developing pulmonary and renal epithelium." Am J Physiol **274**(3 Pt 1): L351-359.

Pohl, B. S. and W. Knochel (2004). "Isolation and developmental expression of Xenopus FoxJ1 and FoxK1." Dev Genes Evol **214**(4): 200-205.

Ramsay, R. G. and T. J. Gonda (2008). "MYB function in normal and cancer cells." Nat Rev Cancer **8**(7): 523-534.

Reiß, M. (2009). Facharztwissen HNO-Heilkunde: Differenzierte Diagnostik und Therapie. Heidelberg, Springer.

Rice, J. C., K. Nishioka, et al. (2002). "Mitotic-specific methylation of histone H4 Lys 20 follows increased PR-Set7 expression and its localization to mitotic chromosomes." Genes Dev **16**(17): 2225-2230.

Satir, P. (1980). "Structural basis of ciliary movement." Environ Health Perspect **35**: 77-82.

Satir, P. (1995). "Landmarks in cilia research from Leeuwenhoek to us." Cell Motil Cytoskeleton **32**(2): 90-94.

Satir, P. and S. T. Christensen (2007). "Overview of structure and function of mammalian cilia." Annu Rev Physiol **69**: 377-400.

Schneider, T. D., J. M. Arteaga-Salas, et al. (2011). "Stage-specific histone modification profiles reveal global transitions in the Xenopus embryonic epigenome." PLoS One **6**(7): e22548.

Schotta, G., M. Lachner, et al. (2004). "A silencing pathway to induce H3-K9 and H4-K20 trimethylation at constitutive heterochromatin." Genes Dev **18**(11): 1251-1262.

Schotta, G., R. Sengupta, et al. (2008). "A chromatin-wide transition to H4K20 monomethylation impairs genome integrity and programmed DNA rearrangements in the mouse." Genes Dev **22**(15): 2048-2061.

Sive, H. L., R. M. Grainger, et al. (2000). Early development of Xenopus laevis : a laboratory manual. Cold Spring Harbor, N.Y. :, Cold Spring Harbor Laboratory Press.

Stooke-Vaughan, G. A., P. Huang, et al. (2012). "The role of hair cells, cilia and ciliary motility in otolith formation in the zebrafish otic vesicle." Development **139**(10): 1777-1787.

Strahl, B. D. and C. D. Allis (2000). "The language of covalent histone modifications." Nature **403**(6765): 41-45.

Stubbs, J. L., L. Davidson, et al. (2006). "Radial intercalation of ciliated cells during Xenopus skin development." Development **133**(13): 2507-2515.

Stubbs, J. L., I. Oishi, et al. (2008). "The forkhead protein Foxj1 specifies node-like cilia in Xenopus and zebrafish embryos." Nat Genet **40**(12): 1454-1460.

Stubbs, J. L., E. K. Vladar, et al. (2012). "Multicilin promotes centriole assembly and ciliogenesis during multiciliate cell differentiation." Nat Cell Biol **14**(2): 140-147.

Summerton, J. E. (2007). "Morpholino, siRNA, and S-DNA compared: impact of structure and mechanism of action on off-target effects and sequence specificity." Curr Top Med Chem **7**(7): 651-660.

Taira, M., H. Otani, et al. (1994). "Expression of the LIM class homeobox gene Xlim-1 in pronephros and CNS cell lineages of Xenopus embryos is affected by retinoic acid and exogastrulation." Development **120**(6): 1525-1536.

Takebayashi-Suzuki, K., N. Arita, et al. (2007). "The Xenopus POU class V transcription factor XOct-25 inhibits ectodermal competence to respond to bone morphogenetic protein-mediated embryonic induction." Mech Dev **124**(11-12): 840-855.

Tan, F. E., E. K. Vladar, et al. (2013). "Myb promotes centriole amplification and later steps of the multiciliogenesis program." Development **140**(20): 4277-4286.

Tollervey, J. R. and V. V. Lunyak (2012). "Epigenetics: judge, jury and executioner of stem cell fate." Epigenetics **7**(8): 823-840.

Torres, M., E. Gomez-Pardo, et al. (1995). "Pax-2 controls multiple steps of urogenital development." Development **121**(12): 4057-4065.

Tran, U., L. M. Pickney, et al. (2007). "Xenopus Bicaudal-C is required for the differentiation of the amphibian pronephros." Dev Biol **307**(1): 152-164.

Turner, B. M. (2005). "Reading signals on the nucleosome with a new nomenclature for modified histones." Nat Struct Mol Biol **12**(2): 110-112.

Vasilyev, A., Y. Liu, et al. (2009). "Collective cell migration drives morphogenesis of the kidney nephron." PLoS Biol **7**(1): e9.

Vick, P., A. Schweickert, et al. (2009). "Flow on the right side of the gastrocoel roof plate is dispensable for symmetry breakage in the frog Xenopus laevis." Dev Biol **331**(2): 281-291.

Vize, P. D., E. A. Jones, et al. (1995). "Development of the Xenopus pronephric system." Dev Biol **171**(2): 531-540.

Vize, P. D., D. W. Seufert, et al. (1997). "Model systems for the study of kidney development: use of the pronephros in the analysis of organ induction and patterning." Dev Biol **188**(2): 189-204.

Walentek, P., S. Bogusch, et al. (2014). "A novel serotonin-secreting cell type regulates ciliary motility in the mucociliary epidermis of Xenopus tadpoles." Development **141**(7): 1526-1533.

Wallingford, J. B. (2010). "Planar cell polarity signaling, cilia and polarized ciliary beating." Curr Opin Cell Biol **22**(5): 597-604.

Wang, L., C. Fu, et al. (2013). "miR-34b regulates multiciliogenesis during organ formation in zebrafish." Development **140**(13): 2755-2764.

Werner, M. E. and B. J. Mitchell (2012). "Understanding ciliated epithelia: the power of Xenopus." Genesis **50**(3): 176-185.

Wessely, O. and U. Tran (2011). "Xenopus pronephros development--past, present, and future." Pediatr Nephrol **26**(9): 1545-1551.

Whitfield, J. F. (2004). "The neuronal primary cilium--an extrasynaptic signaling device." Cell Signal **16**(7): 763-767.

http://www.omim.org/entry/244400. Retrieved Jan. 2014.

Yang, J., X. Liu, et al. (2002). "Rootletin, a novel coiled-coil protein, is a structural component of the ciliary rootlet." J Cell Biol **159**(3): 431-440.

Yu, X., C. P. Ng, et al. (2008). "Foxj1 transcription factors are master regulators of the motile ciliogenic program." Nat Genet **40**(12): 1445-1453.

Zariwala, M. A., M. R. Knowles, et al. (2007). "Genetic defects in ciliary structure and function." Annu Rev Physiol **69**: 423-450.

Zhang, J., D. W. Houston, et al. (1998). "The role of maternal VegT in establishing the primary germ layers in Xenopus embryos." Cell **94**(4): 515-524.

Zhang, Y. and D. Reinberg (2001). "Transcription regulation by histone methylation: interplay between different covalent modifications of the core histone tails." Genes Dev **15**(18): 2343-2360.

Zhang, Y. J., L. Zhao, et al. (2013). "Xenopus radial spoke protein 3 gene is expressed in the multiciliated cells of epidermis and otic vesicles and sequentially in the nephrostomes." Dev Genes Evol **223**(3): 183-188.

ACKNOWLEDGEMENTS

I want to express my sincere gratitude to Prof. Ralph Rupp, my supervisor, for giving me the opportunity to carry out my research project. I highly appreciate his encouragements, guidance, valuable advice, and his dedication to teach and share his knowledge. His enthusiasm for scientific research has inspired me and I want to thank him for his mentoring along my way to explore the world of scientific research.

My gratitude also goes to Prof. Peter Becker for enabling a friendly, international and motivating scientific atmosphere in the institute.

Additionally, I am grateful for the financial support provided by the "Förderung für Forschung und Lehre" (FöFoLe) program of the LMU as well as Prof. Jürgen Heesemann for supporting this research project.

I want to express my appreciation to Dr. Laurent Kodjabachian and Mrs. Virginie Thomé (Institut de Biologie du Développement de Marseille-Luminy, France) for the fruitful collaboration on the miR-449-project and their helpful suggestions.

I also thank Prof. Ulrich Welsch and Frau Beate Aschauer from the Anatomical Institute (Lehrstuhl II) of the LMU for their help with the scanning electron microscopy analysis.

My sincere gratitude also goes to my lab. Thank you for your kindness, friendship, support and the fun we had together. Special thanks go to Edith, Barbara and Gabi for their help and advice. Thanks to Max, Steffi, Adrian, Alessandro, Julian and Daniil. Last but not the least, I thank Dario for helping me with the cilia project, providing helpful protocols, discussions and advice.

I am also thankful to the experimental animals without which the study would not have been possible.

Finally, I want to thank my family, especially my parents and my sister, for their constant love, support and wisdom. Thanks to Paw and Mae for the many stimulating discussions, advice and for being who they are.